

Perfectly reproducible and stable plasma columns can be achieved by using the electric field component of radiofrequency and microwave waves. These plasma columns can be much longer than the electromagnetic field applicator that generate the travelling waves sustaining them. These waves are guided by the interface between the outer surface of the dielectric discharge tube and the ambient air. This article proposes a model for describing such travelling wave discharges (TWDs) that perfectly matches the experiments, unlike all existing articles.

Michel Moisan

Groupe de physique des plasmas, Université de Montréal, Montréal H3C 3J7, Québec

Abstract

A new category of plasma appeared in the late 1970s. It consists of a plasma column contained in a cylindrical dielectric discharge tube and maintained by the electric field component of radio frequency (RF) and microwave (MW) waves. These waves propagate at the interface between the outer surface of the tube and the ambient air (or vacuum). These plasmas are also perfectly stable and reproducible. This plasma column is known as a travelling wave discharge (TWD) and has the unique property of increasing in length with the RF and MW power absorbed. Its electron density decreases linearly along its axis until it stops abruptly at a non-zero electron density value, marking the end of wave propagation. The slope of its distribution depends solely on externally defined operating parameters, namely the carrier gas pressure p , the wave frequency f and the inner radius of the discharge tube R (part I). The model presented in this article is the only one to date capable of accurately reproducing all experimental data, particularly those relating to the end of the column, a feat that no other published model has been able to achieve (part II). Interest in TWDs began with the arrival of efficient RF and MW field applicators (wave launchers), which occupy only a few centimetres of the resulting plasma column, which can eventually extend to several metres. Devices such as the Surfatron, Surfaguide, Waveguide-Surfatron, Ro-Box and TIAGO (the latter of which achieves plasma in ambient gas) are already in widespread use. The fact that all these devices have been patented testifies to the interest in the potential applications of TWDs and, of course, their originality. Another outstanding feature of TWDs is their unrivalled wide range of operating parameters p (from a few mTorr (Pa) tested up to twice atmospheric pressure), f (from a few MHz to at least 10 GHz); and R (from 0.5 mm to at least 150 mm). As a result of these exceptional features, today, most publications on TWDs are focused on applications, and this sector is expanding constantly.

Keywords: Plasma physics, RF and microwave discharges, discharges sustained by electromagnetic surface waves/travelling waves.

⁺ This article is dedicated to the memory of Professor Ivan Zhelyazkov (1938-2021), a plasma physics theorist (St. Clement of Ohrid University, Sofia, Bulgaria).

Part I: Experiments show that the axial distribution of the electron density of TWDs is solely determined by the externally set parameters p , f and R , and not by the properties of the plasma column as is currently erroneously accepted.

1. Introduction

In practical terms, plasma columns sustained by travelling waves are characterized by the way in which the electron density is distributed along the axis of the column. It decreases linearly from the start to the end of the column, abruptly stopping at a non-zero electron density; this marks the end of wave propagation and, consequently, the end of the plasma column. All published papers to date explain this distribution by invoking an electromagnetic (EM) *surface wave* that propagates either along the plasma column itself or along the interface between its outer edge and the inner wall of the dielectric discharge tube, but this is erroneous. This paper is the first to demonstrate that, in travelling wave discharges (TWDs) held in a dielectric tube, the travelling wave propagates along the interface between the outer wall of the tube and the surrounding medium.¹ According to the *discharge stability criterion* (Sec. 1.5), the wave attenuation coefficient $\alpha(z)$ must be proportional to the electron density $n_e(z)$, i.e. $\alpha(z) = \frac{b}{\bar{n}_e(z)}$, where b is a constant. This ensures the linearity of the electron density axial distribution under all operating conditions, including at the end of the plasma column — a phenomenon that none of the published models can reproduce correctly. In addition, it makes that ions do not affect the power transfer from the wave to the plasma, whether in the RF or MW range.

It is the electric field of the wave that heats up the electrons, thus ionizing the discharge gas. This establishes a relationship between the energy dissipated by the wave at a given axial position and the energy acquired by the electrons at that position. Consequently, the axial distribution of electron density can also be considered to correspond to an axial distribution of the energy supplied to the electrons by the wave.

1.1. The first identification of plasmas supported by microwaves as TWDs

MW gas discharges, the length of which increases with the applied power, were first identified in an experimental article by Tuma (1970) as being generated by an EM surface wave. In support of this, the author referenced the work of Trivelpiece (1958, 1967) and Gould and Trivelpiece (1959)

¹ An easy way to check this is to close your hand around the discharge tube when it is switched on and observe how the light is partially blocked along its length. The degree of disturbance to the plasma column then depends on how much your hand overlaps the wall of the tube. At the very least, we can conclude that a significant proportion of the electromagnetic power of the wave is transmitted on the outside of the discharge tube.

concerning non-ionising surface waves that propagate along the positive column of a direct current (DC) discharge.

However, plasma columns had been observed to respond in this way to increasing microwave power long before, but this had not been correctly interpreted. They were often simply described in the literature as 'plasma columns emerging from an MW resonant cavity'. For instance, Fehsenfeld *et al.* (1965) wrote that 'in all sources except 2A and 2B, a discharge may extend several centimetres in the tube outside the cavity', while Epstein *et al.* (2014) stated that 'the plasma column, which spreads beyond the resonator, is spatially uniform... it represents the afterglow of the microwave discharge inside the cavity'. At the time, excepting Tuma's paper, there was no indication that they would be maintained by an EM travelling wave as opposed to direct EM radiation or radiation from an antenna. This confusion remains for most of them to this day.

1.2. Various types of TWDs

Reported TWDs most commonly occur in a cylindrical dielectric tube. However, plasma columns can emanate from the outlet of an open-ended dielectric tube and extend freely for several centimetres into the surrounding environment; these plasmas are sometimes called filaments as their diameter is around one millimetre or less. They can also be generated at the tip of a conductive nozzle that introduces gas into the environment (TIAGO system: see Appendix D in Part II). Furthermore, plasmas can be sustained along the dielectric plate that closes the top of a cylindrical metal container, producing planar TWDs, which are of interest in many microelectronic processes (Sugai, Ghanashev and Nagatsu, 1998).

1.3. The rapid early spread of TWDs in the literature is due to the availability of efficient wave launchers (EM field applicators), such as the Surfatron, Surfaguide and Ro-Box

Interest in these plasmas has grown considerably since the introduction of the EM field applicators proposed and patented by Moisan and his team (see Moisan *et al.*, 1977; Moisan and Zakrzewski, 1989; Appendix A). These applicators facilitate straightforward impedance tuning to produce highly efficient, stable and perfectly reproducible plasma columns over an unequaled range of operating conditions. These include gas pressures p ranging from a few mTorr (a few Pa) to at least twice atmospheric pressure, EM field frequencies f ranging from radio frequencies (RF) as low as a few MHz to microwaves above 100 MHz (mainly 2.45 GHz), and an inner radius R of the dielectric tube ranging from 0.5 mm to at least 150 mm. Passing through all possible values of p , f and R results in an electron density spanning 18 orders of magnitude ($2.2 \times 10^8 \text{ cm}^{-3}$ (Fig. 11)– $4.1 \times 10^{26} \text{ cm}^{-3}$ (Fig. 16)!, which is unprecedented compared to any kind of gas discharges.

These technical advances have provided theorists with a vast and compelling body of experimental data, with over 600 papers and several books having been published to date. However, it is a common misconception that these discharges are caused by an EM wave travelling along the plasma column itself (e.g. Gordiets *et al.*, 2000), along the (theoretical) interface between the plasma column and the vacuum (e.g. Margot and Moisan, 1993), or along the interface between the plasma column and the inner wall of the discharge tube (e.g. Navratil *et al.*, 2013).

1.4. The TWD model developed in this paper² is based on the verified fact that electron density decreases linearly along its entire length, whatever the values of parameters p , f and R .

Theorists question this linearity when they compare their calculations of the axial distribution of electron density with experimental results. Regardless of their assumptions or calculation methods, they are unable to reproduce the linearity that we claim to observe throughout the plasma column. To establish the validity of this assertion, we will use a recognised statistical method, applying it to the data in all the figures in this document that describe the axial distribution of electron density.

Section 3 uses least-squares regression to statistically analyse the axial distribution of electron density data points from our laboratories and those of other countries. This demonstrates that, when considering more than five data points, the regression's *coefficient of determination* (r^2) is consistently close to one. In fact, our study not only confirms the linearity of the axial electron density distribution but shows that the slope of this distribution depends solely on the operating parameters p , f and R . This means that the dispersion properties of the EM wave that sustains the discharge and the kinetic properties of the plasma do not affect the axial distribution of electron density. As stated for the first time in ArXiv Moisan v1 (2021), "Plasma columns supported by the propagation of an electromagnetic surface wave have no influence on the properties of the wave, which depend only on the operating conditions". As demonstrated further in the current paper, these discharges are supported by an EM wave guided along the interface between the outer wall of the discharge tube and the surrounding vacuum (or ambient air). Since the interface along which the guided wave propagates depends exclusively on the dielectric permittivity of the discharge tube and the surrounding vacuum, the general belief that plasma properties influence wave propagation is necessary incorrect.

In order to maintain continuity in the text, a brief remark is necessary at this point before the question is fully addressed: the first part of the plasma column, which extends from the EM field applicator output for some distance, is generated by the antenna-like radiation of the wave launcher (see Section 3.2). As explained in detail in Section 3.1, a TWD only forms beyond this section.

1.5. The discharge stability criterion determines the linearly decreasing axial electron density distribution

As will be fully demonstrated in Sec. 4.1 of Part II, the slope of the axial electron density distribution of TWDs is governed by the discharge stability criterion. This is the process by which the wave's power is transferred to the electrons, maintaining a stable and reproducible plasma column. This implies that the electron density must decrease axially in a monotonic manner, regardless of the guided wave's specific dispersion characteristics. As previously mentioned, the slope of the axial electron density distribution is ultimately determined only by the operating parameters p , f and R , as detailed experimentation in Sec. 3 confirmed.

The fact that six different diagnostic techniques support the linearity of the observed axial electron density distribution (see Appendix B) provides an additional level of confidence in this assertion.

² The current model has developed progressively over the years. The first published version appeared in the ArXiv repository (Moisan, 2021), and the model has since evolved to reach version 15.

1.6. Organizing the study as Part I

Firstly, Section 2 provides an overview of the different devices that have been used to produce TWDs. Historically and currently, many of these devices have not been recognised as wave launchers. A next step is to discuss the design of EM field applicators that can produce stable and reproducible long columns of plasma from travelling EM waves, focusing on their key features. A critical issue in this respect is ensuring the full transfer of RF and MW power to the field applicator. Initially, this functions as an antenna that radiates into space, without being in an EM field configuration that ensures TWDs. Section 3 shows, as already indicated, that the axial distribution of electron density remains linear throughout the column, regardless of the TWD's operating conditions (p , f and R). As this had been challenged by theorists, we had to perform a least-squares regression of the experimental data on all the reported axial distributions of electron density, as already mentioned. The validity of these data is increased by the fact that they originate from five different national research groups. This is followed by Appendices A (initial patent applications) and B (six different methods of electron density diagnostic).

2. Design of EM field applicators intended for producing plasma columns with travelling waves and their essential characteristics

2.1. Plasma columns supported by MWs were originally obtained empirically, without adequate theoretical support, and under rather inefficient operating conditions

As mentioned in Section 1.1, MW discharges originating from 'resonant cavities' were initially reported without a suitable explanation, and under suboptimal operating conditions. The ability to vary the length of the plasma column at will, as well as to achieve high levels of excitation and ionisation, fascinated the scientific community. A resonant cavity is a closed, conductive enclosure in which a standing wave pattern can be established, resulting in a high-intensity electromagnetic field due to wave interference. The cavity may be circular, with the cylindrical discharge tube typically passing through its geometric centre. Alternatively, it may be a region within a closed segment of a waveguide, such as a rectangular one, from which the discharge tube emerges. The literature proposes numerous types of resonant cavity, typically ensuring that their dimensions correspond to an integer or half of the full wavelength of the EM field. This maximises the intensity of the electric field by establishing a standing wave (see Appendix C in Part II). It was also found that the best results for maximising the extent of the discharges outside the cavity were achieved by delimiting an EM field zone as narrowly as possible within the cavity, thereby possibly maximising the local intensity of the electric field component of the wave.

The question of how to improve impedance matching quickly arose. For instance, it was discovered that the impedance adjustment on most of these early microwave plasma devices had to be reset each time the discharge was restarted. Furthermore, this tuning had to be achieved through a lengthy and often frustrating process of trial and error, resulting in unreliable discharge reproduction. Ideally, the field applicator would incorporate two impedance adjustment mechanisms to optimise the coupling of RF and MW power generators to a given load: one to minimise the imaginary part of the impedance and the other to minimise the difference between the

real part of the input impedance of the field applicator and the characteristic impedance Z_p of the plasma column. In this case, the plasma column embedded in the dielectric discharge tube is considered a transmission line along which the EM wave propagates. The closer the net impedance of the field applicator is to that of the power generator, the longer the plasma column is observed for a given power. This results in lower energy losses that would otherwise heat and damage equipment components. These 'feats' have resulted in several short papers, mainly focusing on technical improvements in plasma column generation.

These considerations have guided the design of what should be more accurately called EM field applicators. As we shall see in Section 2.2, examining the characteristics of the Surfatron closely helps to clarify the correct operating conditions for generating long and efficient plasma columns.

Some of the practical problems encountered in this area warrant reporting. Citing van Dalen *et al.* (1978) concerning the Beenakker cavity (1976): “(a) Sometimes we could not get the plasma started at all. (b) Although the reflected power could be tuned to a minimum, it always remained high (10–50 W). (c) Sometimes, the reflected power did not change gradually but jumped erratically with a slight variation in the metal tuning screws. (d) The coaxial connector with the antenna loop became very hot. (e) The tuning range of the metal screws in our cavity was too small for proper tuning, especially when conditions were different to those of a helium plasma in a thick-walled quartz tube. Retaining the metal screws thus implied adapting the inner diameter of the cavity.” Other types of resonant cavity have also been developed to improve impedance matching. Examples include variable-size MW cavities (Fredericks and Asmussen Jr., 1971) and parallelepiped cavities mounted on a waveguide. The latter are larger than cylindrical cavities, reported as allowing for better MW coupling (Dessaux *et al.*, 1983).

Finally, it was recognised that plasmas obtained from resonant cavities were maintained by EM surface waves (Mallavarpu *et al.*, 1978). This means that these plasmas were not produced by resonant cavities in the strict sense, but rather by a concentration of the EM field within a *wave-launching gap*. This concept was introduced at the Université de Montréal (UdeM) and is discussed in more detail in Sections 2.2 and 2.3 below.

The advent of these different types of microwave-induced tubular plasma has encouraged research into better EM field applicators. This has been achieved by comparing the applicators under various operating conditions. Ultimately, the EM field applicator known as the Surfatron was developed, overcoming all the aforementioned issues (see Selby and Hieftje, 1987, for a review of the Surfatron's advantages).

2.2. The Surfatron and Surfaguide are EM field applicators optimally designed to support long, reproducible TWD plasma columns and perfectly suited to microwave energy generators.

As mentioned, these devices have been patented by Moisan and his colleagues (see Appendix A). Not only are they much more efficient at transferring MW power to gas discharges, they also solve most, if not all, of the limiting issues previously encountered with other MW-supported discharges. These problems include ambiguous impedance matching and unreliable restart performance. Notably, the Surfatron exhibits the same impedance tuning characteristics in the RF domain (tested between 27 and 100 MHz) as in its MW range (100–2450 MHz). Perfect impedance matching in the RF domain is a distinctive attribute of the Surfatron. Unlike other RF plasma devices (e.g. ICPs), it does not require a separate impedance matching box: using these often results in high

power loss as the matching box heats up considerably. In contrast, the Surfatron provides TWDs with the best possible operating conditions across an unrivalled range of operating parameters p and R , with f extending from 27 MHz (for Surfattrons of a very long length) to 2450 MHz.

In this context, the original concept of a wave-launching interstice (gap) confining the EM field is of major interest, since it enables TWDs to be generated with great efficiency and ease. This concept is described in Section 2.2.2 below.

2.2.1. *The Surfatron is an effective and efficient example of a MW field applicator for generating stable and reproducible plasma columns*

Fig. 1 shows typical photographs of the TWDs obtained using a 915 MHz Surfatron in argon gas at atmospheric pressure within a 6/8 mm inner diameter/outer diameter (ID/OD) fused silica discharge tube. The absorbed power is 300 W in each photo:

- a) As there is no Faraday cage surrounding the discharge tube, high-frequency (HF) radiation (i.e. RF and MW radiation) from the antenna-like radiation region is not contained.
- b) The discharge tube is enclosed in an FC with a radius of 22.5 mm, which is well below the wave cut-off radius for a circular waveguide at 915 MHz.³ Here, the FC length is limited to 30 mm — the minimum length required to prevent HF radiation in the room, as evidenced by measuring instruments remaining unaffected.
- c) The discharge tube is again enclosed in a 22.5 mm radius FC which is now 305 mm long and extends beyond the plasma column length. The axial slot in the FC enables E -field intensity and spectroscopic measurements to be made along the plasma column without the MW field leaking into the room through it. Note that when the same 300 W MW power level is used to feed the Surfatron, the plasma column length fully enclosed in the FC at cut-off is longest. This is because no MW space-wave power escapes from the antenna-like domain into the room.

³ When the radius of a circular waveguide surrounding a plasma tube is small enough to reach its cutoff frequency, no high-frequency waves can propagate freely inside it at this frequency or any lower one. The fundamental mode of a circular waveguide (i.e. the lowest frequency at which a wave can propagate through it) is the TE_{11} mode. The corresponding wavelength is given by $\lambda_c = 2\pi R_{FC(c0)}/1.841$. At 915 MHz, a Faraday cage with an R_{FC} radius of less than 96.1 mm reaches its cutoff frequency. At 2450 MHz, this radius is 35.9 mm (Wendt *et al.*, 1958).

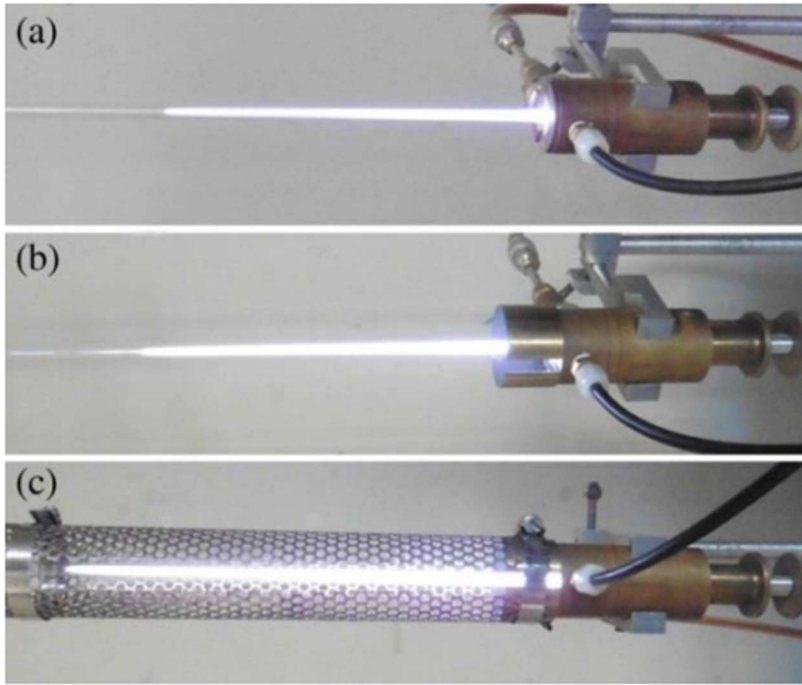


FIG. 1. Photographs showing the plasma column obtained with a 915 MHz Surfatron in a fused silica tube 6/8 (mm) ID/OD: a) no surrounding FC at all; b) with a radius of 22.5 mm, the FC is already well below the cutoff radius for a circular waveguide, which is at 96.1 mm at 915 MHz (footnote 3); the cage length is here 30 mm, which is the minimum FC length preventing MW field radiation in the room from affecting much the measurements; c) enclosed in a 22.5 mm radius FC, 305 mm long, which goes beyond the plasma column length. Absorbed power is 300 W in each photo. The FC's axial slit allows EM E -field intensity and spectroscopic measurements to be taken along the plasma column without any leakage of MW radiation in the room (Moisan, Levif and Nowakowska, 2019).

2.2.2. The wave field initially concentrated in the EM field interstice (the gap) radiates through the opening of the field applicator toward the discharge tube in the same way as an antenna

In our study of TWDs, we found experimentally that that the MW radiation that interfered with the laboratory's measuring instruments was coming from the surfatron gap. The presence of a Faraday cage of minimal length and under cut-off prevented the antenna-like radiation emitted from the gap to flow in space. It reduced the power dissipated by this radiation by up to 30% of the total incident power of the surfatron (Moisan, Levif and Nowakowska, 2019).

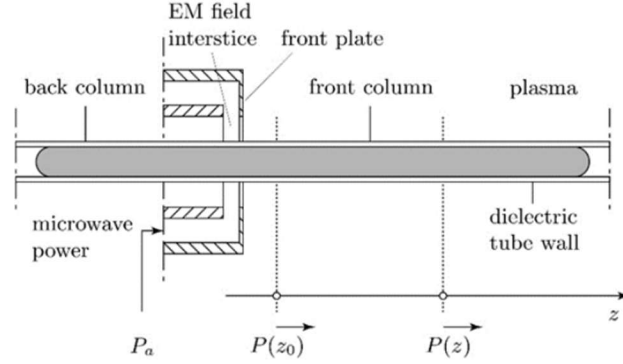


FIG. 2. Schematic representation of the configuration of the wave launching gap (EM field interstice), which is found in all UdeM EM field applicators and achieves reproducible, energy-efficient TWDs. The typical gap width is 2 mm. $P(z_0)$ marks the point at which the flow of travelling-wave power begins after the antenna-like radiation contribution. (Moisan, Levif and Nowakowska, 2019).

Without going into antenna theory in detail, let's take a closer look at the type of radiation emitted by an antenna. The space surrounding an antenna can be divided into three regions: the reactive near-field, the radiating near-field, and the radiating far-field (Johnson, 1993). These regions are designated to identify the field structure in each. i) The reactive near-field region extends only a short distance from the antenna and can be neglected; ii) In the radiating near-field region, the \mathbf{E} and \mathbf{H} fields of the wave are neither proportional in intensity nor perpendicular to each other or in phase. These vary with position, and the wave is evanescent rather than propagating. This region extends from the antenna for a distance equal to a fraction of the travelling wave's wavelength λ_0 , depending on the configuration of the electromagnetic field applicator (see Table I below); iii) The far-field radiating region begins at the end of this region. In this region, the wave propagates as an EM wave until the end of the plasma column (Balanis, 2016). We believe that, as soon as the antenna radiation turns electromagnetic in structure, it can excite the guided (and thus slightly slower) EM wave that generates the TWD plasma column.

Unlike conventional antennas, which are described by spherical geometry, the cylindrical configuration is better suited to mapping the fields of TWDs. In the far-field region, the spatial distribution of wave power can be calculated as a function of the \mathbf{E} field intensity to determine the radiation pattern. For TWDs, this reveals a main lobe and secondary lobes, with the majority of the radiated energy concentrated in the main lobe (Nowakowska, Lackowski and Moisan, 2020).

Considerations on the EM field interstice (Fig. 2). The EM field interstice (gap) plays an essential role in generating efficient TWDs, whether using Surfatron, Surfaguide, Ro-Box (Moisan and Zakrzewski, 1991) or other devices with a similar objective. The width of the gap on a Ro-Box is also 2 mm, as on a Surfatron. However, the width (height) of a Surfaguide is at its optimal level when its impedance is matched to that of the plasma column then considered a transmission line (see Sec. 2.2.3).

Some of the characteristics of the Surfatron faceplate determining the EM field interstice are shown in Fig. 3. This indicates that perfect impedance matching (full power absorption) can be achieved by adjusting the axial position of the capacitive coupler of the Surfatron faceplate with a thickness of 2 mm (Moisan and Zakrzewski, 1991). Good power coupling can be obtained over a greater axial distance of the capacitive coupler with a faceplate thickness of only 0.5 mm relatively to 2 mm.

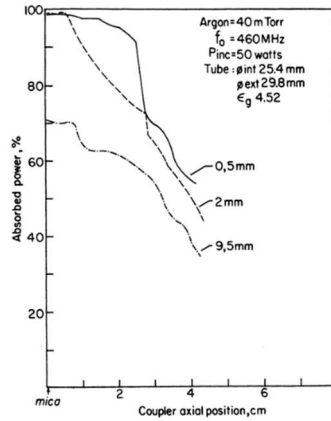


FIG. 3. Percentage of MW power absorbed for a Surfatron fitted with a capacitive coupler with axial displacement along its length (see Fig. A1 in Appendix A, also Moisan and Zakrzewski, 1991). For a given microwave power and a faceplate thickness of 2 mm or less, very little power can be reflected at the input of the field applicator, demonstrating the possibility of achieving near-perfect impedance matching. The thinner the Surfatron faceplate (e.g. 0.5 mm), the greater the axial range of impedance matching (Moisan, Beaudry and Leprince, 1975).

Experimentation has also revealed that the easier the TWD is to turn on, the sharper the inner edge of the faceplate is in the area where the discharge tube passes through. This is particularly evident at high operating frequencies, for example with a 2450 MHz Surfatron and Surfaguide. The higher the field frequency, the greater the minimum electron density required for ignition, necessitating a higher field strength.

As stated above, L_{space} , the length of the plasma column resulting from near-field radiation (antenna-like radiation) is a fraction of the wavelength λ_0 of the EM wave in free space. Table I confirms this for different frequencies and EM field applicators, including for the MW plasma produced using the Beenakker cavity (Lebedev, 1997), as discussed by Moisan, Levif and Nowakowska (2019). In this Table the two narrowest EM-field applicators in the direction perpendicular to the discharge tube, the Surfaguide and the Beenakker cavity, lead to the lowest L_{space} / λ_0 ratio.

TABLE I Length of the plasma column in the space-wave radiation region, L_{space} , and its ratio to λ_0

Frequency (MHz)	Wave launcher	L_{space} (mm)	L_{space} / λ_0
360	Surfatron	330 ± 10	0.40
915	Surfatron	43 ± 1	0.13
2450	Surfatron	28 ± 2	0.23
2450	Surfaguide	7 ± 1	0.06
2450	Beenakker cavity	17	0.14

Note on the Beenakker cavity from the paper by Lebedev (1997). The radial component of the E -field radiation along the outer wall of the discharge tube was detected using a radially oriented antenna made from a tiny semi-rigid coaxial cable, the end of which had been stripped of 1 to 2 mm of its conductive wall. It first increases axially to reach a maximum intensity value at approximately $z = 17$ mm from the cavity, after which it decreases about linearly till $z = 90$ mm (Moisan, Levif and Nowakowska, 2019). The E -field antenna was also axially set for reading at 8 mm (near-field radiating region) and then at 90 mm from the launcher (far-field radiating region). At 8 mm, the E -field intensity decreases slowly in a radial direction away from the discharge tube, whereas it radially decreases exponentially from $z = 17$ to $z = 90$ mm (the end of the plasma column).⁴

2.2.3. *The Surfaguide: the simplest EM field applicator to build for achieving TWDs at 2450 MHz, and capable of reaching operating powers of several kW*

Various Surfatron-like devices were first built in the early years to obtain long columns of plasma over a wide frequency range (100-2450 MHz), a frequency agility that proved decisive in revealing the properties of TWDs. Subsequently, at least 125 small axial length Surfatrions operating at 2450 MHz were marketed by the French company Sairem, and widely used for the study of TWD plasmas mainly at atmospheric pressure, but at powers not exceeding 350 W.

However, the development of applications requiring plasmas with higher electron densities has led to the creation of discharges of several kW with, for example, a Surfaguide at 915 MHz (diamond deposition: Schelz, Campillo and M. Moisan, 1998) and Surfaguides at 2450 MHz (purification of rare gases: Rostaing *et al.*, 2000, elimination of greenhouse gases in fabs: Rostaing *et al.*, 1996 and 1999). The Surfaguide has now become the most popular EM field applicator for TWDs because of its simplicity of construction and ease of use, as well as its higher operating power than the Surfatron. Its dimensions have even been tailored so that it is no longer necessary to readjust its impedance matching under variable operating conditions (but for a limited set of operating conditions as shown in Sec. 2.2.3.2), making it ideal for industrial applications. In fact, the Surfaguide is currently the EM field applicator whose properties are best known in terms of TWD production and whose near-field radiation power loss is the lowest (Table I).

2.2.3.1. *Specific dimensions of the Surfaguide and its equivalent electrical circuit.* The Surfaguide is most commonly made from a standard rectangular WR-340 (R26) waveguide and consists of the three distinct parts shown in Fig. 4a. These are: a central section with a reduced height h of the narrow waveguide wall and length l_2 , and two sections that increase linearly in elevation from height h to full height b (the width of the narrow waveguide wall) at their ends. Each of these sections has a length l_1 .

This scheme enables allows a continuous and gradual transition between the central section and the two ends of the waveguide, which have standard dimensions. This avoids the generation of

⁴ The rather slow decrease of the E -field radial intensity along the plasma column axis up to $z = 17$ mm is ascribed to space-wave radiation (near-field radiation region) while the exponential radial decay observed along the 17 to 90 mm segment (far-field region) is clearly an attribute of TWDs (alias SWDs). This is confirmed by Fig. A12 (see Appendix E in Part II) plotted radially along a Surfatron TWD.

standing waves. One end connects to the microwave power input, and the other end connects to the moving short-circuit plane (tuning plunger) of length l_s (Fleisch *et al.*, 2007).

The central section of the Surfaguide has a circular hole in each broad wall, through which the discharge tube passes. A segment of the tube is sketched in Fig. 4a. The space between the two corresponding holes inside the Surfaguide forms the launching gap (see Fig. 2). Fig. 4b shows the equivalent electrical circuit of the Surfaguide, divided into three sections as shown in Fig. 4a, with the connections between them represented by a transformer turn ratio k_T . The equivalent circuit of the various TWD field applicators designed at UdeM can be found in Moisan, and Zakrzewski (1991).

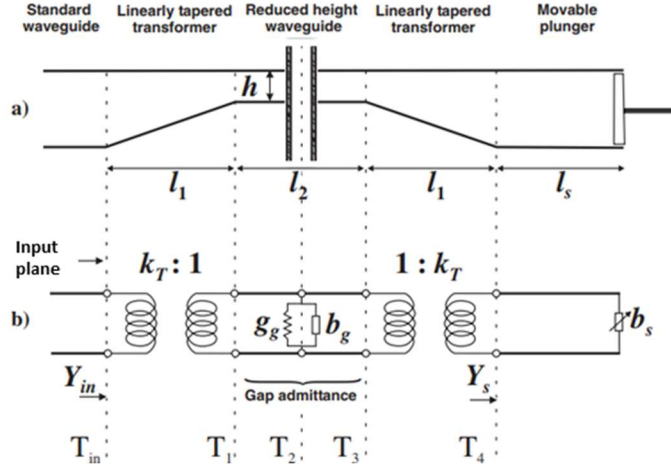


FIG. 4. (a) Schematic representation of the EM field applicator known as the Surfaguide. The vertical dotted lines show the location of the discharge tube (sketched by a segment of it) and delimit the applicator's different dimensions; (b) the equivalent electrical circuit of the Surfaguide. The transformation ratio k_T is used to connect two contiguous sections, the corresponding admittance of which is given by $y = g + j b$ where g is the conductance and b (here) the susceptance in each section of the applicator field. The admittance is the inverse of the impedance Z (Fleisch *et al.*, 2007).

The reduced height h of the field applicator should not be made as narrow as possible in the belief that this will increase the intensity of the \mathbf{E} field in the launch aperture: in fact, the value of h , together with the position of the movable plunger, provides a means of acting on the impedance of the Surfaguide so that the characteristic impedance of the TW plasma column (considered as a transmission line) corresponds approximately to that of the Surfaguide at its launching gap (Moisan, and Nowakowska, 2018). In the case of a rectangular waveguide with broad and narrow wall values a and b , respectively, the EM wavelength λ_g in the waveguide, corresponding to the wavelength λ_0 in free space, is given for TE_{mn} modes by (Lorrain and Corson, 1972):

$$\lambda_g = \frac{\lambda_0}{\sqrt{1 - \frac{\lambda_0^2}{4} \left(\frac{m^2}{a^2} + \frac{n^2}{b^2} \right)}}, \quad (1)$$

which in the case of the TE_{10} fundamental mode ($m=1, n=0$) comes to:

$$\lambda_g(TE_{10}) = \frac{\lambda_0}{\sqrt{1 - \frac{\lambda_0^2}{4} \left(\frac{1}{a^2} \right)}} \quad (2)$$

with the corresponding waveguide impedance:

$$Z_g = \sqrt{\frac{\mu_0 \lambda_g b}{\varepsilon_0 \lambda_0 a}} \quad (3)$$

where $b = h$ in the central section of the Surfaguide, implying here that Z_g decreases as h decreases. The optimum h dimension was determined by experimentally examining the tuning characteristics of the Surfaguide under a range of specific operating conditions, as detailed in the next section.

2.2.3.2. *Determination of the range of discharge operating parameters for which no impedance retuning is necessary when using a Surfaguide with a correctly dimensioned narrow wall width.* Fig. 5 illustrates the experimental configuration employed to generate a TWD plasma column with a Surfaguide, as well as to diagnose the level of reflected power in relation to the position of the movable short (tuning plunger).

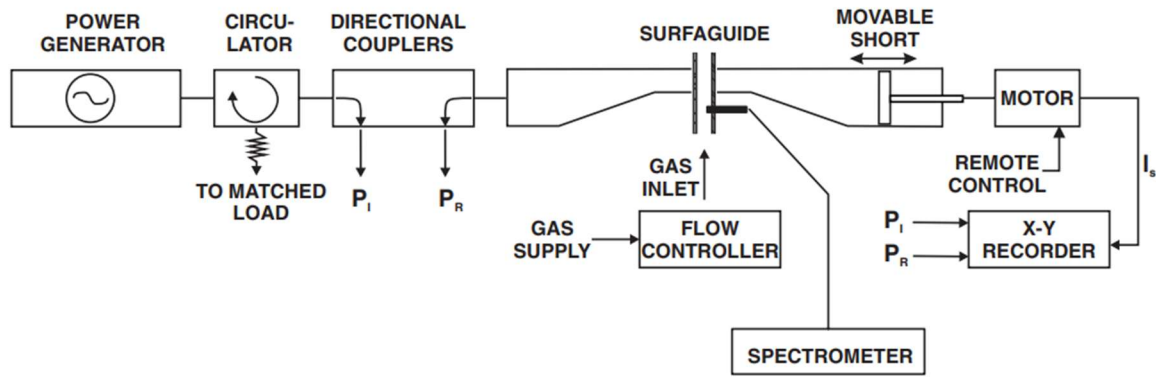


FIG. 5. Schematic diagram of the experimental arrangement used to generate a TWD with a Surfaguide, as well as analyse the reflected power P_R as a function of the position of the movable plunger, for a given narrow wall width h (Fleisch *et al.*, 2007).

The reflected power P_R is tracked as a function of the position of the moving short, looking for the widest range of operating conditions that do not require readjustment. This scenario is examined in Fig. 6 for three reduced heights $h = 10, 15$ and 25 mm: it is $h = 15$ mm that provides the broadest range of operating conditions for which no readjustment of the plunger position is needed. In Figs. 6b, 6e and 6h specifically, the tuning characteristics (reflected power P_R over incident power P_I vs. plunger position l_s over waveguide wavelength λ_g) remains close to perfect impedance matching under a large range of N_2 gas flow (30-120 slm), MW input powers (2-5 kW) and N_2 and Ar mixture compositions (Fleisch *et al.*, 2007). The ability to implement plasma processes across a wide range of operating parameters without constantly readjusting the Surfaguide's impedance is a definite advantage in industrial processes: this example demonstrates how efficiently SF_6 molecules, which are used in plasma reactors for chip manufacturing, can be removed without plunger retuning when $h = 15$ mm (Kabouzi *et al.*, 2003).

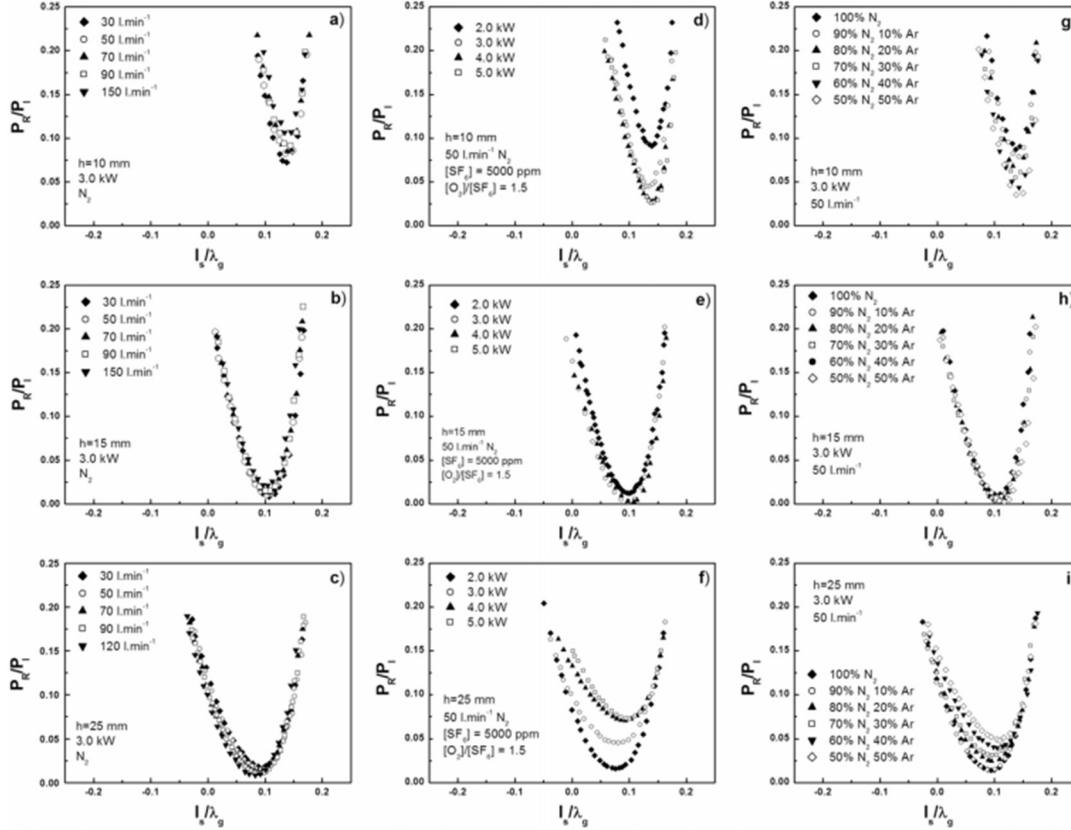


FIG. 6. Surfguide tuning characteristics (reflected power over incident power as a function of plunger position over waveguide wavelength) considering three different heights h , for various discharge operating conditions: (a)–(c) influence of the N_2 gas flow rate at a with incident microwave power, (d)–(f) influence of the incident microwave power for a given gas mixture comprising O_2 and SF_6 and a fixed gas flow rate, (g)–(i) influence of the concentration of admixed Ar gas in N_2 at a constant incident microwave power (Fleisch *et al.*, 2007).

3. 3. The linearity of the axial distribution of the electron density of TWDs depends exclusively on the operating parameters p, f and R

3.1. The linearity of the axial distributions of electron density obtained from experimental data is statistically reliable

In Glaude *et al.* (1980), the data points of the experimentally determined axial distributions of electron density along a TW-maintained plasma column were approximately linearly related to each other, as judged by the operator. This was also the case, for instance, in Fig. 3a of Chaker and Moisan (1985). It was not until the early 2000s at UdeM that the experimental points were subjected to linear least-squares regression using specialised software, which had not been readily available previously. This recognised statistical method was used to ascertain the linearity of the axial

electron density distributions, which were often disputed in the literature. Fig. 7b, obtained using this statistical technique, confirms the validity of the approximate fit of the data in Fig. 7a. This shows that the measured points naturally align with linearity. The very high statistical determination coefficients, r^2 , confirm this: 0.996 for the antenna-like radiation zone and 0.994 for the TWD in Fig. 7b.

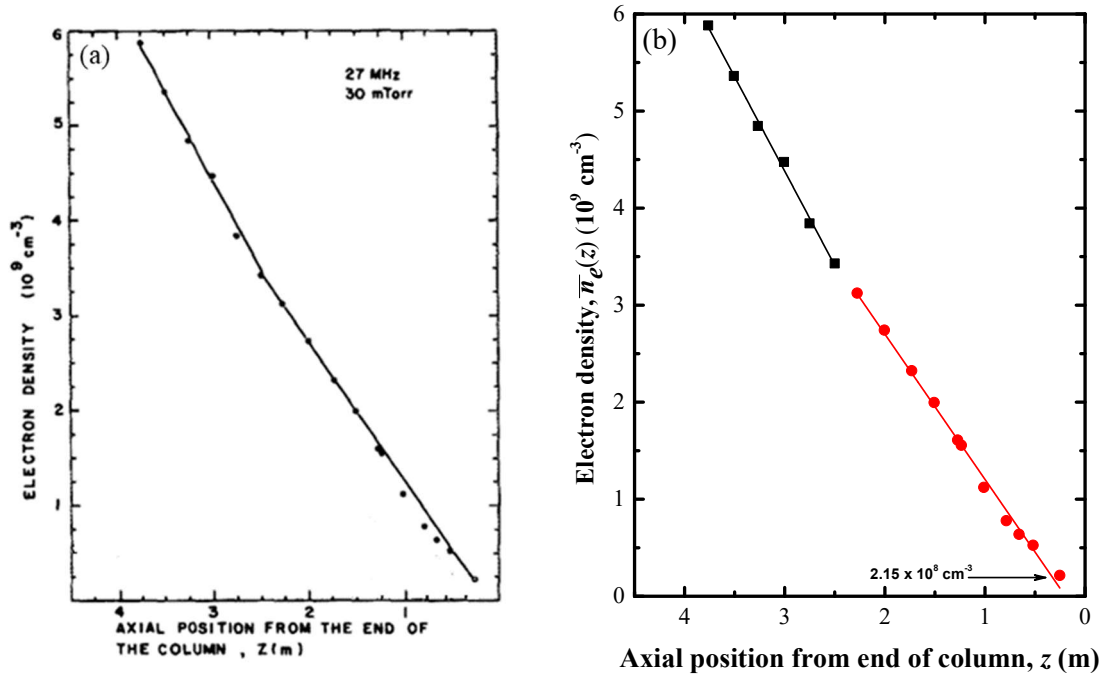


FIG. 7: a) Electron density determined by the TW phase-variation method along the plasma column (see Appendix B) at an argon pressure of 30 mTorr (7.5 Pa) in a discharge tube with an inner radius of 32 mm and at a wave frequency of 27 MHz. This curve was first published in 1985 as part of Fig. 3a in Chaker and Moisan (1985): the data points were connected approximately to the eye by two successive straight lines; b) same data as in Fig. 7a, but processed by a least-squares regression, confirming the existence of two independent straight lines, with $r^2 = 0.996$ for the antenna-like radiation zone and $r^2 = 0.994$ for the TWD.

Remark: Interpreting experimental data with r^2 close to 1 as evidence of a perfectly linear axial profile of electron density is not justified a priori: it merely indicates a strong linear correlation. In fact, deviations above or below the mean value of the data points are masked when considering the quadratic value of the r^2 coefficient. In practice, this means that slight non-linearity in the data cannot be ruled out at this stage, even though r^2 is close to unity. It is therefore possible that the axial electron density distribution of TWDs is slightly non-linear, but this would not be detectable unless the range of electron density considered extends over three or four orders of magnitude. The largest observed range of electron density in a single measurement is less than two orders of magnitude for given discharge conditions. This article will focus on the observed linearity in the axial distribution of electron density, gradually clarifying its nature/origin and ultimately reaching a definitive physical conclusion: this distribution is intrinsically linear and decreases axially, ending abruptly when the propagation of the travelling wave stops.

Assuming that the straight line closest to the field applicator in Fig. 7 results from a TWD is a mistake because, as mentioned earlier, it ignores the fact that this zone, which starts at the outlet of the EM field applicator's interstice (Fig. 2), is necessarily determined by its antenna-like behaviour (designated the 'space-wave radiation zone'). This generates an unguided radiation wave that spreads through space with some intensity lobes. This intrinsic radiation zone precedes any TWD plasma column axially (see Sec. 3.2.1 below). The axial distribution of electron density in this zone can take many shapes⁵, and its length depends on frequency as well as on the structural characteristics of the field applicator (Nowakowska, Lackowski and Moisan, 2020). As shown in Table I, the axial extension of this radiation zone, starting at the gap of a Surfatron, is between 0.13 and 0.4 λ_0 (EM wavelength in free space). At 27 MHz, this equates to a range of 1.4–4.4 metres. If we consider the segment close to the launcher segment in Fig. 7b, the radiation zone extends approximately 1.3 m long, which is consistent with the findings of Moisan, Levif and Nowakowska (2019).

Fig. 7b already shows a general feature of the axial distribution of electron density: the electron density in Fig. 7 does not decrease continuously to zero but instead stops abruptly at a non-zero value. In the present case, the observed electron density at the end of the column is approximately five times higher than the minimum required for TW propagation, namely $\bar{n}_{e(\text{re})} = 4.8 \times 10^7 \text{ cm}^{-3}$ (equation (6) below). This is because, although the gas pressure is low enough to ensure a small collision frequency ν , the wave (angular) frequency ω is here too low to correspond to the conditions $\nu/\omega \ll 1$ of equation (6) (further on for details).

3.2. The axial gradient of the electron density depends solely on the operating parameters p , f and R

As stated in the footnote ⁶, the discharge gas should be characterized by its density N (and its nature) rather than its pressure p . So far, efforts to model the axial gradient of electron density along surface wave discharges (SWDs) have highlighted its dependence on the similarity-law factor $\nu f/R$ (Aliev, Boev and Shivarova, 1982). Here f and R are true operating parameters, meaning they are fully set externally while the electron-neutral collision frequency for momentum transfer, ν , is not since it can vary axially. We therefore suggest replacing ν with N , although this remains to be proven analytically. This would give the following expression for the axial gradient of the electron density:

$$\frac{d\bar{n}_e}{dz} = -C_0 \frac{fN}{R} \quad (4)$$

⁵ Fig. 8a below illustrates that the axial electron density distribution in the antenna-like region is linear at low argon pressures (20–40 mTorr) but becomes bumpy at higher pressures (80 mTorr and above).

⁶ The role and importance of the gas in a discharge is usually represented by its pressure, p , an easily accessible and adjustable quantity. However, a more appropriate parameter is the gas density, N , since p depends on the gas temperature, $N = p/k_B T$ (k_B is Boltzmann's constant). This indicates that p is not a distinctive physical parameter of the discharge, as it can correspond to different N and T pairs. Furthermore, the value of N does not vary axially within the discharge tube. This makes it a condition that is fixed by the operator at the outset, unlike ν which develops with plasma kinetics (Aliev, Schlüter and Shivarova, 2000).

where f , N and R are now all true externally set parameters, and C_0 is a constant. In any case, for practical reasons, the influence of the discharge gas is most often expressed in terms of p instead of N :

$$\frac{d\bar{n}_e}{dz} = -C'_0 \frac{fp}{R}. \quad (5)$$

3.2.1. Minimum electron density (at the end of plasma column) as a function of wave frequency and the role of the collisional parameter ν/ω when exploring the entire TWD pressure range

This section focuses on the minimum electron density required for travelling wave propagation. The cessation of this propagation marks the end of the plasma column. Throughout this paper, we will verify experimentally that, in our configuration, the minimum electron density allowing travelling wave propagation at a frequency f and in the low collision regime ($\nu/\omega \ll 1$) is obtained from the following relation (Aliev, Schlüter and Shivarova, 2000):

$$\bar{n}_{e(\text{re})}(\text{cm}^{-3}) \simeq 1.2 \times 10^4 (1 + \varepsilon_g) f^2 (\text{MHz}) \quad (6)$$

where ε_g is the relative dielectric permittivity of the discharge tube material (3.78 for fused silica and 4.52 for many types of Pyrex glass). When ν/ω is no longer much less than unity, the minimum electron density found is higher than that given by equation (6). The higher the gas pressure, the higher the electron density at the end of the column, a situation not always recognized as such in, for example, Palomares *et al.* (2010b).

It should be noted that, although relationship (6) was initially demonstrated for a plasma column assumed supported by a surface wave propagating along the interface between the plasma column and the inner wall of the discharge tube, it nonetheless experimentally accurately provides $\bar{n}_{e(\text{re})}$ in the case of an EM wave travelling along the interface between the outer wall of the dielectric tube and the surrounding vacuum (see the discussion concerning Fig. A3, right panel). The intensity of the wave's \mathbf{E} field (and therefore the electron density) is reduced by the permittivity of the discharge tube as the wave passes through it to heat the electrons in the gas.

3.2.2. Linearity of the axial distribution of electron density as a function of gas pressure

3.2.2.1. *Low gas pressure domain (0.02-0.3 Torr, 2.7-40 Pa).* Fig. 8a shows $\bar{n}_e(z)$, the radial averaged electron density, as a function of axial position, from the end of the plasma column at five argon gas pressures (with a nearly twofold increase at the next pressure). The electron density has been determined using a TM_{010} mode resonant-cavity method (see Appendix B). Beyond a certain axial position relative to the field applicator (here, a Surfatron), the axial distribution of the electron density becomes linear. The curved line of the electron density at higher axial positions than the straight line in the figure belongs to the antenna-like radiation region. Recall from Table I that this region extends over a distance between 0.13 and $0.4 \lambda_0$ from the exit of the field applicator (Moisan, Levif and Nowakowska, 2019).

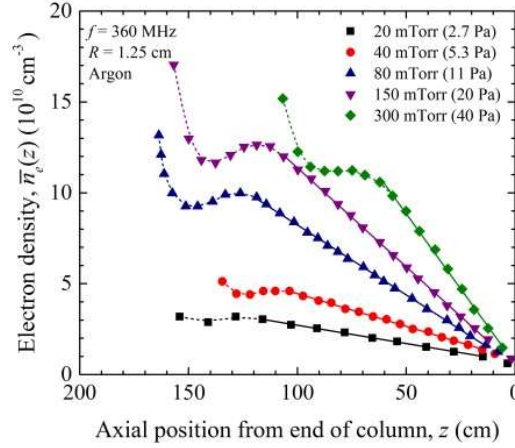


FIG. 8a. Measured axial distribution of the radially averaged electron density through the resonant TM_{010} cavity method, plotted from the end of the plasma column, along the discharge sustained by the propagation of a 360 MHz TW, at five argon gas pressures. This was conducted in a Pyrex-brand glass discharge tube (Dow Corning; relative dielectric permittivity $\epsilon_g = 4.52$) of an inner radius of 12.5 mm and external radius of 15 mm (Glaude *et al.*, 1980).

Fig. 8b corresponds to the 0-50 cm axial section of Fig. 8a. These curves were plotted using linear least-squares regressions on (many) data points, yielding coefficients of determination r^2 very close to unity (see the figure caption for their values) for gas pressures between 20 and 300 mTorr. The observed axial electron density distributions are clearly straight lines that extend to the end of the plasma column. the slope of their axial electron density distribution steepens with increasing pressure, as predicted by relationship (5).

Fig. 8b also shows that the minimum electron density $\bar{n}_{e(re)}$ (6) that allows the wave to propagate under low-collision regime ($\nu/\omega \ll 1$) is reached at 20 mTorr for 360 MHz. This clearly indicates that the travelling wave supporting the plasma column obeys the relation (6) at its end. Glaude *et al.* (1980) actually calculated that under current operating conditions, ν is about $1 \times 10^8 \text{ rad s}^{-1}$, which, at 360 MHz, gives a value of about $\nu/\omega = 0.04$: this verifies that, in the present case, $\nu/\omega \ll 1$.

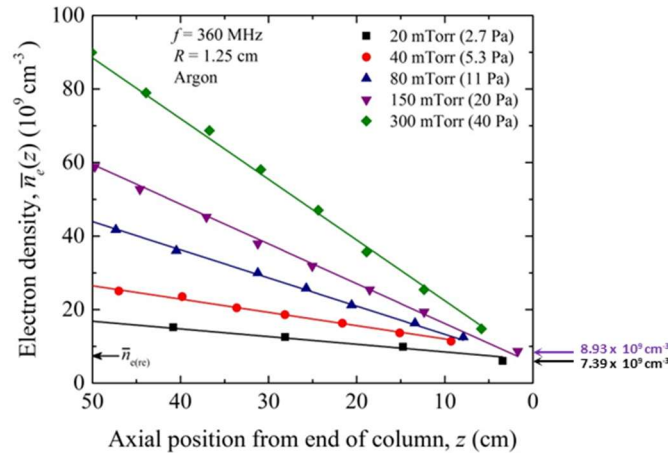


FIG. 8b. An enlargement of the 0-50 cm axial segment in Fig. 8a. The experimental data points for a given gas pressure correspond to a straight line to the end of the plasma column, with $r^2 = 0.984, 0.995, 0.995,$

0.999, and 0.999 at 20, 40, 80, 150, and 300 mTorr, respectively. Assuming that $v/\omega \ll 1$, the corresponding minimum theoretical electron density (6) is $\bar{n}_{e(\text{re})} = 7.4 \times 10^9 \text{ cm}^{-3}$, as indicated by the arrow inside the figure frame. The minimum measured electron density values at 20 and 40 mTorr are designated by arrows outside, showing that the $\bar{n}_{e(\text{re})}$ value is reached at 20 mTorr.

3.2.2.2. *Intermediate pressure range case (0.12-7.2 Torr; 16-960 Pa).* This situation corresponds, given the gas pressure and TW frequency, to the collisional regime varying from $v/\omega \ll 1$ to $v/\omega < 1$. Linearity of the TWD axial distribution of electron density is again verified with $r^2 = 0.995$ in both Figs. 9a and 9b.

According to relation (5), the axial gradient of electron density $\frac{d\bar{n}_e}{dz}$ depends on the radius of the discharge tube as $1/R$. This means that the ratio of the slopes of the electron axial density in Figs. 9a and 9b should be $R_b/R_a = 1.7$. However, the ratio of the measured slope values, $6.35/4.77 = 1.33$, is lower. One possible explanation is that there is some radial contraction of the plasma column (the plasma does not entirely fill the discharge tube radially) in the larger tube radius (Fig. 9b): the radius of the plasma column is smaller on average axially than R_b . The axial profile of the electron density $\bar{n}_e(z)$ has been obtained by recording the axial phase variation of the EM travelling wave, then determining the electron density using the wave phase diagram (see Appendix B).

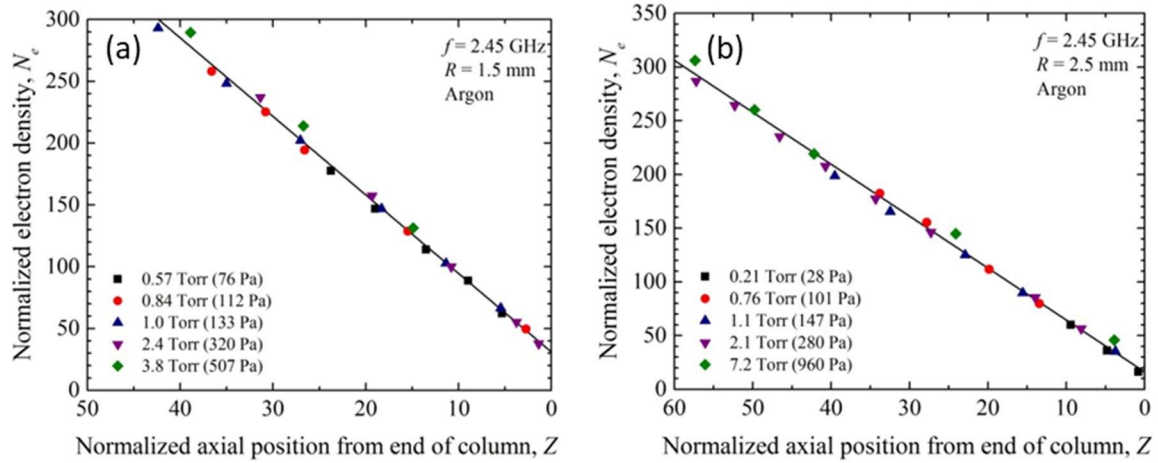


FIG. 9 (foreign laboratory). Axial distribution of the electron density of TWDs maintained at 2450 MHz at different argon gas pressures in the collisional regime ranging from low to medium pressures in discharge tubes ($\epsilon_g = 4.8$) of two different radii: a) $R_a = 1.5 \text{ mm}$ and b) $R_b = 2.5 \text{ mm}$; the figures are adapted from Sola, Cotrino and Colomer (1998) where N is here the normalized electron density and Z the normalized axial position. In both tubes r^2 is found to be 0.995.

3.2.2.3. *Atmospheric pressure domain and tube radius dependence.* Fig. 10 shows the observed axial distribution of the radially averaged electron density along a TWD-supported plasma column at twice atmospheric pressure in argon gas in three discharge tubes with radii smaller than one mm (Moisan, Pantel and Hubert, 1990). The electron density was determined using the broadening of the H_β line (486.1 nm) (see Appendix B) in an argon-hydrogen gas mixture containing 0.5 % hydrogen.

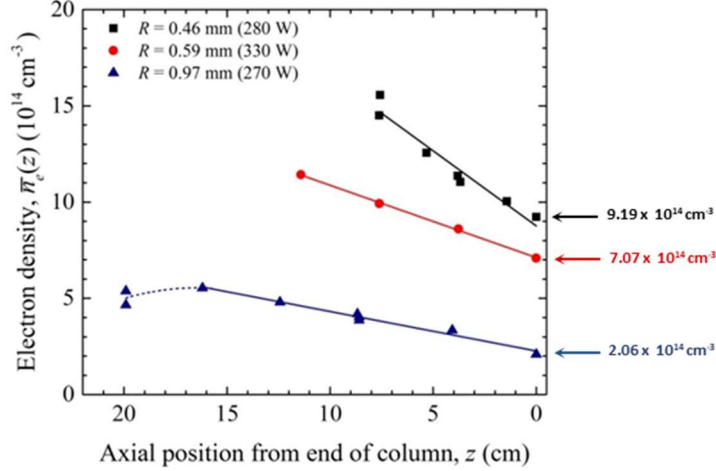


FIG. 10. Measured axial distribution of the radial mean electron density displayed from the end of the plasma column supported by a 915 MHz TW in fused silica discharge tubes. The tubes have three different inner radii, but they are all thick-walled with an external radius of 8 mm. The experiment was conducted in argon gas at twice atmospheric pressure (Moisan, Pantel and Hubert, 1990). The measured electron density was by H_β Stark broadening with 0.5 % added hydrogen (see Appendix B). The calculated minimum electron density at 915 MHz (6) is $\bar{n}_{e(\text{re})} = 4.8 \times 10^{10} \text{ cm}^{-3}$, which is four orders of magnitude lower than the measured electron density, as expected for such a high gas pressure. Coefficient of determination $r^2 = 0.935, 0.999, 0.977$ following the increase of the tube radius.

Although the ratio v/ω is much larger than unity at (twice) atmospheric pressure, the data nevertheless follow a straight line, except at the $z = 20$ cm point for the $R = 0.97$ mm tube, which belongs to the space wave radiation region of the field applicator (Surfatron). The slope in Fig. 10 follows the $1/R$ dependence of equation (5) at least qualitatively, since the gas pressure in the tube is not necessarily equal to the input pressure p . This is because the restriction to gas circulation increases as the radius of the tubes decreases sufficiently.

As mentioned previously, the discharge tubes shown in Fig. 10 all have thick walls. In contrast, all the other tubes presented in this document have relatively thin walls. For instance, Fig. 8 illustrates an inner radius of 12.5–13 mm and an outer radius of 15 mm. Therefore, as in the study by Kovačević *et al.* (2021), one might hypothesise that when the dielectric tube is sufficiently thick, the EM wave will lose power as it travels through this medium (see Section 5.2.5 for calculations). However, the experiment contradicts this hypothesis. Fig. 10 shows that the linearity of the axial electron density remains unaffected by a loss of wave power, which would otherwise increase with axial position and affect linearity as the wave propagates inside a thick dielectric tube. The absence of wave power loss in the dielectric tube is consistent with our model, in which the guided wave primarily propagates along the interface between the outer wall of the discharge tube and the surrounding vacuum.

For the reasons already mentioned in 3.1.2, the value of the electron density at the end of the column in high-pressure gas discharges should exceed the minimum electron density (6) for TW propagation, which at 915 MHz and with $\epsilon_g = 3.78$ is $\bar{n}_{e(\text{re})} = 4.8 \times 10^{10} \text{ cm}^{-3}$, whereas the electron density measured at the end of the column (as shown in the figure) is $2 \times 10^{14} \text{ cm}^{-3}$ in the 0.97 mm radius tube and even higher in the smaller tubes: it is four orders of magnitude higher than in the low-collision regime: nonetheless, linearity is unaffected.

The pressure range we have just examined in this section 3.2 is extremely wide, ranging from a few mTorr to twice the atmospheric pressure. It therefore corresponds to major changes in the recombination mechanism of charged particles, moving from the diffusion regime (free and then ambipolar) to volume recombination (atomic and molecular): the kinetics of the discharge are therefore strongly modified by its passage through these different regimes. However, even with such extreme variations, the linearity of the axial distribution of the electron density remains, as expected from our model.

3.3. Linearity of the axial distribution of the electron density in TWDs as a function of wave frequency

Figs. 8 at 360 MHz, 10 at 915 MHz and 9 at 2450 MHz have already shown that a large variation in the wave frequency of TWDs does not affect the linearity of their axial distribution of electron density. This section extends the study to frequencies as low as 27 and 50 MHz, which belong to the RF domain. As ions can absorb energy from the E field of the wave below 100 MHz (Moisan, Ganachev and Nowakowska, 2022), we investigate whether this has any effect on the linearity of the axial distribution of electron density.

3.3.1. Covering part of the RF domain up to the beginning of the microwave range (27-200 MHz) of the TWDs.

Fig. 11 shows the value of $\bar{n}_e(z)$, the radially averaged measured electron density of these TWDs (using the TM₀₁₀ resonant cavity method), at four frequencies of the traveling wave ranging from a portion of the RF domain to the approximate beginning of the MW range, with axial position starting from the end of the plasma column (Chaker, Moisan and Zakrzewski, 1986). Due to the low gas pressure of these TWDs (30 mTorr, 4 Pa) and the fact that $v/\omega \ll 1$, the minimum measured electron density values (at the end of the plasma columns) should correspond to the calculated value $\bar{n}_{e(re)}$ (6). We observe that at each of these frequencies, the axial distribution of electron density decreases linearly, as confirmed by the r^2 values of the least squares regressions approaching unity (see figure caption for these values). Additionally, according to relation (5), the slope of these lines increases with increasing TW frequency.

Since the beginning of studies on SWDs, it has been observed that increasing the EM power transmitted to the field applicator under fixed operating conditions extends the length of the plasma column without affecting the linearity of the axial distribution of electron density or its slope. The 100 MHz curve in Fig. 11 illustrates this well: the arrow pointing towards 36 W shows the axial position of the start of the TW plasma column relative to its end at this power value; increasing the MW power, for example, to 58 W does not alter the slope of the existing plasma column segment, only its length.

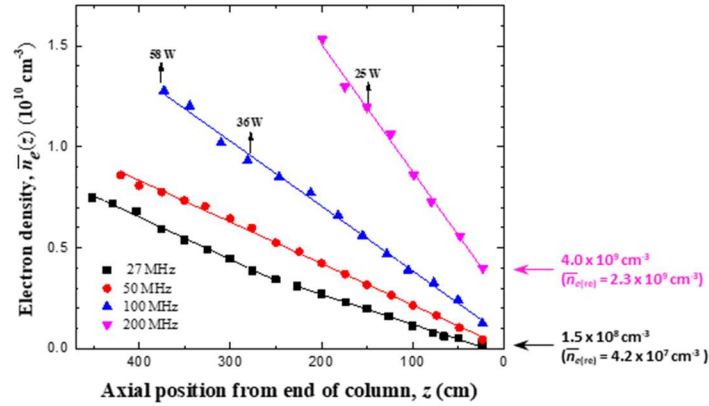


FIG. 11. Measured radial mean value of the electron density axial distribution from the column end using the TM_{010} resonant cavity method. The discharge was obtained by launching an EM travelling wave excited at four different frequencies in argon gas at a pressure of 30 mTorr (4 Pa) in a fused silica tube with an inner radius of 32 mm (Chaker, Moisan and Zakrzewski, 1986). The straight lines are the result of least-squares regression of the data, providing coefficients of determination of $r^2 = 0.990, 0.999, 0.998$ and 0.998 respectively as the frequency increases. For the 27 MHz case, two different slope values can be identified for the curve: $1.5 \times 10^7 \text{ cm}^{-4}$ between $z = 0$ and $z = 250$ cm, and $2.1 \times 10^7 \text{ cm}^{-4}$ between $z = 250$ and $z = 350$ cm (see Fig. 7b at 27 MHz for details on the antenna-like radiation region).

Unlike in the microwave range, in the RF domain of 27 and 50 MHz, the \mathbf{E} field of the wave heats both the electrons and the ions in the discharge: nonetheless, the linearity of the axial electron density distribution remains unaffected. One possible reason for this is the (coming) relationship (25) where $\alpha(z) = \frac{b}{\bar{n}_e(z)}$ (b is a specific constant), which means that the attenuation coefficient of the wave power is related only to the electron density. This means that the ions do not come into play in the power transfer from the wave to the charged particles (see Sec. 3.3.4 for more information).

3.3.2. The 200-2450 MHz MW range.

Fig. 12 shows the measured axial distribution of the average radial electron density at 210 MHz and 2450 MHz, with an argon gas pressure of 200 mTorr (27 Pa). Linear least squares regressions give $r^2 = 0.991$ for the antenna radiation segment and $r^2 = 0.984$ (based on four points only) for the TWD segment at 210 MHz. At 2450 MHz, $r^2 = 0.997$ for the TWD segment; however, the antenna-like segment is too small to be visible. Conversely, at 210 MHz, the antenna zone is longer than the TWD zone itself (Moisan, Levif and Nowakowska, 2019).

According to equation (5), the slope of the distribution at 2450 MHz should be much steeper than at 210 MHz a priori, since the operating frequency being approximately ten times higher. In this case, however, the slope at 2450 MHz is barely steeper than that at 210 MHz (TWD zone). This is because the TWD plasma column in a 4.5 mm radius tube is partially radially contracted at 2450 MHz but no at all at 210 MHz. It is generally found that, for given operating conditions, the slope of the axial electron density distribution decreases as radial contraction increases. Substituting in (5) the value of the inner radius of the discharge tube, R , for that of the plasma column, r_p , does not

solve the problem. However, qualitatively speaking, it seems that the greater the difference between R and r_p with increasing radial contraction, the gentler the slope.

The measured minimum electron density at the end of the plasma column, indicated by an arrow in Fig. 12, is found to be $3.23 \times 10^{11} \text{ cm}^{-3}$ and $8.67 \times 10^{11} \text{ cm}^{-3}$ at 210 MHz and 2450 MHz, respectively. By contrast, the minimum value of $\bar{n}_{e(\text{re})}$ calculated from equation (6) (assuming $v/\omega \ll 1$ and with $\varepsilon_g = 4.52$) is 2.9×10^9 and $3.9 \times 10^{11} \text{ cm}^{-3}$ at 210 MHz and 2450 MHz: the observed electron density at the end of the column is close to $\bar{n}_{e(\text{re})}$ only at 2450 MHz because then the v/ω ratio is much less than one (low-collision regime).

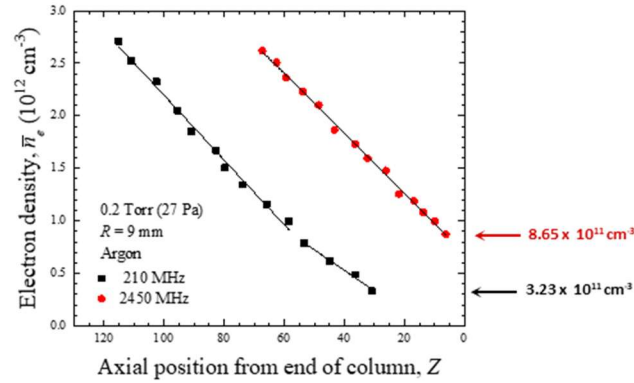


FIG. 12. Measured axial distribution of the electron density (using the TM_{010} cavity method) of a TWD held in argon at 27 Pa inside a fused silica tube with an inner radius of $R = 4.5 \text{ mm}$, at frequencies of 210 and 2450 MHz, both curves obtained with a Surfatron. Least-squares linear regression yields at 210 MHz, $r^2 = 0.991$ for the antenna-like driven plasma segment and $r^2 = 0.981$ (only 4 points) for the travelling wave-sustained one. At 2450 MHz, however, there is no sign of an antenna-like zone, with $r^2 = 0.997$ for the TWD segment (adapted from Chaker, Moisan and Zakrzewski, 1986). The arrow outside the figure frame indicates the lowest observed electron density.

Figs. 11 and 12 confirm that the linearity of the axial electron density distribution is maintained across the entire 27–2450 MHz frequency range, although there are corresponding significant changes in the plasma properties: it does not depend on them, as erroneously currently accepted. Our opposition to the current incorrect belief is further strengthened by the finding that the corresponding operating conditions domain encompasses electron density values spanning 18 orders of magnitude (Fig. 11: $2.2 \times 10^8 \text{ cm}^{-3}$ – Fig. 16: $4.1 \times 10^{26} \text{ cm}^{-3}$). Such a large variation in electron density would normally be expected to alter the electron energy distribution function (EEDF): indeed, the EEDF is most probably not Maxwellian in the low-density electron plasma at 27 MHz but should gradually tend toward a Maxwellian shape as the electron density increases with the wave frequency coming up to 2450 MHz. Nonetheless, this extremely large variation in electron density does not affect the linearity of the axial electron density distribution. Clearly, TWD behaviour is independent of EEDF characteristics, contrary to the beliefs of theorists (see Sec. 5 in Part II).

3.3.3. TWDs at 915 and 2450 MHz in neon

Fig. 13 compares the axial distribution of the radial mean electron density observed at 915 MHz and 2450 MHz in a 3 mm radius tube at atmospheric pressure, this time, in neon gas. Analysis of

the data for the axial distribution of electron density using least squares regression again reveals a linear relationship. However, the r^2 value is lower than those quoted above due to the smaller number of experimental points (only four and five data points at 915 MHz and 2450 MHz, respectively). As expected from relationship (5), the slope at 2450 MHz is steeper than at 915 MHz (Kabouzi *et al.*, 2002).

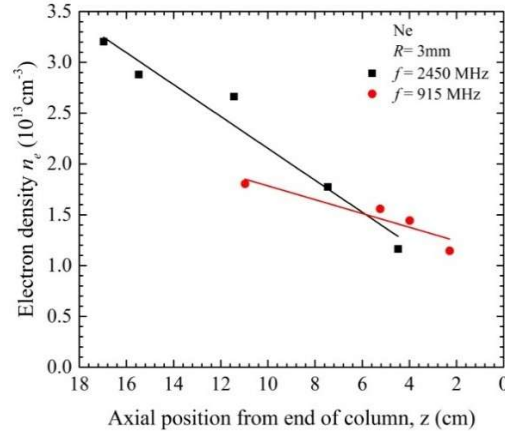


FIG. 13. Measured axial distribution of the radially averaged electron density of a TWD sustained at 915 MHz and 2450 MHz as displayed from the end of the plasma columns. The experiment was conducted in a fused silica discharge tube with an inner radius of 3 mm containing neon gas at atmospheric pressure (Castaños-Martínez, 2004). The electron density was determined from the broadening of the H_β line (486.1 nm) caused by hydrogen atoms supplied by a minimal amount of water vapour in the discharge gas. The coefficients of determination of the least-squares regression were $r^2 = 0.80$ and 0.95 for 915 MHz and 2450 MHz, respectively. It should be noted that assigning r^2 values to a small number of data points is debatable.

3.3.4. The ion density increases at the expense of the electron density in TWDs when the frequency of the travelling wave is lowered from MW towards the RF levels. However, the linearity of the axial distribution of electron density remains unaffected

Our model assumes that the energy supplied to the electrons by the E -field component of the wave causes them to heat up, resulting in the subsequent ionisation of the discharge gas. However, at frequencies below 100 MHz (i.e. in the RF range), the ions also heat up, absorbing some of the energy from the wave's E -field. Nevertheless, Fig. 11 clearly showed that operating at frequencies below 100 MHz does not affect the linear behavior of the axial distribution of electron density, which additionally always obeys relation (5).

However, the slope of the axial distribution of the electron density becomes smaller than predicted by (5) as the frequency decreases from 100 to 50, more to 27 MHz, due to a decrease in the energy given to electrons in favour of ions. Table III confirms, through the measurements from Table II, our assertion that the slope of the axial distribution of the electron density decreases more rapidly than expected when the value of the frequency is lowered in the RF range. In fact, in the MW range, the quotient of the slopes agrees with the exact ratio of their frequencies (relation (5)), as shown in Table III with the ratio 200/100, whereas this is not the case for 200/27: at 27 MHz, the lowest frequency in the table, a great part of the energy of the E field is taken away from the electrons, making the ions relatively more numerous as the frequency of the wave is lowered.

TABLE II Measured slope of electron density from Fig. 11 (relative value)

27 MHz	1.7
50 MHz	2.1
100 MHz	3.2
200 MHz	6.3

TABLE III	Frequency ratio	Measured slope ratio	Measured slope ratio/frequency ratio
50/27	1.85	1.23	0.66
100/27	3.70	1.88	0.51
100/50	2.00	1.52	0.76
200/27	7.41	3.71	0.50
200/50	4.00	3.0	0.75
200/100	2.00	1.97	0.98

3.4. Linearity of the axial distribution of the electron density of TWDs as a function of the inner radius of the discharge tube

Since $\frac{d\bar{n}_e}{dz} = -C'_0 \frac{fp}{R}$ (5), the smaller the discharge tube radius, the steeper the slope of the plasma column density gradient.

3.4.1. Low-collision regime

Figure 14 shows the measured mean radial electron density along the plasma column supported by a 100 MHz travelling wave in a fused silica discharge tube with an inner radius of either 3.2 cm or 6.2 cm, in argon gas at a pressure of 1.8 Pa (10 mTorr) (Chaker, Moisan and Zakrzewski, 1986). As shown in the figure and caption, a straight line with a high degree of confidence is obtained for both R values when a least-squares regression is performed on the axial electron density data points. More precisely, the measured slopes (expressed in relative units) for $R = 3.2$ cm and $R = 6.2$ cm are 13 and 5.9, respectively. Recalling (5) the inverse slope ratio of the small tube radius to the large tube radius is $5.9/13 = 0.45$, while the corresponding inverse radius ratio ($6.2/3.2$) is slightly larger at 0.52.

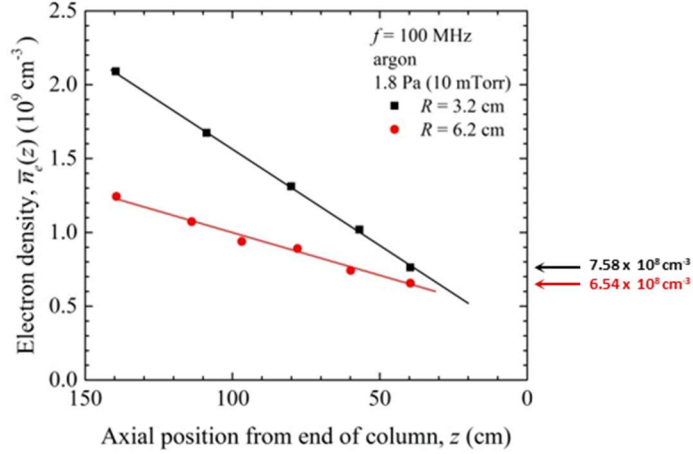


FIG. 14. Measured axial distribution of the mean radial value of the electron density with respect to the end of the plasma column supported by a 100 MHz travelling wave. The experiment was conducted for two values of the internal radius R of the discharge tube, in argon gas at the (very) low pressure of 1.8 Pa (10 mTorr) (Chaker, Moisan and Zakrzewski, 1986). The electron density in the $R = 32$ mm tube was determined using a TM_{010} resonant cavity method, while the axial phase variation of the TW was used for the larger $R = 62$ mm tube (Margot-Chaker *et al.*, 1988). The values of r^2 are 0.993 and 0.986 for $R = 32$ mm and 62 mm, respectively. According to equation (6), the calculated electron density at the end of the TWD plasma column at 100 MHz and assuming $v/\omega \ll 1$, is $\bar{n}_{e(\text{re})} = 6.62 \times 10^8 \text{ cm}^{-3}$, which corresponds, within the experimental error, to the value measured in the tube of larger radius.

3.4.2. High-collision regime

Figure 10 above showed the measured axial distribution of the radially averaged electron density in a TWD supported at 915 MHz in argon gas at (twice) atmospheric pressure. Recall that it specifically concerned discharge tubes with three different internal radii and the same thick outer wall radius. The r^2 value of their axial electron density distribution confirmed its linearity. At the same time, this indicates that, even at pressures as high as atmospheric pressure, the lower the value of R , the steeper the corresponding slope of the axial electron density distribution, in agreement with relationship (5).

3.4.3. Radial contraction of the plasma column does not affect the linearity of the axial distribution of the electron density of TWDs

In the low-collision regime, the TWD plasma typically fills the discharge tube radially. However, radial plasma contraction does occur at pressures approaching one Torr or more if the value of one or more of the following parameters reaches a certain relative magnitude: the inner radius of the discharge tube; the frequency of the wave; and the discharge gas mass (Kabouzi *et al.*, 2002, Castaños-Martínez and Moisan, 2011).⁷ In the case of Fig. 15, radial contraction of the plasma is bound to happen at atmospheric pressure, because the tube radius is large enough and the wave

⁷ The radial contraction of TWD plasma columns is a characteristic of high-pressure electrical discharges in sufficiently large tubes. Plasma contraction in rare gas discharges is related to the influence of the gas temperature T_g upon the concentration of molecular ions X_2^+ . In contracted discharges, T_g decreases strongly toward the discharge tube wall, ensuring the increase of X_2^+ . Since the density of molecular ions is greater toward the wall, the loss of electrons by volume dissociative recombination is higher, ionization is less important, resulting in a contracted plasma (Ridenti, Spyrou and Amorim, 2014).

frequency high. However, in this case, the lower mass of neon compared to argon means that the plasma column is likely to heat less and thus contract less than an argon TWD under the same operating conditions. As shown in the figure, radial contraction causes the plasma column's radius to decrease continuously towards its end, resulting in an increasingly nonuniform plasma column.



FIG. 15. Photograph showing a radially contracted TWD sustained at atmospheric pressure in neon gas in a tube with an inner radius of 6 mm and operating at 915 MHz. As can be seen, the radius of the plasma column decreases continuously towards its end, making it structurally increasingly nonuniform in the axial direction (Castaños-Martínez and Moisan, 2011).

Assuming an already contracted TWD plasma column, increasing the internal radius of the discharge tube causes the plasma column to move further and further radially away from the inner wall of the discharge tube at a given axial position. At the same time, the slope of its axial electron density distribution becomes gentler (Castaños-Martínez, 2004; Castaños-Martínez and Moisan, 2011). The degree of contraction increases as the thermal conductivity of the gas increases: for given conditions, this means successively helium, neon, argon, krypton and xenon in the case of noble gases. For instance, at 915 MHz, plasma contraction is evident in a 3 mm radius argon tube at atmospheric pressure but absent in a neon and helium tube (Fig. 4.26 in Moisan and Pelletier, 2012).

A plasma column subject to radial contraction, as shown in Fig. 15, is structurally an axially inhomogeneous medium. Nevertheless, its axial distribution of electron density remains linear (not shown), as in the case of an uncontracted plasma column. The reason for this is that the traveling wave that maintains the plasma column does not propagate on it, but along the outer wall of the discharge tube surrounded by vacuum (or ambient air): therefore, we should not expect a dependence on the properties of the plasma column, but rather on the permittivity of the dielectric tube, which is constant axially.

3.5. Linearity of the axial distribution of electron density as a function of the discharge gas flow rate

It is interesting to consider how variations in gas flow within a discharge tube affect the axial distribution of electron density in a TWD. According to equation (4), the linearity of the axial distribution of electron density in a discharge tube with a constant cross-section should not be affected by the gas flow rate, since the gas density N is constant along the tube's length. However, increasing the flow velocity of a gas in a tube decreases its inlet pressure (Bernoulli's law of gases). This results in a lower N value and consequently a lower slope of the axial electron density distribution, as observed.

The experiment was carried out in argon at atmospheric pressure in a fused silica tube with an internal radius of 0.75 mm to prevent radial contraction of the plasma and filamentation (Martínez-

Aguilar *et al.*, 2019). Gas flow rates of 0.25 and 1 standard litre per minute (slm) were used in an open-ended tube. The discharge was at 2450 MHz using a surfaguide, — an E -field applicator with a launching gap on either side of the waveguide structure (see Fig. 4a) — producing two plasma columns. Depending on the direction of the gas flow, these columns are described as either 'forward' or 'backward'. The two columns initially receive an equal share of the power emitted by the surfaguide. However, the columns in the opposite direction to the gas flow are shorter, as shown in Fig. 16 and explained in the theoretical work of Kabouzi *et al.* (2007). The electron density was obtained from the broadening of the H_β 486.1 nm Balmer line ((Palomares *et al.*, 2009)). Key points to note from this figure are that the axial distributions of electron density remain linear in all cases and that the slope corresponding to the greatest gas flow (smallest value of N) is the smallest in both directions, which is consistent with the role of N in relation (4).

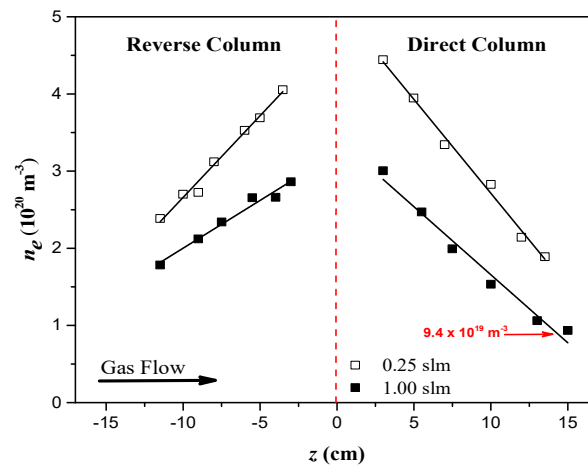


FIG. 16 (foreign laboratory). Experimental axial distribution of the TWD electron density accounting for the argon gas flow direction (forward and backward) and two gas flow rates at atmospheric pressure with $R = 0.75$ mm and $f = 2450$ MHz. The electron density was determined by the broadening of the H_β Balmer line (486.1 nm). The data points from Martínez-Aguilar *et al.* (2019) were processed using least-squares regressions, yielding r^2 values of 0.985 and 0.992 for the 0.25 slm backward and forward columns, respectively, and 0.971 and 0.974 for the 1 slm backward and forward columns, respectively. This confirms the linearity of these axial distributions. The predicted minimum electron density for travelling wave propagation $\bar{n}_{e(\text{re})}$ (6) at 2450 MHz is 1.7×10^{16} m⁻³ whereas the TW is observed to stop propagation at 9.4×10^{19} cm⁻³, meaning cessation of wave propagation occurs more than three orders of magnitude above $\bar{n}_{e(\text{re})}$.

3.6 Linearity of the axial distribution of electron density in TWDs of molecular gases

As all previous figures concerned TWDs in atomic gases such as argon and neon, it is worth examining what happens to TWDs generated in molecular gases. We know that these discharges are mainly composed of molecular ions at low electron density. However, at high electron density, the increased rate of molecular dissociation means that they comprise an ever-greater proportion of atomic ions (Kabouzi *et al.*, 2002; Kabouzi *et al.*, 2007). As we shall see, the difference in

concentration of atoms and molecules in these discharges has no effect on the linearity of their axial electron density distribution.

3.6.1. Nitrogen

Fig. 17 illustrates the axial electron density distribution in an N_2 TWD sustained within a Pyrex™ glass tube ($\epsilon_g = 4.52$) featuring a substantial inner radius of 22.5 mm and operating at a low MW frequency of 500 MHz, with at a gas pressure of 0.5 Torr (~67 Pa). These combined conditions correspond to a radially uncontracted discharge (Dias *et al.*, 1998).

Electron density was determined using the Langmuir probe technique (see Appendix B). According to Grosse *et al.* (1994a), the technique was initially intended to "gather information about the actual EEDF", but it has since been found to "act as a source of inhomogeneity in the plasma" due to the disturbance it causes to wave propagation. This method provides electron density values that are significantly lower than the minimum value calculated for TW propagation, $\bar{n}_{e(re)} = 1.66 \times 10^{10} \text{ cm}^{-3}$ (indicated by the arrow outside the figure frame). We have previously confirmed the existence of this minimum value experimentally, using both the TM_{010} resonant cavity method (see Figs. 8b, 11 and 12) and the axial phase variation of the travelling wave (see Fig. 14). Therefore, a TWD cannot have an electron density lower than $\bar{n}_{e(re)}$. Despite this inconsistency, the axial distribution of electron density obtained using this method is as linear as that obtained using the various diagnostic methods mentioned above. This also means that the linearity of the axial distribution of electron density is maintained, even when dealing with a molecular discharge gas rather than an atomic one.

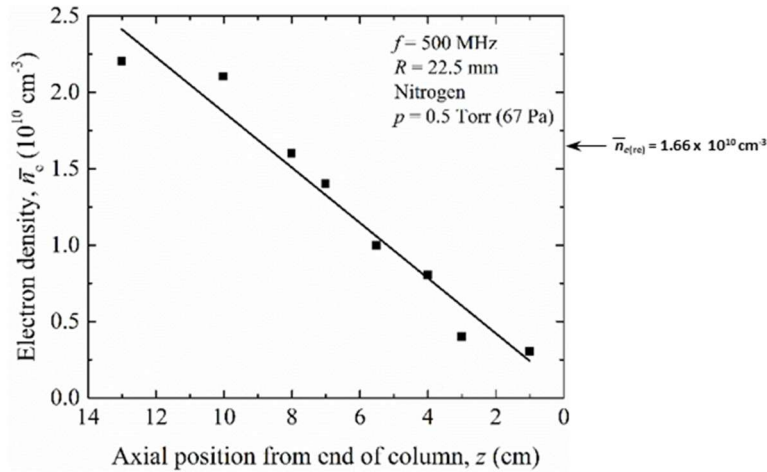


FIG. 17 (foreign laboratory). Axial electron density distribution determined by using the Langmuir probe technique for a TWD sustained in N_2 gas at 67 Pa within a dielectric discharge tube ($\epsilon_g = 4.52$) with an inner radius $R = 22.5$ mm at 500 MHz. The corresponding minimum electron density for wave propagation along the TWD (6), $\bar{n}_{e(re)} = 1.66 \times 10^{10} \text{ cm}^{-3}$, is shown on the outside of the figure frame. Least-squares regression of the data points from Dias *et al.* (1998) gives a linear fit with $r^2 = 0.986$.

3.6.2. Hydrogen

Fig. 18 shows the measured axial distribution of electron density in an H_2 TWD operating under the same conditions as N_2 in Fig. 17, also using a Langmuir probe to diagnose electron density (Gordiets *et al.*, 2000). Data point $Z = 28$ (normalised axial position) is attributed to the antenna

radiation region of the field applicator (Moisan, Levif and Nowakowska, 2019) and is therefore not part of the TWD plasma column. As briefly mentioned in relation to N_2 TWD, the microwave field actually disrupts the probe measurements, as it causes it to collect a time-varying current. This shifts the apparent floating potential towards more negative values, leading to distortion of the probe characteristic and its second derivative. This results in the minimum electron density starting well below $\bar{n}_{e(\text{re})} = 1.66 \times 10^{10} \text{ cm}^{-3}$. Nevertheless, we observe that linearity of the axial distribution of electron density is preserved whatever the kind of molecular discharge gases. This lends further support to our model.

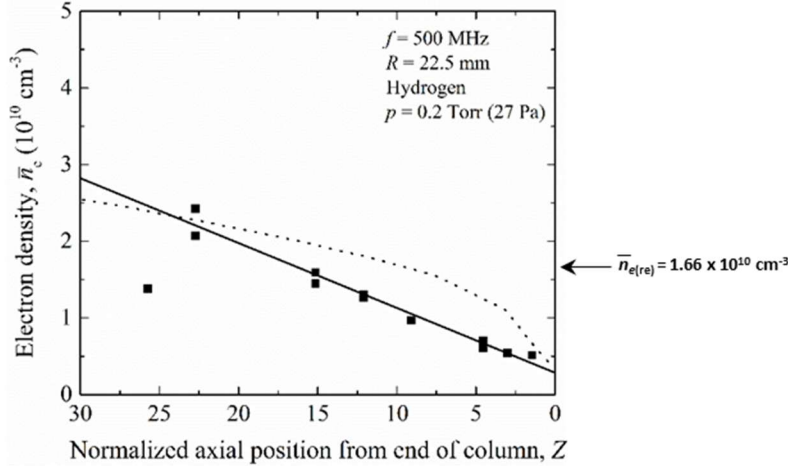


FIG. 18 (foreign laboratory). Measured axial distribution of the electron density in a TWD held at 500 MHz in H_2 gas at 27 Pa within a PyrexTM glass discharge tube ($\epsilon_g = 4.52$) with an inner radius of 22.5 mm, as determined using the Langmuir probe diagnostic method. Excluding the value at the largest Z (related to the antenna-like region of the field applicator), the least-squares regression yielded an r^2 value of 0.948. The whole figure was restructured from Gordiets *et al.* (2000) where the dotted curve is theoretical. It deviates significantly from the experimental results and will be discussed in Sec. 5.2.6.

3.7. *If the plasma column contracts radially, a diagnosis of electron density that considers only part of the radial distribution of electrons will not produce a linear axial distribution of electron density*

3.7.1. *The total number of electrons in a radial section of a TWD plasma at a given axial position is proportional to the power dissipated by the travelling wave at that position*

Recalling the concept of power absorbed per electron (Moisan, Ganachev and Nowakowska, 2022), it is easy to agree that the total number of electrons produced in a radial section of the plasma column is proportional to the amount of power absorbed from the wave that generated them at that particular axial position.

If there is no radial contraction of the plasma column, its radial structure remains constant, i.e. does not vary along the axis. Therefore, whichever portion of the radial electron distribution is considered in the diagnostic technique, this remains axially proportional to the total electron distribution, and consequently to the power dissipated by the travelling wave along the axis. In this case, a linear distribution of electron density should be observed.

In the TM_{010} resonant cavity, the total electron density is considered because the entire radial distribution of electrons is exposed to the EM field within the cavity. Similarly, the electron density diagnostic by the axial variation of the wave phase yields an average total electron density for each radial section of the plasma column at each axial position (see Appendix B).

In both diagnostic techniques, the graph of the radially averaged electron density is therefore proportional to the power lost by the wave at that axial position. This observation, previously made just before Sec. 1.1., provides an innovative new perspective on the axial distribution of electron density, revealing an additional law of energy conservation, which links the wave and the electrons of the plasma column (first proposed by Aliev, Boev and Shivarova in 1982).

3.7.2. *This is the case of electron density diagnosis, in which only some of the electrons in the radial distribution are considered while the plasma column undergoes radial contraction*

Consider, for example, Fig. 19a, which illustrates the Thomson scattering (TS) system employed for measuring the electron density within a Surfatron plasma column. The intersection of the laser beam and the focal spot of the triple grating spectrometer (TGS) (whose slit is parallel to the laser beam axis) defines the TS detection volume. Due to the narrowness of the laser beam ($75\ \mu\text{m}$), only a very limited part of the electron radial distribution is detected.

Two situations can be envisaged:

- i) there is no radial contraction of the plasma column (see case 3.7.1 above). Fig. 19b shows that this occurs at sufficiently low gas pressure (below 0.65 mbar), yielding an axial electron density distribution that is linear.
- ii) in Fig. 19b, at gas pressures of 20 mbar and above, linearity is lost, as the radial electron density profile has contracted, according to the author of the paper.

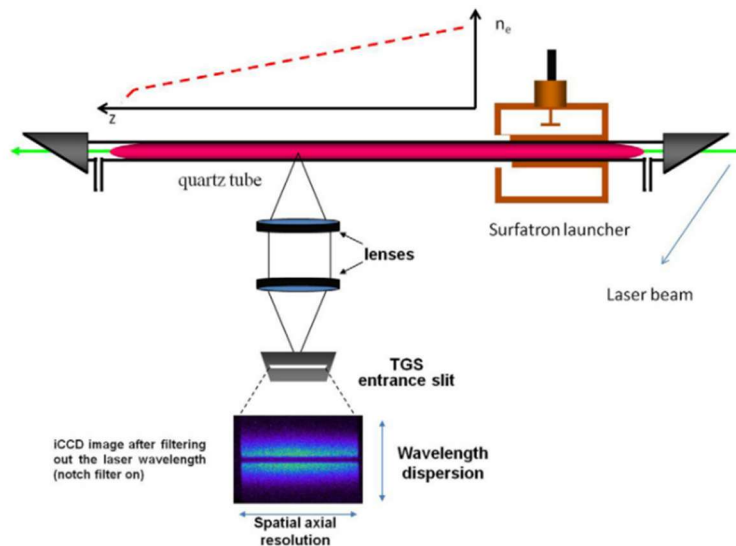


FIG. 19a (foreign laboratory). Diagram displaying the Surfatron plasma source and the TS diagnostic detection system. It illustrates how the entrance slit of the triple grating spectrometer (TGS) is focused on a small radial portion of a given section of the plasma column (Carbone *et al.*, 2012).

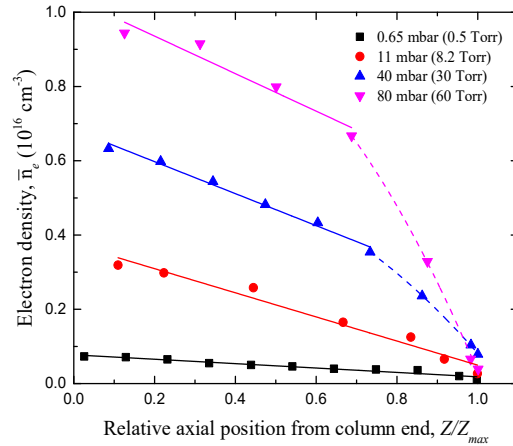


FIG. 19b (foreign laboratory). Axial electron density distribution determined by Thomson scattering along a Surfatron plasma column maintained at 2450 MHz in argon at four different gas pressures, inside a 3 mm radius fused silica tube (adapted from Hubner 2013a and 2013 b).

Note: Contrary to the linearity observed throughout Section 3, Fig. 7 at 270 W in Moisan, Pantel and Hubert (1990) shows experimentally a deviation from the linearity of the axial distribution of electron density, where the TWD is maintained at 915 MHz in a 0.97 mm radius tube at atmospheric pressure in argon. The axial electron density distribution of the plasma column at 270 W curves towards the end, which according to our model should not do so. We attribute this bending to an error in the data processing. In contrast, the 500 W and 700 W curves in Fig. 7 (Moisan, Pantel and Hubert, 1990) both show a linear electron density distribution along the entire length of the plasma column. As Fig. 12 in the current paper demonstrates, the axial electron density distribution of TWDs remains linear throughout the TWD, regardless of the total RF/MW power supplied.

This section concludes that the axial distribution of electron density in TWDs is linear under all adequate diagnostics and depends only on the operating parameters p , f and R . This new inference was first expressed by Moisan in the initial version of its article on Arxiv (v1, June 2021). This contradicts the widespread belief in the field that it depends on plasma column properties.

The next section will demonstrate how travelling waves dissipate their energy while maintaining a TWD. It will also outline the mechanisms responsible for the linear distribution of electrons observed in these TWDs.

APPENDIX A: THE INITIAL PATENT APPLICATIONS THAT LED TO THE SURFATRON. THE SURFAGUIDE AND RO-BOX EM FIELD APPLICATORS (TRAVELLING WAVE LAUNCHERS)

-*Surfatron*. The original patent application for the EM field applicator, later named the *Surfatron*, was filed by the Agence Nationale de la Valorisation de la Recherche (ANVAR), a French government agency, and was designed by Michel Moisan, Philippe Leprince, Claude Beaudry and Émile Bloyet. It was registered on 31 October 1974 by the Institut National de la Propriété Industrielle (INPI, National Agency for Industrial Property), it was given the number FR7436378A and the title:

Perfectionnements apportés aux dispositifs d'excitation, par des ondes HF, d'une colonne de gaz enfermée dans une enveloppe (Improvements to devices for exciting with HF waves a column of gas enclosed in a casing).

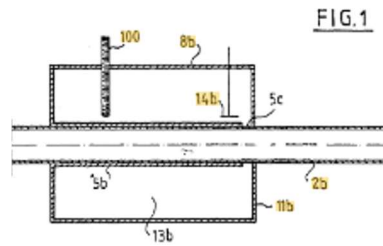


FIG. A1 (FIG. 1 in the initial patent disclosure). Schematic description of the cylindrical EM field applicator of the reentrant-type cavity, which encompasses a dielectric discharge tube coaxially (2b). It shows the radially movable high-frequency (HF) power coupler with its capacitive plate perpendicular to its end (14b). This coupler is located near the leakage interstice (gap) between the EM field and the tube (5c); this ensures impedance matching with the HF generator. A tuning screw (100) could also facilitate impedance matching of this device, which was later named the 'Surfatron'. Moisan, Zakrzewski and Pantel (1979) emphasise that the applicator enables stable, reproducible and energy-efficient generation of TWDs.

On 28 May 1975, a supplement to the first application was registered with priority over FR7436378A. This supplement was designated as the certificate of addition FR7533425 and was entitled:

-Surfaguide. Perfectionnements aux dispositifs d'excitation, par des ondes hyperfréquences, d'une colonne de gaz dans une enveloppe allongée (Improvements to microwave excitation devices for a column of gas in an elongated envelope).

FIGS. A2a and A2b (FIG. 2 and FIG. 2A in the original patent disclosure) show a schematic representation of a waveguide-type EM field applicator, later designated as a 'Surfaguide'. This applicator is fed by a coaxial high-frequency (HF) power connection (135) to a MW generator. At the opposite end of this connection is a movable impedance-tuning piston (136).

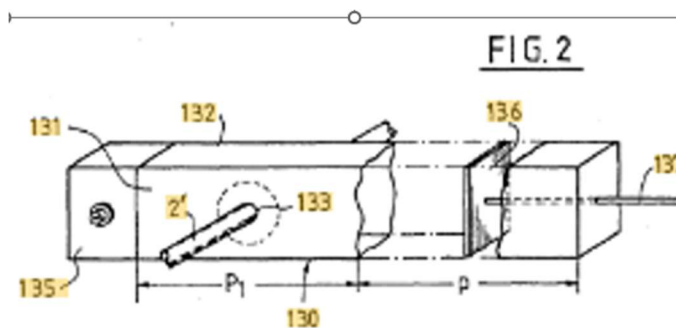


FIG. A2a: first step in the design of the future waveguide-based EM field applicator.

In Section 3, we demonstrated that the observed axial distribution of electron density decreases at a constant slope until it reaches a non-zero value at the axial position where the EM wave can no longer propagate. It is essential to verify the perfect linearity of this experimental distribution, because any theoretical model that fails to reproduce it accurately can then be considered erroneous or incomplete in our model. Here are the various electron density diagnostics used:

-1 The discharge tube passes through the central hole of a flat, narrow, cylindrical conductive cavity operating in the TM_{010} resonant eigenmode

The plasma is represented by its equivalent and relative permittivity ϵ_p , which can be calculated and/or calibrated with respect to the shift of the cavity resonance peak observed on an oscilloscope screen relative to the known permittivity of low-loss dielectric liquids (e.g., benzene). Varying the RF/MW power sets the length of the TWD plasma column relative to its end. This enables the different segments of the plasma column to pass through the cavity in succession, allowing the frequency shift of the resonance peak of each segment to be recorded relative to the resonance peak at the end of the plasma column. The axial distribution of the electron density can then be reconstructed segment by segment (Glaude *et al.*, 1980). One variant of this method involves calibrating the light emission intensity from several plasma segments (positioned at different points along the plasma column) against the corresponding electron density in the cavity. The intensity of light emitted along the column is fully recorded and compared with the light emission calibration in relation to electron density.

In all cases, the resonant cavity approach is limited by the fact that it becomes impossible to obtain a well-defined resonance peak above a certain level of electron density and gas pressure due to damping and distortion. Additionally, the resonant cavity of a large-diameter discharge tube must be much larger than the orifice for it to work properly, which makes it unwieldy and heavy. The resonant cavity method was used in Figs. 8, 11, 12 and 14.

-2 Determining the axial distribution of the electron density is achieved by recording the wavelength λ of the travelling wave through its phase variation along the plasma column

This phase variation is detected using an E -field antenna⁹, which moves along the discharge tube, close to its outer surface. Its signal feeds the first leg of a double balance mixer. The second leg is connected to the MW generator and acts as a phase reference. The mixer's output signal provides the axial variation of the wave phase, shown as curve c of the left panel of Fig. A3, for example. The corresponding electron density can then be determined from the calculated phase diagram.

A *phase diagram* plots of ω/ω_{pe} (where ω is constant) versus βR where the wave number $\beta = 2\pi/\lambda$ and λ is the recorded wavelength. Here, the phase diagram is calculated under the assumption of a cold plasma column with a locally uniform electron density, and surface-wave propagation along it (Zakrzewski *et al.*, 1977).

Surprisingly, the agreement between the data points and the solid curve representing the calculations in Fig. A3 (right panel) is quite good. However, it should be noted that the calculated

⁹ It is made from an approximately 2 mm diameter semi-rigid coaxial cable terminated over a few mm length by its bare conductor, directed radially toward the outer wall of the discharge tube.

curve overshoots above $(1 + \epsilon_g)^{-1/2}$ due to the authors' assumption that the travelling wave propagates in the ionised discharge gas. In contrast, our model claims that the travelling wave primarily moves along the interface between the outer wall of the discharge tube and the surrounding vacuum (see Appendix E). The factor $(1 + \epsilon_g)^{-1/2}$ nonetheless correctly marks the end of wave propagation in terms of electron density (Aliev, Schlüter and Shivarova, 2000), thus excluding the calculated overshoot above $(1 + \epsilon_g)^{-1/2}$ in the diagram.

Margot-Chaker *et al.* (1988) developed a detailed technique using the phase diagram to determine the electron density along TWDs. This method was applied to generate Figs. 7, 9 and 14 ($R = 62$ mm) and has the advantage that it can be used with discharge tubes of a larger diameter and at a higher gas pressure than with resonant cavities. However, beyond a certain pressure limit, the TW phase diagram ceases to vary significantly with β : it then becomes impossible to accurately determine the electron density (see, for example, Moisan, Pantel and Hubert, 1990).

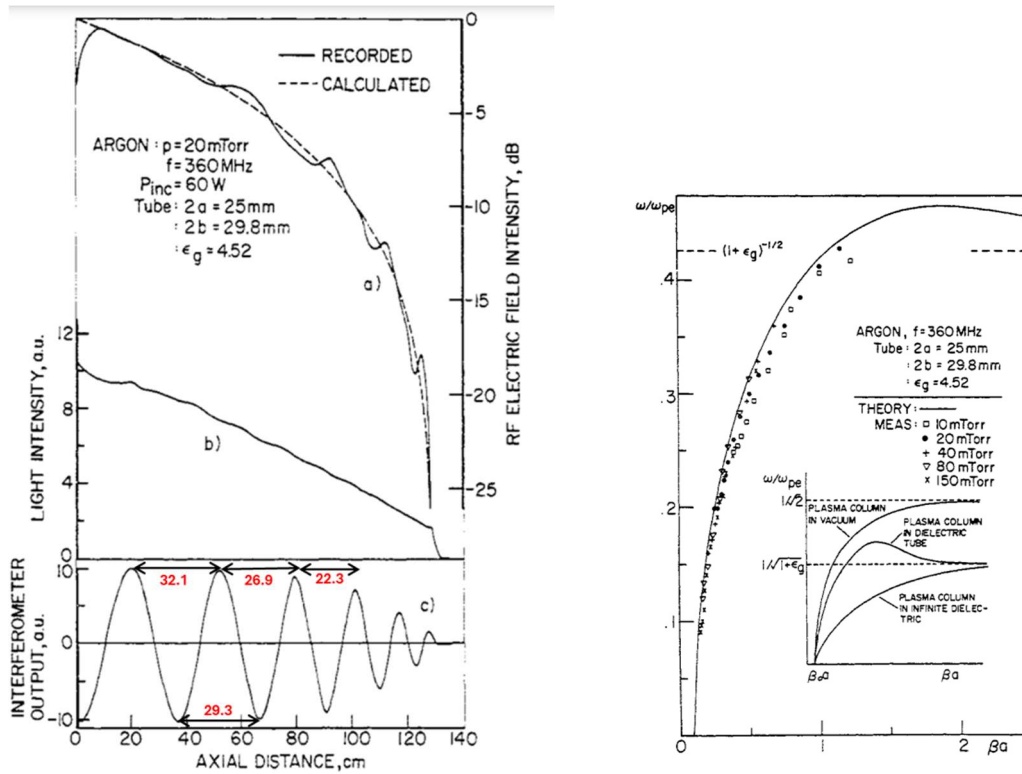


FIG. A3.

Left panel: a) the electric field intensity of the travelling wave recorded axially along the external wall of the discharge tube using a semi-rigid coaxial cable acting as an antenna. The antenna is directed perpendicular to the discharge tube at less than a mm from its outer wall (see footnote 9); b) axial light intensity recorded along the outside of the discharge tube; c) variation of the TW phase signal at the output of the double-balance mixer as a function of axial position (Zakrzewski *et al.*, 1977).¹⁰

¹⁰ The wavelength of the EM travelling wave in a vacuum, λ_0 , at 360 MHz is 83.28 cm, while Fig. A3c (left panel) shows a wavelength of 32.1 cm at one given axial position along the plasma column. Since the phase velocity of an EM wave is $v_{ph} = \omega/\beta$ where $\beta = 2\pi/\lambda$, the guided wave is travelling at this point at 38% of the speed of light in a vacuum, decreasing as the electron density decreases toward the column end.

Right panel: the phase diagram data points are compared to the calculated solid curve, which assumes a surface-wave discharge extending axially along the plasma column. The data points were determined using the TM_{010} resonant cavity method. The maximum observed value of ω/ω_{pe} is $(1 + \epsilon_g)^{-1/2}$, which corresponds to the minimum electron density obtained under low-collision regime according to equation (6). This marks the end of the plasma column. This value was determined using the TM_{010} resonant cavity method (Zakrzewski *et al.*, 1977).

3- Electron density diagnostic from the Stark broadening of the H_β emission line (486.1 nm)

Hydrogen atoms are made available in the discharge gas in the following ways:

- i) in the argon plasma at twice atmospheric pressure in Fig. 10, 0.5% added hydrogen was used, which did not alter the length of the pure argon plasma column (Moisan, Pantel and Hubert 1990);
- ii) in the neon plasma at atmospheric pressure (Fig. 13), the hydrogen atoms came from a minimal amount of added water vapour, such that its addition did not modify the length of the plasma column (Castaños-Martinez, 2004);
- iii) the percentage of H_2 admixed with argon at atmospheric pressure in Martinez-Aguilar *et al.* (2019) is unspecified (Fig. 16);
- iv) the gas in the TIAGO plasma torch operating at atmospheric pressure was a 9:1 argon-hydrogen mixture (see Fig. A10 in Appendix D).

-4 Electron density diagnostic through the Thomson laser scattering method

Figure 19a shows that the method of recording electron density from Thomson scattering provides a relatively high level of spatial resolution. This method can be used to diagnose a TWD plasma in a non-intrusive way. "This is an active spectroscopic method based on the scattering of laser photons by free electrons in the plasma. It does not need any model to account for the state of equilibrium departure" (Palomares *et al.*, 2010a and 2010b).

Fig. A4 refers to a Surfatron plasma at 2450 MHz and a pressure of 20 mbar in a 3 mm diameter discharge tube and with $\epsilon_g = 3.84$. It shows that excluding the data points closest to the Surfatron due to the antenna-like radiation from the EM field applicator, the axial distribution of the electron density is linear.

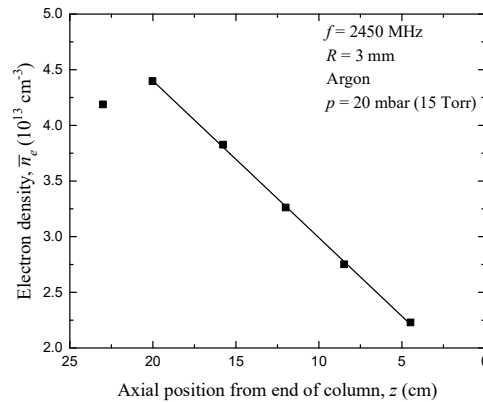


FIG. A4 (foreign laboratory). Axial electron density distribution obtained through Thomson laser scattering along a Surfatron plasma at 2450 MHz in a $R = 3$ mm tube at 20 mbar (15 Torr), by selecting a few electrons in the radial cross-section of the plasma column knowing that there is no radial contraction (Palomares *et al.*, 2010a and 2010b). Beyond the data point closest to the field-applicator (antenna-like radiation), the plasma column is linear and ends abruptly at a non-zero electron density, as expected from TWDs. Coefficient of determination $r^2 = 0.9993$.

However, this is not the case at higher gas pressures of 40 and 80 mbar (Fig. 19b), where the observed axial electron density distribution is no longer linear. This is primarily because the TWD plasma column undergoes radial contraction at these higher pressures. Then, due to the narrow width of the probing laser beam (see Sec. 3.7.2) and the electron density diagnostic method employed, only a portion of the radial electron density is considered. However, linearity is restored when the entire radial cross-section of electron density is considered (not shown).

5- Electron density diagnosed through the continuum radiation of the argon line at 648 nm, calibrated with a standard tungsten ribbon lamp and expressed in absolute units (Iordanova *et al.*, 2008a and 2008b)

Fig. A5 shows the electron density \bar{n}_e obtained using this diagnostic method in a Surfatron plasma at 2450 MHz and 15 mbar (11.2 Torr) in a $R = 3$ mm tube with $\epsilon_g = 3.84$. Once again, the axial distribution of electron density is perfectly linear when the data point closest to the Surfatron — originating from the antenna-like radiation of the field applicator — is disregarded.

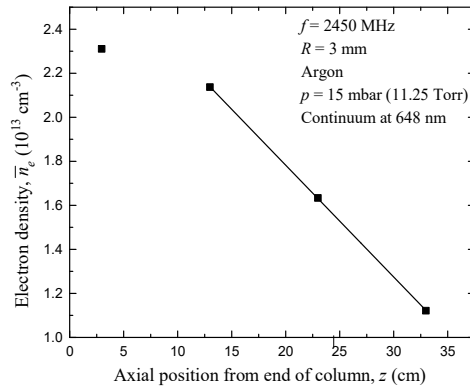


FIG. A5 (foreign laboratory). Axial distribution of electron density measured using continuum radiation from the 648 nm argon line, calibrated using a standard tungsten ribbon lamp. The results are expressed in absolute units (Iordanova *et al.*, 2008a and 2008b). The coefficient of determination (with only three data points!) is $r^2 = 0.99996$.

6- Electron density diagnosed using the ion saturation current of an axially moving Langmuir probe paired with a reference probe placed inside the Surfatron (Gordiets *et al.*, 2000).

The authors indicate that installing of a Langmuir probe in a Surfatron TWD was intended to 'gather information on the actual EEDF', but it 'acts as a source of inhomogeneity in the plasma' (Grosse, Schluter and Tatarova, 1994b). This disturbance causes some of the electron density values shown in Figs. 17 and 18 to fall below the minimum electron density \bar{n}_e (6), which

contradicts the results obtained using all the other diagnostic methods for TWDs cited in this paper thus far.

In summary, all measurement methods produce the same axial electron density distribution for TWDs. This is characterised by a linear decrease of electron density from start to finish, followed by an abrupt end at a non-zero value. This result remains consistent regardless of the measurement technique employed, provided the antenna-like EM radiation region of the field applicator is avoided and provide, in the case of plasma radial contraction, that the whole radial distribution of electrons is considered.

REFERENCES

- Aliev, Y.M., A. G. Boev, and A. Shivarova, 1982, "On the non-linear theory of a long gas discharge produced by an ionizing slow electromagnetic wave", *Phys. Letters* **92**, 235-237.
- Aliev, Y.M., H. Schlüter, and A. Shivarova, 2000, "Guided-wave-produced plasmas". Springer: Berlin.
- Balanis, C. A., 2016, "Antenna Theory Analysis and Design", John Wiley & Sons.
- Beenakker, C. I. M., 1976, "A cavity for microwave-induced plasmas operated in helium and argon at atmospheric pressure", *Spectrochimica Acta* **31B**, 483-486.
- Bertrand L., J. M. Gagné, B. Mongeau, B. Lapointe, Y. Conturie, and M. Moisan, 1977, "A continuous HF chemical laser: production of fluorine atoms by a microwave discharge", *J. Appl. Phys.* **48**, 224-229.
- Carbone, E.A.D., S. Hubner, M. Jimenez-Diaz, J. M. Palomares, E. Iordanova, W. A. A. D. Graef, A. Gamero, and J. J. A. M. van der Mullen, 2012b, "Experimental investigation of the electron energy distribution function (EEDF) by Thomson scattering and optical emission spectroscopy", *J. Phys. D: Appl. Phys.* **45**, 475202 (12pp). doi:10.1088/0022-3727/45/47/475202.
- Castaños-Martínez, E., 2004a, "Influence de la fréquence d'excitation sur les phénomènes de contraction et de filamentation dans les décharges micro-ondes entretenues à la pression atmosphérique", *Mémoire de Maîtrise, Département de physique, Université de Montréal.*
- Castaños-Martínez, E., Y. Kabouzi, K. Makasheva, and M. Moisan, 2004b, "Modeling of microwave-sustained plasmas at atmospheric pressure with application to discharge contraction". *Physical Review E* **70**, 066405.
- Castaños-Martínez, E., and M. Moisan, 2011, "Expansion/homogenization of contracted/filamentary microwave discharges at atmospheric pressure", *IEEE Transactions on Plasma Science* **39**, 2192-2193.
- Chaker, M., and M. Moisan, 1985, "Large-diameter plasma columns produced by surface waves at radio and microwave frequencies", *J. Appl. Phys.* **57**, 91-95. doi:10.1063/1.335401.
- Chaker, M., M. Moisan, and Z. Zakrzewski, 1986, "Microwave and RF surface-wave sustained discharges as plasma sources for plasma chemistry and plasma processing", *Plasma Chemistry and Plasma Processing* **6**, 79-96, doi:10.1007/BF00573823.

- Dessaux, O., P. Goudmand, and B. Mute, 1983, "Evidence for heterogeneous mechanisms in the active nitrogen-CO reaction", *J. Quant. Specfros. Radial. Transfer.* **30**, 137-141.
- Dias, F.M., E. Tatarova, and C. M. Ferreira, 1998b, "Spatially resolved experimental investigation of a surface wave sustained discharge in nitrogen", *Journal of Applied Physics* **83**, 4602-4609.
- Epstein, I. L., M. Gavrilović, S. Jovičević, N. Konjević, Yu. A. Lebedev, and A. V. Tatarinov, 2014, "The study of a homogeneous column of argon plasma at a pressure of 0.5 torr, generated by means of the Beenakker's cavity", *Eur. Phys. J. D.* **68**, 334-343. DOI: 10.1140/epjd/e2014-50182-7.
- Fehsenfeld, F. C., K. M. Evenson, and H. P. Broida, 1965, "Microwave discharge cavities operating at 2450 MHz", *Rev. Sci. Instr.* **36**, 294-298.
- Fleisch, T., Y. Kabouzi, M. Moisan, J. Pollak, E. Castaños-Martínez, H. Nowakowska, and Z. Zakrzewski, 2007, "Designing an efficient microwave-plasma source, independent of operating conditions, at atmospheric pressure", *Plasma Sources Sci. Technol.* **16**, 173-182, doi:10.1088/0963-0252/16/1/022.
- Fredericks, R. M., and J. Asmussen Jr., 1971, "Retuning and hysteresis effects of a RF plasma in a variable size microwave cavity", *J. Appl. Phys.* **42**, 3847-3849. doi.org/10.1063/1.1660786.
- Glaude, V.M.M., M. Moisan, R. Pantel, P. Leprince, and J. Marec, 1980, "Axial electron-density and wave power distributions along a plasma-column sustained by the propagation of a surface microwave", *Journal of Applied Physics* **51**, 5693-5698, doi:10.1063/1.327568.
- Gordiets, B., M. Pinheiro, E. Tatarova, F. M. Dias, C. M. Ferreira, and A. Ricard, 2000b, "A travelling wave sustained hydrogen discharge: modelling and experiment", *Plasma Sources Science and Technology*, **9**, 295-303.
- Grosse S., H. Schluter, E. Tatarova, 1994a, "On electron energy distribution function measurements in microwave discharges sustained by propagating surface waves", *Plasma Sources Science and Technology* **3**, 545-555. doi: 10.1088/0022-3727/27/2/019.
- Grosse S., H. Schlüter, and E. Tatarova, 1994b, "Axial dependence of the electron energy distribution function in microwave discharges sustained by propagating surface waves", *Physica Scripta* **50**, 532-539. doi: 10.1088/0031-8949/50/5/009.
- Hübner, S., N. Sadeghi, E. A. D. Carbone, and J. J. A. M. van der Mullen, 2013a, "Density of atoms in Ar*(3p54s) states and gas temperatures in an argon surfatron plasma measured by tunable laser spectroscopy", *J. Appl. Phys.* **113**, 143306 (9pp). doi.org/10.1063/1.4799152.
- Hübner, S., 2013b, "Poly-diagnostic study of low pressure microwave plasmas", Technische Universiteit Eindhoven, Netherlands.
- Iordanova, E., N. de Vries, M. Guillemier, and J. J. A. M. van der Mullen, 2008a, "Absolute measurements of the continuum radiation to determine the electron density in a microwave-induced argon plasma". *Journal of Physics D: Applied Physics*, **41**, 015208.
- Iordanova, E., N. de Vries, M. Guillemier, and J. J. A. M. van der Mullen, 2008b, "Absolute measurements of the continuum radiation to determine the electron density in a microwave-induced argon plasma", *J. Phys. D: Appl. Phys.* **41**, 015208 (8pp). doi:10.1088/0022-3727/41/1/015208.
- Johnson, R.C., 1993, "Antenna engineering handbook (third edition)", McGraw Hill, New York.

- Kabouzi Y., M. D. Calzada, M. Moisan, K. C. Tran, and C. Trassy, 2002, "Radial contraction of microwave-sustained plasma columns at atmospheric pressure", *J. Appl. Phys.* **91**, 1008-1019. <https://doi.org/10.1063/1.1425078>.
- Kabouzi, Y., M. Moisan, J. C. Rostaing, C. Trassy, D. Guérin, D. Kéroack, and Z. Zakrzewski, 2003, "Abatement of perfluorinated compounds using microwave plasmas at atmospheric pressure", *Journal of Applied Physics*, **93** 9483-9496.
- Kabouzi, Y., D. B. Graves, E. Castaños-Martinez, and M. Moisan, 2007, "Modeling of atmospheric-pressure plasma columns sustained by surface waves", *Physical review E* **75**, 016402, doi: 10.1103/PhysRevE.75.016402.
- Kovačević, M.S., L. Kuzmanović, M. M. Milošević, A. Djordjevich, 2021, "An estimation of the axial structure of surface-wave produced plasma column", *Physics of Plasmas* **28**, 023502.
- Lebedev, Y. A., 1997, "Some properties of an atmospheric-pressure long plasma column generated by a TM₀₁₀ cavity", *J. Moscow Phys. Soc.* **7**, 267-271.
- Lorrain, P., and D. Corson, 1972, "Electromagnetic fields and waves", WH Freeman Company, San Francisco, USA.
- Mallavarpu, R., J. Asmussen, and M. C. Hawley, 1978, "Behaviour of a microwave cavity discharge over a wide range of pressures and flow rates", *IEEE Trans. Plasma Science* **PS-6**, 341-354.
- Margot, J., and M. Moisan, 1993, "Characteristics of surface-wave propagation in dissipative cylindrical plasma columns", *J. Plasma Physics* **49**, 357-374.
- Margot-Chaker, J., M. Moisan, Z. Zakrzewski, V. M. Glaude, and G. Sauvé, 1988, "Phase sensitive methods to determine the wavelength of electromagnetic waves in lossy nonuniform media: The case of surface waves along plasma columns", *Radio Science* **23**, 1120-1132, doi:10.1029/RS023i006p01120.
- Martínez-Aguilar, J., C. González-Gago, E. Castaños-Martínez, J. Muñoz, M. D. Calzada, and R. Rincón, 2019, "Influence of gas flow on the axial distribution of densities, temperatures and thermodynamic equilibrium degree in surface-wave plasmas sustained at atmospheric pressure", *Spectrochimica Acta Part B: Atomic Spectroscopy* **158**, 1-9.
- Moisan, M., C. Beaudry, and P. Leprince, 1975, "A small microwave plasma source for long column production without magnetic field", *IEEE Transactions on Plasma Science* **PS-3**, 55-59.
- Moisan, M., P. Leprince, C. Beaudry, and E. Bloyet, 1977, "Improvements relating to devices and methods of using HF waves to energize a column of gases enclosed in an insulating casing", US Patent Number 4,049,940.
- Moisan M., Z. Zakrzewski, and R. Pantel, 1979a, "The theory and characteristics of an efficient surface wave launcher (surfatron) producing long plasma columns", *J. Phys. D.: Appl. Phys.* **12** 219-237.
- Moisan M., Z. Zakrzewski, R. Pantel, and P. Leprince, 1984, "A waveguide-based launcher to sustain long plasma columns through the propagation of an electromagnetic surface wave", *IEEE Trans. Plasma Science* **PS-12**, 203-214.
- Moisan, M., and Z. Zakrzewski, 1989, "New surface wave launchers to produce plasma columns and means for producing plasmas of different shapes", US Patent Number 4,810,933.

- Moisan, M., R. Pantel, J. Hubert, 1990, "Propagation of surface wave sustaining a plasma column at atmospheric pressure", *Contributions to Plasma Physics* **30**, 293-314. doi:10.1002/Ctpp.2150300213.
- Moisan, M., and Z. Zakrzewski, 1991a, "Plasma sources based on the propagation of electromagnetic surface waves", *Journal of Physics D: Applied Physics* **25**, 1025-1048.
- Moisan, M., G. Sauvé, Z. Zakrzewski, and J. Hubert, 1994, "An atmospheric pressure waveguide-fed microwave plasma torch: the TIA design", *Plasma Sources Science and Technology* **3**, 584-592, doi: 10.1088/0963-0252/3/4/016.
- Moisan, M., Z. Zakrzewski, D. Kéroack, and J.-C. Rostaing, 2002c, "Dispositif de traitement de gaz par plasma", PCT/FR2001/003293 (WO 2002/035575), Assignee : Air Liquide, France.
- Moisan, M., and J. Pelletier, 2012, "Physics of collisional plasmas: Introduction to high-frequency discharges", Springer: Berlin.
- Moisan, M., and H. Nowakowska, 2018, "Contribution of surface-wave (SW) sustained plasma columns to the modeling of RF and microwave discharges with new insight into some of their features. A survey of other types of SW discharges (Topical review)", *Plasma Sources Science and Technology* **7** 073001 (43pp), doi: 10.1088/1361-6595/aac528.
- Moisan, M., P. Levif, and H. Nowakowska, 2019, "Space-wave (antenna) radiation from the wave launcher (surfatron) before the development of the plasma column sustained by the EM surface wave: a source of microwave power loss", *AMPERE Newsletter* **98**, 9-19.
- Moisan, M., 2021, "Maintaining a discharge using a travelling electromagnetic wave results in a linear decrease in electron density along the plasma column", arXiv: 2106.11404.
- Moisan, M., I. P. Ganachev, and H. Nowakowska, 2022, "Concept of power absorbed and lost per electron in surface-wave plasma columns and its contribution to the advanced understanding and modeling of microwave discharges", *Physical Review E* **106**, 04520.
- Navrátil, Z., L. Dosoudilová, J. Hnilica, and T. Bogdanov, 2013, "Optical diagnostics of a surface-wave-sustained neon plasma by collisional-radiative modelling and a self-absorption method", *J. Phys. D: Appl. Phys.* **46**, 295204 (9pp), doi 10.1088/0022-3727/46/29/295204.
- Nowakowska, H., M. Lackowski, M. Moisan, 2020, "Radiation losses from a microwave surface-wave (SW) sustained plasma source (surfatron)", *IEEE Transactions on Plasma Science* **48**, 2106-2114. doi:10.1109/TPS.2020.2995475.
- Palomares, J. M., J. Torres, M. A. Gigosos, J. J. A. M. van der Mullen, A. Gamero, and A. Sola, 2009, "Balmer H β line asymmetry characteristics in a high pressure, microwave-produced argon (TIA) plasma", *Appl. Spectroscopy* **11**, 1223-1231.
- Palomares, J.M., E. Iordanova, E. M. van Veldhuizen, L. Baede, A. Gamero, A. Sola, J. J. A. M. van der Mullen, J.J.A.M., 2010a, "Thomson scattering on argon surfatron plasmas at intermediate pressures: Axial profiles of the electron temperature and electron density", *Spectrochimica Acta Part B: Atomic Spectroscopy* **65**, 225-233.
- Palomares, J. M., E. I. Iordanova, A. Gamero, A. Sola, and v d Mullen, 2010b, "Atmospheric microwave-induced plasmas in Ar/H $_2$ mixtures studied with a combination of passive and active spectroscopic methods", *J. Phys. D: Appl. Phys.* **43**, 395202 (9pp). doi:10.1088/0022-3727/43/39/395202.

- Pelletier, J. H. L., A. Lacoste, T. Lagarde, M. Moisan, Y. Arnal, and Z. Zakrzewski, 1999, "Diviseur de puissance pour dispositif à plasma", French patent application filed on 13 September 1999 as FR 99/11422, PCT publication under WO 01/20710. "Equal part microwave power divider into many ports along a waveguide, ensuring absence of influence of any port on others", US patent 6,727,656. Assignee: CNRS, Université de Montréal and Metal Process (French company).
- Ridenti, M. A., N. Spyrou, and J. Amorim, 2014, "The crucial role of molecular ions in the radial contraction of argon microwave-sustained plasma jets at atmospheric pressure", *Chemical Physics Letters* **595–596**, 83-86. doi.org/10.1016/j.cplett.2014.01.050.
- Rostaing, J. C., F. Coeuret, C. de Saint Étienne, and M. Moisan, 1996 and 1999, "Procédé et installation de traitement de gaz perfluorés et hydrofluorocarbonés en vue de leur destruction", French patent 2 751 565 (26 July 1996), European patent application EP 0820801 A1 (08/07/1997). US patent 5 965 786 (12/10/1999) and 5 993 612, US 6 190 510 and 6 290 918. A process using plasma to purify a gas by dissociating impurity molecules and eliminating them (used, for instance, for purifying krypton and xenon gases).
- Rostaing, J.C., F. Bryselbout, M. Moisan, and J. C. Parent, 2000, "Méthode d'épuration des gaz rares au moyen de décharges électriques de haute fréquence", *C. R. Acad. Sci. Paris*, **t. 1**, Série IV, 99-105.
- Schelz, S., C. Campillo, and M. Moisan, 1998b, "Characterization of diamond films deposited with a 915 MHz scaled-up surface-wave-sustained plasma", *Diamond and Related Materials* **7**, 1675-1683.
- Selby, M., and G. M. Hieftje, 1987, "Taming the surfatron", *Spectrochimica Acta* **42B**, 285–298.
- Sola, A., J. Cotrino, and J. Colomer, 1998, "Reexamination of recent experimental results in surface-wave-produced argon plasmas at 2.45 GHz: Comparison with the diffusion-recombination model results", *Journal of Applied Physics* **64**, 3419-3423.
- Sugai, H., I. Ghanashev, and M. Nagatsu, 1998, "High-density flat plasma production based on surface waves", *Plasma Sources Sci. Technol.* **7**, 192–205.
- Trivelpiece, A. W., 1958, "Slow-wave propagation in plasma waveguides", California Inst. Techn., Pasadena, Electron tube and Microwave Laboratory, Techn. Report 7 (May 1958) and Ph.D. Thesis (June 1958).
- Trivelpiece, W., and R.W. Gould, 1959, "Space charge wave in cylindrical plasma columns", *J. Appl. Phys.* **30**, 1784-1793. doi.org/10.1063/1.1735056.
- Trivelpiece, A. W., 1967, "Slow-wave propagation in plasma waveguides", San Francisco Press, San Francisco.
- Tuma, D. T., 1970, "A quiet uniform microwave gas discharge for lasers", *Rev. Sci. Instrum.* **41**, 1519–1520.
- Van Dalen, J. P. J., P. A. de Lezenne Coulander, and L. de Galan, 1978, "Improvements of the cylindrical TM₀₁₀ cavity for an atmospheric pressure microwave-induced plasma", *Spectrochimica Acta* **33B**, 545-549.
- Wendt, G., R. W. P. King, F. E. Borgnis, C. H. Papas, H. Bremmer, L. Hartshorn. and J. A. Saxton, 1958, "Elektrische Felder und Wellen/Electric Fields and Waves" (Berlin: Springer).
- Zakrzewski, Z., M. Moisan, V. M. M. Glaude, C. Beaudry, and P. Leprince, 1977, "Attenuation of a surface wave in an unmagnetized R. F. plasma column", *Plasma Physics* **19**, 77-83.

Part II: Experimentally, the travelling waves that maintain TWDs are observed to be azimuthally symmetric TM waves. Their field components are thus E_r , E_z and H_ϕ , with $E_r^2 > E_z^2$. These generate two Poynting vectors: one that describes the wave power flowing primarily along the outer surface of the dielectric discharge tube and another that is radially directed and carries a smaller fraction of the total wave power, sustaining the TWD.

Michel Moisan

Groupe de physique des plasmas, Université de Montréal, Montréal H3C 3J7, Québec

Part II is organised as follows: Section 4 provides a physical explanation of specific aspects of TWDs, leading to equations that accurately reproduce the characteristics of their plasma column as obtained experimentally in Section 3. Section 5 offers a critical review of a selection of articles dealing with the modelling of the axial distribution of electron density along TWDs, highlighting the erroneous aspects of their modelling. Section 6 concludes the article with a summary and discussion. Appendix C examines the axial distribution of electron density under various standing wave conditions. Appendix D considers the TIAGO plasma torch while Appendix E uses the Poynting vector to determine how the wave power flows and sustain the TWD.

4. Key mechanisms controlling the linearity of the axial electron density distribution in TWDs

As shown in Section 3, the axial distribution of electron density is always linear and depends only on p, f and R , which are parameters set by the operator. This section will investigate the various mechanisms responsible for such a linearity.

4.1. For TWDs to be stable (stationary), the electron density must decrease monotonically towards the end of the column

Early studies on SWDs (Glaude *et al.*, 1980) assumed, based on observation, that the electron density $\bar{n}_e(z)$ along these discharges was proportional to the power dissipated by the wave at each axial position. This made it possible to empirically establish a relationship between the wave power attenuation coefficient $\alpha(z)$ and $\bar{n}_e(z)$ ¹¹. Later, Zakrzewski (1983) sought to determine the conditions necessary for stable discharge, whereby the production and loss of charged particles are balanced in steady state. Consequently, the wave power and electron density, in the case of a long plasma column (i.e. avoiding specifying the characteristics of the end of the column), must decrease monotonically towards its end. This principle emerges from the following inequalities in wave power flow and electron density (Zakrzewski, 1983):

¹¹ This empirical fact was first introduced in a theoretical article by Aliev, Boev and Shivarova (1982), but it was not physically justified (for that purpose, see Sec. 5.1.2 below).

$$dP(z)/dz, d\bar{n}_e(z)/dz > 0 \text{ and } d\bar{n}_e(z)/dz < 0. \quad (7)$$

Zakrzewski (1983) then sought to express the proportionality of $\alpha(\bar{n}_e(z))$ to electron density analytically, proposing the following:

$$\alpha(n) = An^k \quad (8)$$

where k is here an integer and A is a constant, with the electron density n normalised to its value n_{cs} at the start of the TWD plasma column. Recall the following expression from Glaude *et al.* (1980):

$$\frac{dn}{dz} = -2\alpha(n)n(z) \left(1 - \frac{n(z)}{\alpha(n)} \frac{d\alpha(n)}{dn}\right)^{-1}, \quad (9)$$

then from (8) and (9), there comes:

$$\frac{n(z)}{n_{cs}} = \left(1 + 2An_{cs}^k \frac{k}{1-k} z\right)^{-1/k} = \left(1 + \frac{2k}{1-k} \alpha_{cs} z\right)^{-1/k} \quad (10)$$

$$\text{and } \frac{P(z)}{P_{cs}} = \left(\frac{n(z)}{n_{cs}}\right)^{1-k}, \quad (11)$$

where the normalised quantities n_{cs} , α_{cs} and P_{cs} are those at the start of the TWD plasma column. Fig. 20 is a graph of equation (10).

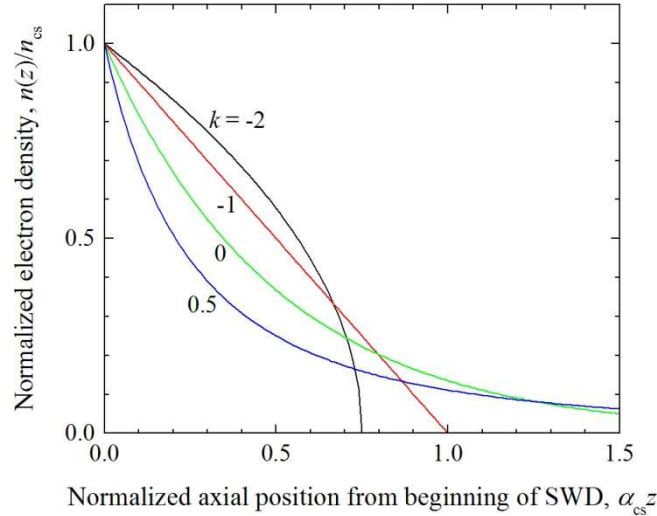


FIG. 20 (foreign laboratory). Electron density calculated as a function of axial position, according to the relation (10). This relation reflects Zakrzewski's (1983) criterion for ensuring the stability of a *long* TWD (meaning ignoring the characteristics of its end). The quantities n_{cs} and a_{cs} are normalised with respect to their values at $z = 0$, assuming $\alpha(n) = An^k$. The $k = -1$ curve corresponds to the linearly decreasing axial distribution of electron density, experimentally observed in Sec. 3 under an extremely large range of operator set values p , f and R .

Fig. 20 shows that the axial profile of the electron density distribution, calculated from relation (10), can be concave ($k = 0.5$ and 0), linear ($k = -1$) or convex ($k = -2$). All of these possibilities comply strictly with the stability criterion $d\bar{n}_e(z)/dz < 0$ (7), which requires monotonical decay of the electron density along the plasma column. These electron density profiles are obtained for

discharges maintained by EM travelling waves of any kind, irrespective of their specific dispersion properties or the kinetic characteristics of the generated plasma column. Of the different values of k shown in Fig. 20, only $k = -1$, which corresponds to the observed axial electron density distribution, remains once the transient period preceding the steady state is over (see below for details).

Zakrzewski (1983) put forward the argument that the SW axial field intensity E_0 is constant along a long plasma column, which guarantees a linear decrease in the axial distribution of electron density. Regarding the end of the plasma column, he incorrectly assumed that the intensity of E_0 would fall sharply. Experimentally, rather, there is a sudden increase in the intensity of E_0 at this point and in its immediate vicinity (Moisan *et al.*, 1991, Moisan, Ganachev and Nowakowska, 2022). In reality, the increase in E_0 at the end of the column is compensated by a reduction in the cross-section S of the plasma column (see Sec. 4.3 below), ensuring that the linearity of the axial electron density distribution of the plasma column is maintained up to its end, as observed throughout Sec. 3.

As briefly mentioned, the fact that the unique $k = -1$ electron density profile is reached under stationary conditions is linked to what occurs during the transient period that precedes the stationary state. More specifically, at the start of this period, the wave propagating towards the end of the column produces distinct plasma clusters on its way (Hamdan *et al.*, 2017). As the discharge evolves towards stability, the electron density along the axis decreases monotonically, leading to the merging of the initial individual plasma segments to form a single plasma column. A possible further mechanism contributing to the linearization of the axial electron density distribution would be the existence of electron density axial curvature (gradient) with profiles other than $k = -1$: these favour the axial transport of electrons, eventually eliminating any curvature of these gradients.¹²

4.2. Derivation of the relationship between $\alpha(z)$, the attenuation coefficient of the travelling wave power, and the axial electron density $\bar{n}_e(z)$, including the column end¹³

The axial distribution of the electron density is determined by the rate at which power is lost by the travelling wave along the plasma column. Assuming that this wave propagates in the z -direction (with $z = 0$ representing the end of the plasma column in this model), the fundamental equations for power flow can be expressed as follows:

$$\alpha(z) \equiv \frac{1}{2P(z)} \frac{dP(z)}{dz} \quad (12)$$

and

$$L(z) = \frac{dP(z)}{dz} \quad (13)$$

¹² Assuming that the discharge tube is longer than the plasma column produced.

¹³ The analytical derivation that follows (inspired from Moisan and Zakrzewski (1991)) is proposed here for the first time.

where $\alpha(z)$ defines the attenuation coefficient of the wave power along z , and $P(z)$ is its power flow¹⁴. $L(z)$ is defined as the power lost by the electrons per unit length due to collisions of all kinds at z , compensated by dP/dz , the absorbed wave power. $L(z)$ can then be expressed as (Moisan, and Zakrzewski, 1991):

$$L(z) = \bar{n}_e(z)\theta(z)S(z) \quad (14)$$

where θ is the power absorbed per electron and S , recall, is the cross-sectional area of the plasma column (Moisan, Ganachev and Nowakowska, 2022), both depending a priori on z but their product being axially constant in accordance with what is imposed in (18) below. The experimentally observed axial distributions of electron density displayed in section 3 unambiguously suggest as a starting point for our model that:

$$\bar{n}_e(z) = n_0 + bz \quad (15)$$

where n_0 is the electron density at the plasma column end and $b \equiv \frac{d\bar{n}_e}{dz}$, the (constant) slope of the axial distribution of electron density. Expressing (14) fully as:

$$L(z) = (n_0 + bz)\theta(z)S(z), \quad (16)$$

then from (13) $P(z)$ can be expressed as an integral over $L(z)$ in the following form:

$$P(z) = \theta S \int_0^z (n_0 + bz) dz + P_0. \quad (17)$$

As previously mentioned, the values of θ and S depend on axial position z but their product, θS , must remain constant. Otherwise, $P(z)$ in (17) would depend on $S(z)$, contradicting the experimentally demonstrated independence of axial electron density (15) from plasma radius variation during radial contraction (see Sec. 4.3 below). After integration and referencing (12) and (17), the following is obtained:

$$P(z) = (n_0 z + \frac{1}{2} b z^2) \theta S + \frac{n_0 \theta S}{2\alpha_0}, \quad (18)$$

identifying the remaining power flow at the column end as:

$$P_0 = \frac{n_0 \theta S}{2\alpha_0}. \quad (19)$$

Therefore finally:

$$P(z) = (\frac{n_0}{2\alpha_0} + n_0 z + \frac{1}{2} b z^2) \theta S. \quad (20)$$

From equations (13) and (21), and bearing in mind that the product θS is independent of z , we have:

$$\alpha(z) = \frac{n_0 + bz}{\frac{n_0}{\alpha_0} + 2n_0 z + bz^2}. \quad (21)$$

¹⁴ Note that this demonstration does not require to specify in which medium(s) the wave propagates and loses its power.

Relation (21) can also be written as follows:

$$\alpha(z) = \frac{b \bar{n}_e(z)}{\bar{n}_e(z)^2 + c} \quad (22)$$

where:

$$c = n_0 \left(\frac{b}{\alpha_0} - n_0 \right). \quad (23)$$

Posing $c = 0$ (see below):

$$b = n_0 \alpha_0, \quad (24)$$

then from (22):

$$\alpha(z) = \frac{b}{\bar{n}_e(z)} \quad (25)$$

where b in (15) is $\frac{d\bar{n}_e}{dz}$ making that:

$$\alpha(z) = \frac{d\bar{n}_e}{dz} \frac{1}{\bar{n}_e(z)} \quad (26)$$

or equivalently:

$$\alpha(z) \bar{n}_e(z) = \frac{d\bar{n}_e}{dz} \quad (27)$$

where $\frac{d\bar{n}_e}{dz}$, recall, is experimentally constant till the very end of the plasma column (Sec. 3) and, therefore, such must be the product $\alpha(z)\bar{n}_e(z)$ all along the plasma column, unlike the result of previous model calculations (Glaude *et al.*, 1980) where this product grew exponentially towards the column end. The independence of $\alpha(z)\bar{n}_e(z)$ from the characteristics of the plasma column comes from the fact that the travelling wave propagates along the interface between the outer wall of the discharge tube and the vacuum (ambient air) surrounding it, as we advocate in this paper, and not along the interface between the outer edge of the plasma column and the inner wall of the discharge tube. The present derivation involves only the electrons in the discharge (as the medium absorbing the wave power), and no other properties of the plasma. Setting $c = 0$ in equation (23) gives $\alpha(z) = \frac{d\bar{n}_e}{dz} \frac{1}{\bar{n}_e(z)}$ (26), which makes that $k = -1$ when writing equation (8) as $\alpha(n) = A/n^{-k}$. This corresponds to the experimentally observed axial electron density distribution.

4.3. The independence of the axial position of the product $\theta(z)S(z)$ ensures a linear electron density distribution up to the end of the plasma column

The axially constant nature of the product $\theta_A(z)S(z)$ is an essential and original feature of our model (see Sec. 4.2). To illustrate this, consider a low-pressure TWD in which the value of θ_A (absorbed EM power per electron) is experimentally constant throughout the plasma column, except at its end where it increases sharply (see Fig. 21a; for detailed physical reasons, see Moisan and Nowakowska, 2018). Simultaneously, the radial luminosity of the plasma decreases at the end

of the column (see Fig. 21b), which indicates a reduction in the plasma's cross-sectional area S . In fact, the product $\theta(z)S(z)$ remains constant throughout the column because the sudden increase observed in θ_A at the end of the column (Fig. 21a) is offset by the corresponding reduction in S . These axial variations can be observed in both the photograph (Fig. 21b) and the plot of the luminous diameter of the plasma column (Fig. 21c).¹⁵

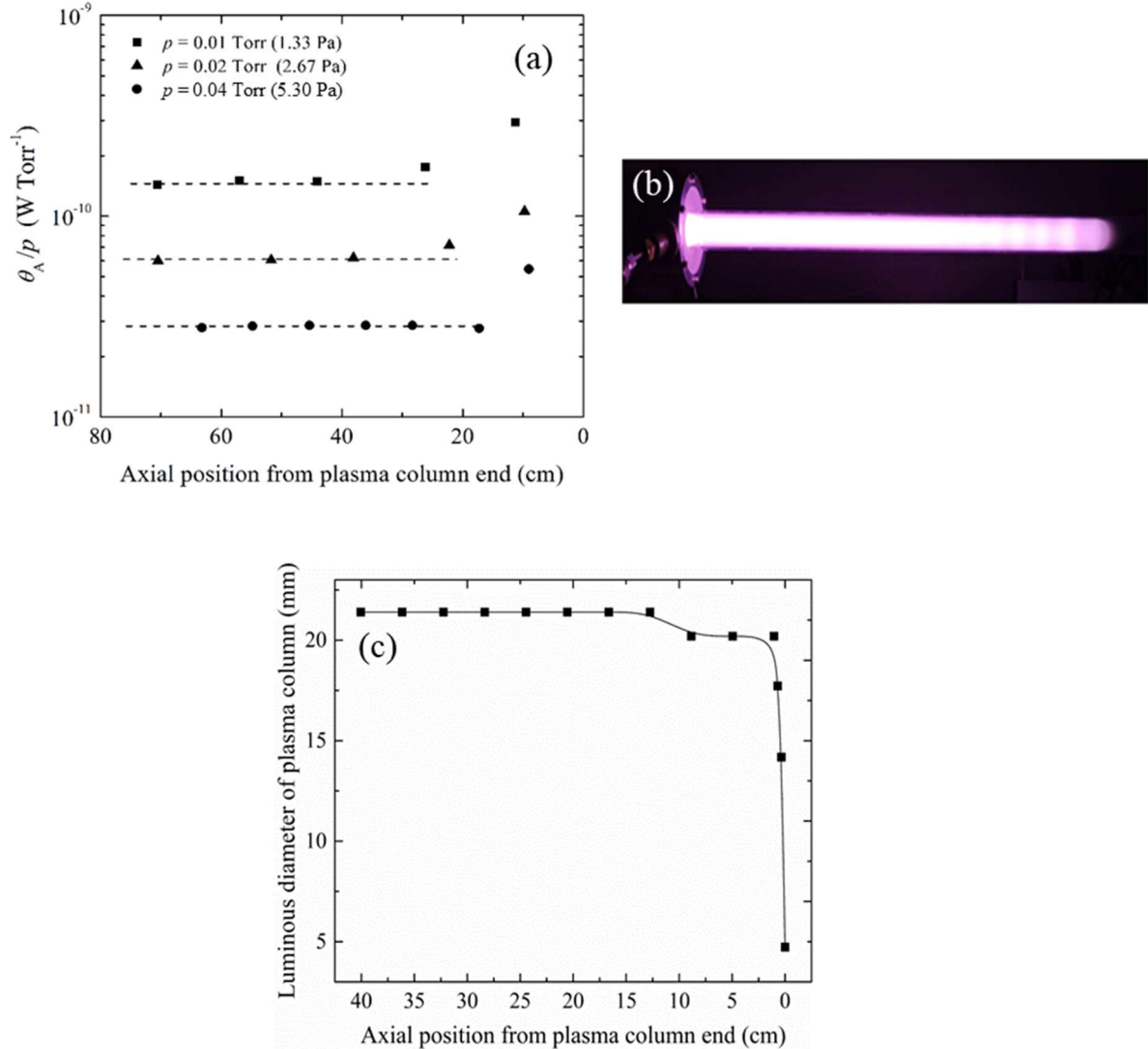


FIG. 21: a) Measured values of θ_A/p as a function of axial position relative to the end of the TWD plasma column sustained at 200 MHz in a tube with inner and outer radii of 13 and 15 mm, for three different gas pressures p in the low-collision regime. For a given gas pressure, the power absorbed per electron (θ_A) does not vary with axial position, except at the end of the column where there is a sudden increase (Moisan *et al.* 1991); b) photograph of an argon TWD at 0.05 Torr (6.7 Pa) sustained at 915 MHz in a tube with an inner radius of 10.7 mm. The wave runs from the left (Surfatron gap) to the end of the plasma column on the right.

¹⁵ Clearly, rigorously checking that $\theta(z)S(z)$ is a constant would require determining $\theta(z)$ and $S(z)$ under the same operating conditions.

The radius of the plasma column decreases towards the end as the plasma becomes rounder. The alternating variations in luminosity at the end of the column are due to the combined reflection of an azimuthally symmetric surface wave ($m = 0$) and a dipolar surface wave ($m = 1$): see Appendix C, case 1; c) The measured luminous diameter of the plasma column (leading to S) indicates that it fills the discharge tube, except at the very end where it decreases abruptly over approximately 10 mm.

The role of the product $\theta(z)S(z)$ in this behaviour was ignored by everyone, most probably because no one considered the possibility of an accompanying reduction in $S(z)$. This made it impossible to adequately resolve the problem raised by the sudden surge in E_0 (and θ) at the end of the column (Moisan *et al.*, 1991), This condition on $\theta(z)S(z)$ is thus essential for obtaining $\alpha(z)\bar{n}_e(z) = \frac{d\bar{n}_e}{dz}$, which leads to $k = -1$, i.e. a linearly decreasing axial distribution of electron density from the beginning to the end of the plasma column.

4.4. Even the shortest experimentally obtained TWD plasma column can be linearly extrapolated to any given length to provide the correct axial distribution of electron density. This is an essential characteristic of TWDs

This feature of TWDs (referred to as SWDs in the literature) is well known and has been documented in experiments (see, for example, Fig. 12 above). Its validity has been demonstrated regardless of the operating parameters p , f and R . The way in which the distribution of electron density decreases axially stems first from our representation of the wave's power distribution as an energy conservation law that links the wave axial power loss to electron heating throughout the discharge process (see Sec. 4.2). As the TW propagates in a vacuum along the surface of the outer wall of the dielectric tube, it dissipates power linearly. This monotonical decay of electron density guarantees the stability of the discharge (Sec. 4.1). Finally, it is the electric field component of the wave that heats the electrons in the discharge gas, thereby ionising the plasma column.

In conclusion, we emphasise that the phenomenon linking wave attenuation and the resulting electron density distribution is expressed by the relationship $\alpha(z) = \frac{b}{\bar{n}_e(z)}$, regardless of the kinetic characteristics of the plasma column. Furthermore, this relationship applies throughout the TWD plasma column. None of the models published to date reproduce this linearity as well in a short TWD plasma column as in a very long one. In fact, all their calculations show significant deviation from linearity at the end of the column, contrary to the linearity observed over its entire length (see Section 3).

5. A critical review of articles on modelling the axial distribution of electron density along so-called surface-wave discharges (SWDs)

While all SWD theorists agree that these MW discharges are controlled by an EM surface wave, either propagating along the plasma column itself or along the interface between the plasma and the inner surface of the dielectric tube, this is incorrect. This inaccuracy has been repeated in more than 500 articles published on SWDs, but our study challenges this analysis. We will discuss why

these authors failed to obtain the perfectly linear axial electron density distribution required by the experiment — a distribution that our model provides. Our analysis of their publications reveals flaws in the wave propagation mode they advocate. These publications, all of which are classified in the SWD category, can be divided into two groups:

- i) The surface wave attenuation coefficient is essentially related to the electron density of the plasma column.
- ii) One of the plasma column's kinetic properties is imposed from outside, in various ways.

5.1. The properties of the surface waves in these papers are determined either analytically or by numerical simulation by assuming propagation in a cold, homogeneous plasma characterised by its relative permittivity. The travelling wave power flow heats the electrons, ionising the discharge gas

5.1.1. Glaude et al. (1980) present experimental results supplemented by numerical calculations

This pioneering paper has paved the way for the study of the fundamental properties of TWD-sustained plasmas. It reveals the characteristic properties of these plasma columns and shows how the electron density $\bar{n}_e(z)$ (related to ω_{pe} in the real part of ε_p , the relative permittivity describing the plasma) depends on the wave frequency $\omega/2\pi = f$ (present in ε_p), on the inner radius R of the discharge tube through $S = \pi R^2$, and p , via the electron-neutral collision frequency for momentum transfer ν (the imaginary part of ε_p). A notable experimental finding is that the number of electrons $\bar{n}_e(z) S \Delta z$ in the cylindrical plasma section of small axial extension z , $z + \Delta z$ is proportional to the power absorbed within it, $P_a(z)$, according to the following equation:

$$\bar{n}_e(z) S \Delta z \theta = P_a(z) \quad (28)$$

where θ is the power absorbed/lost per electron¹⁶ (Moisan, Ganachev and Nowakowska, 2022). Since Glaude *et al.* (1980) assumed that θ is axially constant, the following can be written for two successive short cylindrical plasma segments at z_1 and z_2 :

$$\theta = P_a(z_1)/n(z_1) S \Delta z_1 = P_a(z_2)/n(z_2) S \Delta z_2. \quad (29)$$

The electron density and absorbed wave power values for the first cylindrical segment, as determined by the measurements, enable the iterative calculation process for the second segment to begin since the first segment initially provides the value of θ (see Glaude *et al.*, 1980 for the full procedure). By keeping the three parameters ω , S and ν , which define the operating conditions, constant, the calculations generate a linear axial distribution of electron density, except at the end of the column where "numerical oscillations" are observed. Furthermore, similar calculations, in which one of the parameters ω , S and ν is varied at a time, also lead to a linear axial distribution of electron density (again, except at the end of the column). The slope of these distributions increases with f , ν and decrease with the inner radius of the discharge tube R (via S); this dependence appears as a similarity law of the form $\nu f/R$. Ultimately, the authors demonstrate that the gradient of the

¹⁶ The quantity θ was initially introduced as the inverse of its current value, simply as a constant of proportionality (Glaude *et al.* (1980)) but more appropriately identified afterwards by Chaker *et al.* (1982) as the power required to generate an electron.

axial electron density distribution can be expressed as follows, given the attenuation coefficient of the travelling wave power $\alpha(z)$:

$$dn/dz = -\alpha n. \quad (30)$$

According to the numerical calculations by Glaude *et al.*, this relationship remains approximately constant, ensuring the linearity of the axially decreasing electron density distribution, except at the end of the column where α diverges. It means that the model is incorrect/incomplete.

Conclusion on Glaude et al. (1980): relation (30) is, in fact, formally identical to our relation (26) $\alpha(z) = \frac{d\bar{n}_e}{dz} \frac{1}{\bar{n}_e(z)}$, the difference lying in the way the value of α is assessed. In relation (30), the attenuation coefficient assumes that the travelling wave propagates through the plasma column, the dielectric tube and the surrounding vacuum. In contrast, our model asserts that the travelling wave propagates (and attenuates) guided along the interface between the outer wall of the dielectric tube, and the surrounding vacuum. This follows from the stability criterion (Sec. 4.1) formalised by the relation $\alpha(n) = An^k$ (8), with $k = -1$ leading to a linearly decreasing distribution of electron density from the beginning to the end of the plasma column, in accordance with the experiment. Although Glaude et al.'s paper contains the key elements of TWD wave physics, it does not consider the true propagation medium of the guided wave. As previously mentioned, in our model this medium is the interface between the outer wall of the discharge tube and the vacuum. This solution had not been considered until the present study.

5.1.2. Model of a plasma column sustained by a surface wave focussing on the radial distribution of electron density (Ferreira, 1981)

The main point of the paper is on recovering the observed radial distributions of excited argon atoms obtained with Surfatron plasmas. 'Depending on the working conditions (gas pressure, tube radius and absorbed HF power), the radial profiles are either flat or exhibit a maximum near the wall'. The axial distribution of the electron density is not considered.

5.1.3. The first analytical model to reproduce the linearly decreasing axial distribution of electron density in a plasma column maintained by an EM surface wave (Aliev, Boev and Shivarova, 1982)

Based on the experimental results of Glaude *et al.* (1980), the authors initially assumed an energy conservation law: the electron density at z is proportional to the absorbed wave power at the same axial position. Furthermore, the electrons are heated by the electric field component of the wave, thereby ionising the discharge gas.

They went on, noting that, in the thin-cylinder approximation and for a plasma column surrounded by a vacuum, the only significant power flow occurred in the z -direction and in a vacuum, which fits our model (see Appendix E). They further considered that the expression of the slope of the axial distribution of electron density should include an average (constant) axial value representing the dependence of wave dispersion on plasma properties: this is a basic error of appreciation. As shown in Sec. 3, the axial distribution of electron density depends exclusively on p , f and R . not on the properties of the plasma or wave dispersion. Nonetheless, these approximations produce a linear decrease in the axial distribution of electron density throughout the entire length of the generated plasma column, as observed in the experiment.

The following presentation literally quotes the main points of their article, highlighting their contribution (CGS units are used).

"Consider a weakly damping electromagnetic wave of TM type having both axial and radial electric field components E_z , and E_r , respectively, and an azimuthal magnetic field component B_ϕ . The slow variation along the z -coordinate of the seek for quantities is determined by the energy conservation relation of the surface wave:

$$\frac{d\bar{S}(z)}{dz} = -\bar{Q}(z) \quad (31)$$

where \bar{S} (designing the Poynting vector) is the SW power flow averaged over a wave period:

$$\bar{S} = \frac{c}{8\pi} Re \int_0^{2\pi} d\phi \int_0^\infty r E_r(r) B_\phi^*(r) dr \quad (32)$$

and Re and $*$ denote the real part and the complex conjugate of a quantity, respectively, c being the speed of light in vacuum. As for the value of \bar{Q} , the Joule collisional heating losses in the plasma column per unit axial length, it is given by:

$$\bar{Q} = \frac{1}{2} \int_0^R r dr \int_0^{2\pi} d\phi (Re \sigma) |E|^2 \quad (33)$$

where σ is the conductivity of the low-temperature plasma. Further it is assumed that the frequency of the elastic electron-neutral collisions ν does not exceed the surface wave frequency ($\nu < \omega$), thus neglecting collisional damping. The energy conservation law is expressed, for simplicity, in the thin cylinder approximation (the plasma cylinder of radius R , located in vacuum, is smaller than the skin depth). E_z is the axial electric field component which in the case of the thin cylinder has a constant value over the plasma column cross-section and exceeds considerably the radial electric field component. The plasma (relative) permittivity:

$$\varepsilon_{p1} \approx -(\omega_{pe}^2 / \omega^2) \quad (34)$$

is negative with an absolute value much greater than unity (according to the case of surface waves in the thin cylinder approximation). This condition allows neglecting in the power flow the contribution of the wave propagation in the plasma (the obtained general expression for \bar{S}_z shows that in the thin cylinder case only the power flow forward in the z -direction is considerable and this flow is in vacuum". Finally, assuming that the local value of the electron density is proportional to the absorbed wave power at that same point:

$$|\varepsilon_{p1}| = \beta E_0^2 \quad (35)$$

where β is in their paper some constant and " E_0 is the axial electric field component which in this case of the thin cylinder has a constant value over the plasma column cross-section and exceeds considerably the radial electric field component".

The authors use the SW dispersion relation of a homogeneous cold plasma column surrounded by vacuum whose electron density is provided by (34) and (35). "The analytical results for the axial electron density distribution along the gas discharge axis is in the end:

$$n_e(z) / n_e(0) = 1 - z / L \quad (36)$$

where:

$$L = (R/v\omega)\bar{f}(12\pi e^2/m) n_e(0), \quad (37)$$

L is, here, the length of the produced plasma column, $n_e(0)$ is the electron density value at $z = 0$ where the surface wave generator is situated¹⁷, $\bar{f} = 0.16$ is a wave dispersion average value and m (here only) is the electron mass. In the end, the gradient of the electron density distribution can be expressed as:

$$\frac{dn}{dz} = -(v\omega / R)(\bar{f}^{-1}m/12\pi e^2) \quad (38)$$

where the authors assume that the electron-neutral collision frequency ν does not vary along the plasma column which allows them to preserve the observed axial linearity of the electron density all along the plasma column. Considering, in this condition, ν instead of the gas density N as an operating condition (see footnote 6) amounts to the same thing from a calculation point of view. "The initial value of the wave power (at $z = 0$) determines the length L of the plasma column but it does not influence the electron density axial profile".

Comparison with the experiment showed that the calculated properties of their plasma column, despite the very restrictive assumptions of the model (low-collision regime ($\nu/\omega \ll 1$), thin-cylinder approximation, plasma column in vacuum) gave a correct picture of wider operating conditions.

5.1.4. Aliev, Boev and Shivarova (1984) use the approximation of a thin plasma cylinder as before, but with a plasma column enclosed within a dielectric tube

As in their 1982 paper, they assumed that the contribution of wave dispersion depends on plasma properties, appearing as an average value in the slope expression (which makes that linearity is not affected, but is erroneous as mentioned), although using a more complex expression for \bar{f}_1 . Nonetheless, it leads to a similar expression as (38) (CGS units):

$$\frac{dn(z)}{dz} = - (v\omega / R) (\bar{f}_1^{-1}m/4\pi e^2). \quad (39)$$

They indicate that 'the wave power flux in a vacuum is greater than the energy flux in the plasma', which is a distinctive feature of their modelling and is consistent with our own modelling (see Appendix E). However, their assertion that plasma parameters must be described by nonlinear equations is meaningless for two reasons: first, the axial distribution of electron density is independent of plasma properties (Sec. 3), and second, our fully linear model is consistent with the experimental results.

5.2. Appraising the influence of the kinetic features of the plasma column on the axial distribution of electron density by incorporating some of these elements into the wave equation

¹⁷ Aliev, Boev and Shivarova (1982) were not aware at the time that the TWD plasma column does not begin immediately at the field applicator aperture, as was later documented (Moisan, Levif and Nowakowska, 2019); this results in an antenna-like radiation region.

As our model demonstrates that the travelling wave sustaining the discharge propagates along the interface between the outer wall of the dielectric discharge tube and the surrounding vacuum, it can be inferred that the wave is independent of the plasma column's properties. This contradicts the approach adopted in the following papers.

5.2.1. Mateev, Zhelyazkov and Atanassov (1983) conducted an analytical study of the axial electron density distribution of SWDs, with a particular focus on the role of Maxwell's equations

These are developed in the electrostatic (slow wave) approximation by applying the standard boundary conditions for the field components. The plasma column is represented by the relative (complex) permittivity of a cold, homogeneous, plasma embedded in a vacuum.

As the wave propagates along the plasma column, its energy "dissipated into the medium heats the electrons and they ionize the neutral gas sustaining the plasma column. The wave energy flux decreases during the wave propagation, and it becomes zero at the end of the column".

An original part of their contribution lies in the introduction of "universal" curves, $\bar{n}_e(\zeta)$ and $E^2(\zeta)$, resorting to a dimensionless axial space coordinate $\zeta = vz/\omega R$, which aggregates in the form of the observed similarity law (Glaude *et al.*, 1980) depending on the operating parameters v , ω and R . Another original aspect highlighted by these authors is to consider that the influence of electron density on the properties of the discharge should differ between the low and high gas pressure regimes:

i) "at low pressure, the electron density is proportional to the wave power absorbed per unit length. This occurs when the average lifetime of charged particles is determined by their diffusion towards the inner walls of the discharge tube". In this first approximation, they provide a relationship for the axial gradient of electron density that is similar to equation (38) of Aliev, Boev and Shivarova (1982), namely:

$$\frac{dn}{dz} = 0.73 \times 10^{-8} \frac{\omega v}{2\pi R} (cm^{-4}). \quad (40)$$

ii) at relatively high pressure, electron density is proportional to the total energy of the wave field per unit length. "This occurs when the average lifetime of the charged particles is defined by bulk (volume) recombination".

In both pressure cases, the axial distribution relating to the electron density deviates, although very little, from perfect linearity by showing a slight overall circular curvature extending from the beginning to the end of the plasma column. More dramatically, the axial distribution of electron density at the end of the column clearly shows a downward curvature, which is contrary to experiment (Sec. 4.4): the authors justify this discrepancy by referring to the corresponding increase in the intensity of the wave E field at the end of the column. In any case, their model is inadequate, as axial electron density linearity is not achieved over the full length of the SWD column.

5.2.2. Building upon the theoretical approach of Mateev, Zhelyazkov and Atanassov (1983), Zhelyazkov, Benova and Atanassov (1986) extended it to provide a complete EM treatment of the SW field components

The authors introduced the parameter $\sigma = \omega R/c$, where $\sigma = 0$ corresponds to the electrostatic approximation. They used this parameter to track the evolution of the axial distribution of electron density, moving from the electrostatic approximation to a more complete EM description. They found that, as σ increases, the axial distribution of electron density becomes more linear. Indeed,

the slight overall axial curvature away from linearity observed by Mateev, Zhelyazkov and Atanassov (1983) disappears when σ exceeds 0.2. However, the downward curvature observed by the aforementioned authors at the end of the plasma column persists in the complete EM treatment. This suggests that their calculations are inconsistent with the experimental results and must therefore be rejected on this basis.

5.2.3. Using the thin cylinder approximation, Aliev et al. (1993) propose an analytical derivation that extends the work of Aliev, Boev and Shivarova (1982), specifically considering volume recombination and ambipolar diffusion

This paper makes various approximations and assumptions to obtain analytical expressions for $\frac{d\bar{n}_e}{dz}$ and $E(z)$. The model clearly distinguishes between the roles of the charged particle recombination regime and the influence of the wave dispersion features, as well as the operating conditions of the discharge, namely:

- i) The charged particle loss mechanism acts as a numerical factor a determining the slope of the electron density distribution, which thus remains linear in all cases. The slope of the axial electron density distribution is smaller in the case of volume recombination than in the case of ambipolar diffusion, given the same discharge parameters;
- ii) the wave dispersion still appears as an average value, $\langle f \rangle$, taken over a limited interval of electron density;
- iii) the operating parameters of the discharge are considered in the form of the observed similarity law, namely, $v\omega/R$.

After considering various approximations of interest, it emerges that the axial distribution of electron density is always linear, in accordance with the experiment (see Sec. 3), specifically:

$$\frac{dn}{dz} = -(1/2) v\omega/R m_e/(4\pi e^2) 1/\langle f \rangle \text{ (CGS units)}, \quad (41)$$

except at the end of the plasma column where the electron density, again, falls rapidly. The authors exclude this terminal segment from the region of validity of the thin cylinder approximation. Note that the slope of the electron density distribution is related to the wave dispersion by the mean value $\langle f \rangle$, allowing the authors to assert that the wave dispersion characteristics and the axial plasma density distribution are interdependent: this is fundamentally contrary to reality (Sec. 3). Therefore, their model is both incomplete and erroneous.

5.2.4. Aliev et al. (1995a) introduce the concept of wave power absorption by resonance and compare it with collisional absorption

To simplify the calculations, the authors consider a plasma slab rather than a plasma column. Note that resonance absorption requires a transition region with a longitudinal (axial) gradient of electron density, allowing the resonance condition, $\omega = \omega_{pe}$, to be met at a specific point z along this gradient path: according to the authors, resonance would occur at the beginning and end of the plasma slab. However, this situation does not arise because, at both low and atmospheric pressures (see Sec. 3), the axial electron density profile of an SWD is experimentally linear along the entire plasma slab (column). Therefore, there is no specific transition region at either end of the plasma column to allow for resonance.

5.2.5. *Kovačević et al. (2021) proposed an analytical approximation of the SWD to ensure the axial electron density distribution is fully linear, as required by the experiment*

The authors employed the *square-root analytical approximation* of the surface wave dispersion relation introduced by Babović, Aničin and Davidović (1997). This involves limiting the calculations of the dispersion relation to the $\beta R < 1$ case, where β is here the SW wavenumber. This approach facilitates the determination of the wave power attenuation coefficient $\alpha(z)$ by 'avoiding the more difficult-to-handle cluster of Bessel functions of different types, orders, and arguments'. Using this approximation, the authors obtained linear axial distributions of electron density from the beginning to the end of the plasma column. However, the physical significance of the somewhat restrictive $\beta R < 1$ approximation is not discussed.¹⁸

The authors also examine the contribution of losses arising from the assumption that the wave propagates besides the plasma column in the dielectric discharge tube material. The losses in a dielectric tube increase significantly with both the frequency of the wave field and the thickness of the tube. They therefore conclude that, besides the collisional losses in the plasma column, $\alpha(z)$ should account for dielectric losses in the discharge tube material, since these could impact the linearity of the axial distribution of electron density. Their calculations show that linearity is 'a good approximation' insofar as R_{oi} , the ratio between the outer and inner radius of the tube, is less than 1.5, whereas for a thicker tube, the axial distribution of electron density should become increasingly parabolic as R_{oi} increases.

Such a contribution can be verified experimentally in two ways: by using discharge tubes with particularly thick walls, such as those with an outer radius of 8 mm and an inner radius of less than 1 mm (see Fig. 10), or by varying the frequency of the travelling wave, for example from 200 MHz to 2450 MHz (see Fig. 11). In both cases, the observed axial distributions of electron density remain linear. This result is no surprise since the travelling wave propagates along the surface of the outer wall of the discharge tube in the surrounding vacuum (see Appendix E), therefore without penetrating the discharge tube. However, note that the intensity of the electric field component of the travelling wave, which heats the electrons in the discharge gas, should be lower once passing through the tube dielectric wall.

5.2.6. *Gordiets et al. (2000) examined the kinetics of the plasma column and surface processes, which they claim are self-consistently linked to the electron density axial distribution*

As a matter of fact, the paper first attempts to compile all available information data on the properties of plasma, wave electrodynamics, gas dynamics, thermal balance and surface processes (those occurring on the inner wall of the discharge tube). "The volume and surface kinetics in discharges operating in molecular gases are strongly coupled, and this coupling significantly affects the whole discharge physics". "A SW discharge is sustained by a wave which simultaneously propagates and creates its own propagation structure", an incorrect assumption. In that sense, they claim that anything that happens in the discharge tube is reflected in the axial distribution of electron density. However, this statement is contradicted by the experimental results analysed in Sec. 3, where the electron density distribution only depends on p, f and R , on nothing else. Fig. 18 illustrates the outcome of their approach, clearly showing that their model does not

¹⁸ Their approximation requiring $\beta R < 1$ avoids considering the true end of the plasma column, thus skipping the problem of downward curvature appearing in the calculated axial distributions of electron density by all.

replicate the observed linear axial distribution of electron density. Furthermore, they obtain a downward curvature of $n_e(z)$ at the end of the column, a general feature when assuming that the plasma column and the wave interact. The article is based on many wrong premises.

5.2.7. Aliev et al. (1995b) considered that the wave propagating at the outlet of the EM field applicator and in its immediate vicinity is a true EM wave that is faster than the guided wave generating the TWD. This maintains a plasma column with a higher electron density, resulting in a quadratic axial electron density profile

As demonstrated in Section 2.2.2 and by Moisan, Levif and Nowakowska (2019), the electric field present at the output of the EM wave launcher and extending a certain distance beyond, is that of the radiation generated by an antenna. Furthermore, it is not an EM wave in the strict sense because the \mathbf{E} and \mathbf{H} components of its field in this region are neither of equal intensity, nor in quadrature or phase. Furthermore, the distribution of the electron density recorded in this region cannot be attributed a specific axial profile: for example, at 27 MHz (Fig. 7), this profile is linear, whereas at 360 MHz it is erratic (Fig. 8a). Moreover, the authors postulate that "the nature of this type of discharges combines in a self-consistent nonlinear manner wave and discharge properties", a claim of non-linearity based on incorrect premises.

5.2.8. The Zhelyazkov and Atanassov (1995) report on SWDs

This comprehensive 122-page report is constructed like a textbook and focuses on the main characteristic of plasma columns maintained by EM surface waves: their axial electron density distribution. In all cases studied, Zhelyazkov and Atanassov consistently agreed, directly or indirectly, with the authors reviewed, but wrongly, that the surface wave propagates into the discharge gas or at the interface between the plasma column and the inner surface of the discharge tube and consider this 'a basis for modelling surface-wave plasmas'. However, experiment (Sec. 3) and our model (see Appendix E) show that this is an incorrect approach.

The Zhelyazkov and Atanassov report covers SWDs up to 1995. It is divided into two themes. The first describes the surface waves, which can propagate in two ways (with azimuthal and dipolar symmetry, noted as $m = 0$ and $m = 1$, respectively). The second theme considers the structure and specific properties of the plasma column that the waves are expected to generate. It also examines the impact of a static, homogeneous external magnetic field on the propagation of EM surface waves. The development of the subject in each section follows a chronological order and is sometimes accompanied by contributions from Zhelyazkov and Atanassov themselves. Their comments shed additional light on the subject by identifying and summarising key issues more clearly:

1) The different aspects of SWD modelling are divided into three categories: (i) "approaches in which the surface wave and the plasma column are coupled; (ii) approaches that ignore the wave aspect of the problem but deal in detail with the equilibrium of charged particles in the plasma in the presence of an HF field (generally assumed to be uniform); and finally, (iii) approaches that focus on the propagation and attenuation characteristics of the wave and its power transfer to the plasma, but pay little attention to the equilibrium of the charged particles".

Quoting again the authors of the report:

2) "The axial gradient of the electron density is entirely determined by the discharge conditions (as defined by Moisan and Zakrzewski, 1991), i.e., the composition and pressure of the

gas, the dimensions of the discharge tube and metal enclosure (if any), the permittivity of the tube, the strength of the applied static magnetic field B_0 , the mode and frequency of the wave; the electron density gradient does not depend on the power of the HF wave, which is then considered as a condition separate from the discharge conditions";

3) "a simple model for HF discharges produced by EM travelling waves is based on the assumption that the treatment of the physical processes occurring in the discharge can be divided into two separate parts: the first concerns the maintenance processes within the discharge; the second, the electromagnetic behaviour of the HF waves sustaining the plasma";

4) "the local wave dispersion relation is assumed to be linear as far as the field intensity is concerned. This validity was checked by Zakrzewski *et al.* (1977) up to high wave power levels inclusive. Increasing the surface wave power density (in diffusion regime strictly) leads to a plasma density increase, not to an increase of the wave amplitude into the plasma".

In summary, their report assumes an interaction between the wave and the plasma column throughout, whereas the experiment (Sec. 3) and our model reject this idea: the wave propagates independently of the plasma column. The calculated axial distributions of electron density presented in the report are at best described as 'mostly' linear (hence the need in Sec. 3 for a statistical check of the observed linearity). However, the calculated or simulated theoretical axial distribution of electron density reported certainly do not remain fully linear till the end since they all curve downwards (sometimes upwards). This contrasts with the experiment where the axial distribution is totally linear from start to finish. To be additionally noted, some authors have conducted nonlinear calculations to the extent that the linear axial profile of electron density is considered an approximation of a nonlinear situation. However, experiment again contradicts this and, furthermore, our model correctly reproduces experimental axial distribution of electron density without the need for linear approximations!

Their report is limited to papers published at low gas pressure. At that time, little data little was known about SWDs at atmospheric pressure; in fact, the first well documented SWD publication on such SWDs was published as early as 1990, but in a 'confidential' journal (Moisan, Pantel and Hubert, 1990). As for the existence and characteristics of the antenna-like radiation zone of the field applicator, it had not yet been confirmed experimentally until 2019 (Moisan, Levif and Nowakowska, 2019).

5.2.9. Concluding comments on the reviewed papers

Of all the articles we have just reviewed, only that of Kovačević *et al.* (2021) reports a calculated axial distribution of electron density that remains linear over the entire length of the plasma column. However, this result is due to an approximation that removes calculations from the end of the column. In fact, to reiterate our point, none of the published axial distributions of electron density obtained so far by calculation or simulation end linearly, apart from that of our model. Given that the linearity of the axial distribution of electron density over the entire length of the plasma column is an essential observed characteristic of TWDs (see Sec. 4.4), it follows that all the models presented in the existing literature are incorrect: it is difficult to support such a conclusion in the face of so many authors.

The fundamental error in all these articles also appears in the conclusion that the propagation of the travelling wave is closely linked to the properties of the plasma column produced. However, if we assume instead that the wave propagates at the interface between the outer wall of the dielectric

tube and the surrounding vacuum, this statement becomes irrelevant. Furthermore, the stability criterion for TWDs is another feature that clearly shows that the wave sustaining the discharge is completely independent of the properties of the plasma column, as it only requires a monotonic axial decrease in electron density and power lost by the wave. This strict requirement is related to the fact that, as we propose, the axial distribution of electron density is also the axial distribution of energy lost by the travelling wave.

6. Summary, discussion and conclusion

6.1. Summary

Our model is based on the experimental finding that the axial distribution of electron density in plasma columns supported by EM travelling waves decreases linearly from start to finish. The operating parameters p, f and R are the only influences on this distribution, specifically on its slope, and no other characteristic of these discharges has any effect. This experimental starting point was meticulously confirmed and developed in Sections 3 and 4, respectively. However, this inference continues to be disputed in all theoretical papers published to date. Indeed, all the papers referenced at the end of this article — including our own work up to June 2021 — are affected by the fundamental error of assuming that the propagation of travelling waves along TWDs depends on the kinetic properties of the discharge. In defence, it could be argued that it was only natural to think this way!

A key modelling element introduced in our work is the Zakrzewski stability criterion for discharges sustained by EM travelling waves. This criterion ensures that maintaining a plasma column in this way results in a monotonically decreasing axial electron density and electron energy distribution, regardless of the type of EM travelling wave involved. Using this property to understand the transient period preceding the stationary state of the plasma column is also a significant advance. This demonstrates how the numerous reflections of the EM wave during the transient period— a consequence of the requirement for the electron density to decrease monotonically along the plasma column — gradually eliminate local gradients. Ultimately, only a single linearly decreasing axial electron density distribution remains. Furthermore, as this stability condition is not linked to the dispersion properties of the EM travelling waves, it confirms that the wave feeding the plasma column does not interact with it, contrary to general claims.

This article demonstrates (and does not merely assume) for the first time that the axial distribution of electron density reflects the axial dissipation of wave energy through the electric component \mathbf{E} of the wave, which heats the electrons, in both the RF and MW range; the subsequent ionisation of the discharge gas then maintains the plasma column. In other words, the wave energy attenuation coefficient, $\alpha(z)$, which controls energy transfer, depends solely on the electron density, ultimately expressed as $\alpha(z) = \frac{b}{n_e(z)}$ (26). This confirms our assertion that the travelling wave propagates along the interface between the outer wall of the dielectric tube and the surrounding vacuum. This explains why the wave does not depend on the properties of the plasma column, since it has thus no connection with the plasma column, but rather depends on the dielectric permittivity of the discharge tube.

In the case of the plasma produced by the TIAGO torch at 2450 MHz (see Appendix D), the electron density observed along the plasma filament initially corresponds to the antenna-type radiation zone, extending approximately 2 mm from the nozzle. This is followed by the dart, characterised by a linearly decreasing electron density distribution along the axis, confirming the identification of TIAGO plasma as a TWD.

6.2. Discussion

To eliminate doubts regarding the linearity of the axial electron density distribution, we performed a least-squares regression analysis on all the presented diagrams to validate straight lines drawn in our graphs, some of which originating from other laboratories. Those who oppose the current model like to point out observed deviations from linearity in the axial distribution of electron density: these occurred in cases of radial contraction of the plasma column and in case of an inadequate electron density diagnostic, for example when using Thomson scattering (Sec. 3.7.2).

Several issues raised in this article deserve further study and documentation. For instance, the minimum electron density at which travelling waves cease to propagate in a low-collision regime ($v/\omega \ll 1$), as defined by equation (6), is of particular interest. As this is based on $(1+\epsilon_g)$, it reveals that it depends on the relative permittivity ϵ_g of the dielectric tube, thus strengthening our assertion that wave power is primarily transported on the outer wall of the discharge tube. Furthermore, it should be clarified how the increase in gas pressure leads to a gradual increase in the minimum electron density for wave propagation relative to $\bar{n}_{e(re)}$, as observed in Section 3.

The other following points require clarification/confirmation:

i) gathering experimental data for θ and S under the same operating conditions at the end of the plasma column, to demonstrate that an increase in the local θ value is rigorously compensated for by a reduction in the plasma's cross-sectional area S , ensuring that the product of these two values θS remains constant throughout (see Figs 21a and 21c);

ii) detailed monitoring of the time evolution of the axial electron density distribution, during the transient period in which the initial individual plasma segments merge, causing their axial electron density to decrease monotonically (in accordance with the Zakrzewski criterion). Eventually, all axial gradients (Fig. 20) disappear in favour of a linearly decreasing gradient.

iii) The radial contraction of the plasma column, including the formation of multiple filaments, could be documented more thoroughly.

iv) The substitution of gas density N for p , as we have suggested, requires an analytical derivation leading to (4).

v) Determining how the wave power flows when the TWD is sustained by a $m = 1$ mode would be of interest since the corresponding wave is a linear combination of both TM and TE waves (Margot-Chaker *et al.*, 1989), making power flow more complex than for the TM wave of the $m = 0$ mode (Appendix E).

6.3. Conclusion

We have carefully demonstrated that the linearity of the axial distribution of electron density in TWDs depends exclusively on the operator set parameters p, f and R . This must be accepted as an indisputable experimental fact: consequently, any possible interaction between the wave and the plasma column can be definitively ruled out. Our model challenges the previously unanimously

accepted notion of a surface wave propagating along the plasma column or at the interface between the plasma column and the inner wall of the discharge tube: this represents an important turning point. The only possible scenario for EM travelling waves to support TWDs is for them to propagate on the surface of the outer wall of the dielectric discharge tube, which is in a vacuum (ambient air).

The laboratory's easy access to TWDs with unrivalled operating conditions provides a unique, reproducible, energy-efficient plasma medium. Combined with the present in-depth knowledge of their mechanisms, this makes them powerful research tools for developing new applications in a wide range of fields. In contrast to all other types of RF and MW discharges, it is not necessary to modify the discharge configuration when exploring a wider range of operating conditions as a function of p, f and R , thanks to the flexibility and variety of their operating conditions.

APPENDIX C: VARIOUS STANDING WAVE CONFIGURATIONS IMPROVING THE UNIFORMITY OF THE AXIAL DISTRIBUTION OF THE ELECTRON DENSITY OF TWDs

Maintaining a TWD plasma column using a travelling guided EM wave results in a linear decrease in electron density along the axis, yielding a highly non-uniform plasma column. To mitigate this issue, the column is fed by two guided waves that interfere with each other. This creates various types of standing wave, which reduces the degree of axial non-uniformity of the electron density. The interfering waves may or may not have the same azimuthal symmetry and may be in or out of phase.

- 1- Interference at/near the end of the plasma column of an azimuthally symmetric ($m = 0$) mode travelling wave with its corresponding dipolar ($m = 1$) wave

Fig. 21b (see Section 4.3) showed alternating light and dark circular rings along the axis of the plasma column near its end. These rings are caused by the interference of two travelling waves: one of the symmetric ($m = 0$) type and the other of the dipolar ($m = 1$) type. These waves are reflected at the end of the plasma column. For this to occur, the fR value must be sufficiently high to excite the $m = 1$ mode but not so high that the $m = 0$ wave ceases to exist; the exclusive presence of the $m = 1$ mode begins at $fR = 1.8$ GHz-cm (Margot-Chaker *et al.*, 1989). In Fig. 21b, the discharge tube has a radius of 1.07 cm and the frequency of the wave field that maintains the plasma column is 915 MHz. This gives an fR product of 0.98 GHz-cm, which allows the $m = 0$ and $m = 1$ propagation modes to coexist. However, the faster the amplitude of one of the two waves decreases axially, the more limited the interference zone at the end of the column becomes.

Interestingly, the selection of the propagation of given m modes depends on two of the three operating parameters (f and R) acting in relation to each other (see equation (5)). This can once again be related to the exclusive control exerted by the operating parameters p, f and R over the TWDs (see Section 3), which implies that the properties of the plasma column are not involved in characterising TWDs.

2- Interference between two independently launched azimuthally symmetric ($m = 0$) travelling waves

a) Fig. A6Aa shows the experimental setup involving a Surfaguide associated with a discharge tube of moderate radius. This setup generates a travelling wave of pure azimuthal mode $m = 0$ from the field applicator in two opposite directions (Rakem, Leprince and Marec, 1990): i) A wave is launched towards 'short circuit 1' (the fixed reflector plane) on the far left of Fig. A6a. This backward wave is then reflected, passing through the launch aperture of the Surfaguide towards 'short circuit 2' (the mobile reflector plane) where it is reflected. It therefore propagates in the same direction as the forward wave coming directly from the Surfaguide. These two waves then interfere due to their phase difference.

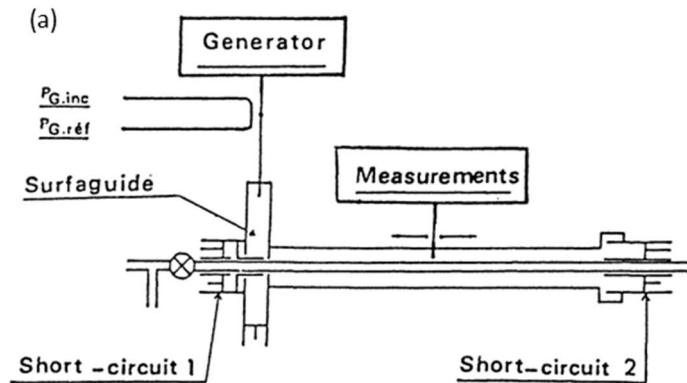


FIG. A6a (foreign laboratory). Schematic setup of a two-wave interference experiment using a Surfaguide, which operates at 2450 MHz with 70 W at 0.5 Torr of argon, in a fused silica tube with inner and outer radii of 2.5 mm and 5 mm, respectively: pure $m = 0$ mode waves are excited (Rakem, Leprince and Marec, 1990).

b) Measured axial intensity of E_r^2 under standing wave conditions

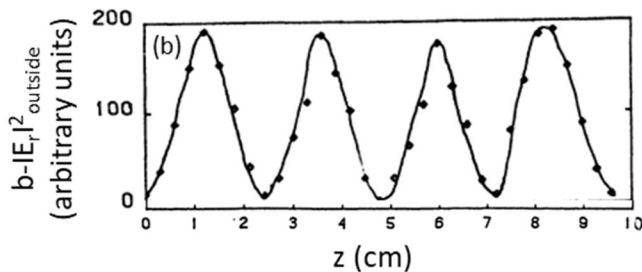


FIG. A6b (foreign laboratory). Measured intensity of E_r^2 , the radial component of the resulting electric field intensity of two interfering waves, under standing wave conditions (Rakem, Leprince and Marec, 1990).

c) Axial variation of radial electron density under standing wave conditions

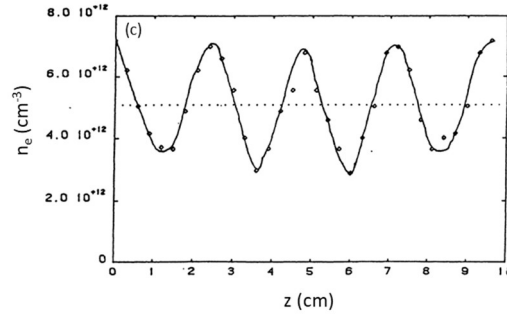


FIG. A6c (foreign laboratory). Axial variation of the radial electron density under standing wave conditions as measured using the EM wave phase variation method (Appendix B). For an absorbed power of only 70 W, the electron density varies axially around an average radial value of $5.1 \times 10^{12} \text{ cm}^{-3}$. In contrast, around 200 W would be required to obtain the same electron density value at the start of a pure travelling wave-sustained plasma column (Rakem, Z., P. Leprince, and J. Marec, 1990).

3- A standing wave configuration has been proposed by Chaker, Moisan and Zakrzewski (1986), which involves two launchers located at opposite ends of the discharge tube that are powered by two separate MW generators, which are therefore not in phase. While this method achieves better axial uniformity than that described in paragraph 2a) above, correctly adjusting the power of each generator to optimise uniformity can be challenging.

4- Two Surfaguides, each operating at 2450 MHz, are positioned at opposite ends of the discharge tube, and are supplied by the same generator, with a 3 dB power divider sharing the power equally between them (Wolinska-Szatkowska, 1988). This creates a standing wave along the plasma column through the interference of two TM $m = 0$ mode waves launched independently but in phase since the same generator is used. Despite this original arrangement proposed, the results obtained are similar to those described in paragraph 2a) above.

5- A single Surfaguide is used to achieve a $m = 1$ mode TWD, setting the standing wave pattern with the help of an axially movable reflecting plane (Zhukov and Karfidov, 2023). The experimental setup is illustrated in Fig. A7 and designated by the authors as an open-air MW interferometer.

It is built around a low-pressure argon gas TWD ($v/\omega \ll 1$), which is sustained within a 2 m-long fused silica discharge tube. The tube has inner and outer radii of 21 mm and 27 mm, respectively. This size is sufficient to excite a $m = 1$ propagation mode at 2450 MHz (Margot-Chaker *et al.*, 1989). The configuration consists of two conducting copper mirrors (M1 and M2) that reflect microwaves. The mirrors are perpendicular to the discharge tube, and the distance between them can be adjusted by moving the mobile M2 mirror. What makes this assembly unique is the presence of a copper reflector mesh with the same internal diameter as the discharge tube. This mesh is inserted transversely into the tube to ensure that the reflective plane of mirror M2 is completely uniform (with no radial discontinuities) given the orifice through which the tube passes. The reflector mesh and mirror M2 can also be moved independently of each other.

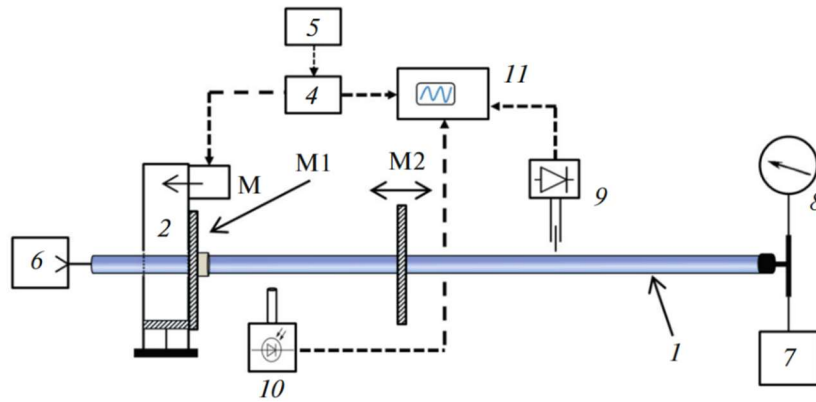


FIG. A7 (foreign laboratory). Schematic diagram of the experimental setup of this interferometer (Zhukov and Karfidov, 2023):

(1) A TWD is achieved in argon gas inside a 2 m long fused silica discharge tube with an inner radius of 21 mm and an outer radius of 27 mm. This excites a $m = 1$ mode wave at 2450 MHz (Margot-Chaker *et al.*, 1989). (2) A waveguide EM field applicator. (3) A 2450 MHz magnetron generator for MW power. (4) A square wave modulator with a 50 ms duration. (5) A delayed pulse generator. (6) A vacuum pump. (7) A gas inlet valve. (8) A vacuum gauge. (9) An MW electric field probe. (10) A collimated radially oriented photodiode. (11) An oscilloscope connected to the electric field antenna (9) for the EM wave and to the photodiode (10). Mirror M1 is fixed, while mirror M2 is axially movable.

This arrangement is designed to determine the axial intensity distribution of the E_z and E_r components of the electric wave field. Compared to a purely axial decrease of electron density, this technique also allows for a more uniform distribution of electron density throughout the plasma column length (see Fig. A6c).

The distance between the mirrors is divisible by an integer number of TW half-wavelengths. As illustrated in Fig. A8, the intensity E_r^2 of the electric field component along the axis is larger than that of E_z^2 .

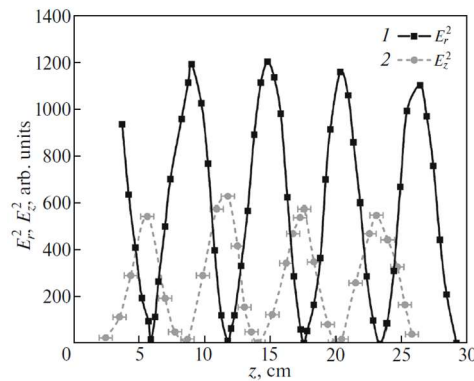


FIG. A8 (foreign laboratory). Measured axial intensity distribution of the electric field components E_z^2 and E_r^2 of the travelling waves, which are confined under a standing wave mode between the two mirrors. The distance between the mirrors is $L = 5/2\lambda = 29$ cm while the radial distance between the MW probes and the tube outer wall is $r = 1.5$ cm (Zhukov and Karfidov, 2023).

6- Unlike the other experimental situations discussed in this appendix, in this case a single wave propagates between a reflector plane that is located at a variable distance from the EM field applicator where the front plate of the wave launcher can also act as a second reflector plane (Rakem, Leprince and Marec, 1992). The aim is to achieve a constant axial distribution of excited argon ions by tracking them using the intensity of the axial emission of excited argon atoms.

Fig. A9 shows the reflector plane in three different axial positions:

- (a) Position A: located beyond the end of the plasma column, reflection is avoided, resulting in a linearly decreasing axial distribution of the intensity I_{ArI} of the excited argon atom emission line, as expected when the atom excitation rate follows the axial distribution of electron density;
- (b) Position B: the reflected power of the wave reaches the EM field applicator, but with minimal power, resulting in a gentler axial slope of I_{ArI} , which is additionally slightly modulated;
- (c) Position C: the reflected power level is sufficiently high between the faceplate of the EM field applicator and the reflector plane to ensure an axially constant I_{ArI} intensity characterized by deeper modulation. This modulation reflects the standing wave pattern resulting from multiples of the wave's half-wavelengths (at 2450 MHz). The authors consider this situation to be like the modulation of the electron density observed inside a resonant cavity. The high Voltage Standing Wave Ratio (VSWR) level achieved enabled wave power densities of up to 2 kW/cm^3 to be reached. An argon ion laser operating with a 1:1 argon: helium mixture has produced a laser beam of a few tens of milliwatts, based on this structure (Rakem *et al.*, 1986).

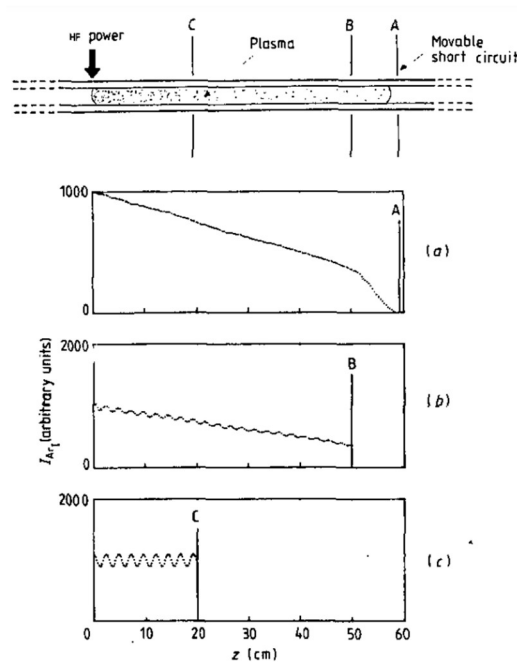


FIG. A9. Axial variation of the intensity of the emission lines from excited argon atoms plotted against the axial position of the reflector plane (Rakem, Leprince and Marec, 1992).

In summary, using standing waves enables the axial electron density of the TW plasma column to be made more uniform than a plasma column supported by a travelling wave alone, where the

electron density decreases linearly along the axis. Improving the axial uniformity of the TW plasma column's characteristic quantities can be useful in applications such as lasers and lighting.

Rogers and Asmussen (1982) were the first to propose exploiting a plasma column supported by 'surface waves' in standing wave mode.

APPENDIX D: THE TIAGO PLASMA TORCH, A HIGH ELECTRON DENSITY TRAVELLING WAVE SUSTAINED DISCHARGE CONFINED IN ITS AMBIENT GAS IN THE ATMOSPHERE

Fig. A10a shows a schematic cross-section of the TIAGO plasma torch. It comprises a hollow, conductive rod that ends in a conical nozzle with an opening typically 1 mm in diameter, which emerges from a Surfaguide (see Sec. 2.2.3). The rod passes through the front and rear broad walls of a modified standard rectangular waveguide section: the height of the waveguide has been reduced along its narrow walls to yield the best impedance matching using the tuning plunger of the Surfaguide (see Section 2.2.3.1). In the present example, a mixture of helium and hydrogen (He/H_2) flows at a rate of 10 slm through the internal conduit of the copper rod and exits as a filamentary plasma through the nozzle into its own ambient gas in the atmosphere. The discharge is maintained at 2450 MHz with 700 W (Ricard *et al.*, 1995). As Fig. A10a shows, the plasma flame consists of a *dart* surrounded by a *plume* that extends beyond the dart itself. The dart constitutes the TWD plasma, while the plume corresponds to its flowing afterglow.

Many small-size TIAGO plasma torches can be assembled on a single waveguide ensuring non-interference and equal sharing of MW power among the various torches (Pelletier *et al.*, 1999). Further information on the TIAGO concept can be found in Moisan, Zakrzewski and Rostaing (2001).

Fig. A10b shows the average electron density along the filamentary plasma relative to the axial distance from the nozzle tip, as obtained from Stark broadening of the H_β line (Ricard *et al.* 1995). The first two points starting from the nozzle exit are not part of the TWD, as they belong to the antenna-like radiation region (Moisan, Levif and Nowakowska, 2019). The last two points should also be excluded, as they are assumed to be affected by ambient N_2 gas penetration into the argon plasma filament. Least squares regression analysis of the remaining data points ($r^2 = 0.999$) reveals a linearly decreasing axial distribution of electron density along the filamentary plasma, starting at 3.5 mm from the nozzle tip. More details on the plasma plume and dart composition can be found in Rincón *et al.* (2013, 2014a, 2014b) and Toman *et al.* (2023).

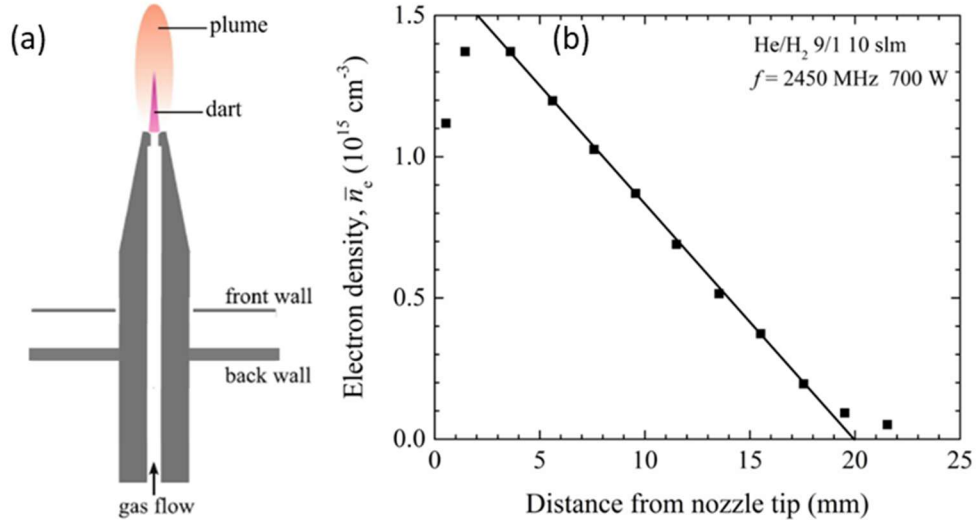


FIG. A10: a) shows a schematic diagram of the TIAGO MW plasma torch. It consists of a hollow conductive rod through which the carrier gas flows to the nozzle through a 1 mm-diameter hole (Ricard *et al.*, 1995). This plasma is supported by an EM travelling wave launched from the Surfaguide gap. The travelling wave gives rise to a dense filamentary plasma (the *dart*) and a surrounding diffuse plasma (the *plume*); b) the figure shows the average electron density obtained from the Stark broadening of the H_β line along the filamentary plasma (Christova *et al.*, 2004, Moisan, Kéroack and Stafford, 2016). The plasma is generated in a premixed He/H₂ 9/1 gas flowing at a speed of 10 standard litres per minute (slm) and sustained at 2450 MHz with a power of 700 W (Ricard *et al.*, 1995).

The fact that the electron density distribution decreases linearly along the plasma filament held by an EM travelling wave indicates that the discharge is controlled by Zakrzewski's stability criterion (see Section 4.1). Under these conditions, the EM travelling wave, whose electric field heats the electrons in the carrier gas, propagates along the exterior of the plasma filament embedded in the ambient gas.

The TIAGO has a proven track record in highly efficient graphene production (Melero *et al.*, 2023). This process was recently improved by over 20% (Morales-Calero *et al.*, 2024) using a Faraday cage around the TIAGO torch. Further improvements could be achieved by reducing the outlet orifice diameter thereby increasing the carrier gas temperature.

APPENDIX E: THE EM TRAVELING WAVE THAT SUSTAINS TWDs PROPAGATES PRIMARILY ON THE SURFACE OF THE DISCHARGE TUBE OUTER WALL, WHICH IS IN A VACUUM (AMBIENT AIR)

As we have repeatedly emphasised, the main issue when modelling the axial distribution of electron density in a plasma column generated by a guided EM travelling wave is the, erroneous, assumption that this wave propagates within the plasma column or along the interface between the plasma column and the inner wall of the containing tube. As previously mentioned, and as will now

be demonstrated, wave power primarily flows along the interface between the outer wall of the discharge tube and the surrounding ambient air.

To prove this, we will first revisit the fundamentals of non-ionising EM surface waves propagating along an existing plasma column, such as the positive column of a direct current (DC) discharge (Trivelpiece and Gould, 1959). This travelling wave was initially referred to as a *space charge wave*. It was later shown that its fundamental propagating mode is an azimuthally symmetric transverse magnetic (TM) wave (e.g. Margot-Chaker et al., 1989), which has two electric field components, E_r and E_z , and a unique magnetic field component, H_ϕ . Fig. A11 shows the radial variation of the two electric field components calculated along the discharge tube while the magnetic field component, which is radially constant, is not shown. We observe that the amplitude of the radial component of the wave electric field E_r is a few times larger than that of its axial electric field component E_z .

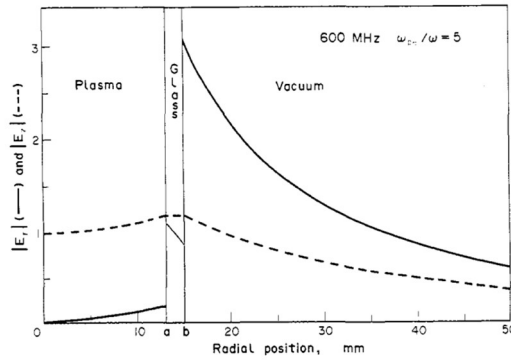


FIG. A11. Calculated radial amplitude of the radial and axial electric field components, $E_r(r)$ and $E_z(r)$ respectively, of the azimuthally symmetric TM mode wave propagating along a preexisting cylindrical DC plasma column enclosed in a dielectric tube surrounded by vacuum. The relative permittivity of the tube is 3.8, with inside and outside radii respectively a and b . The intensities are normalized by requiring $E_z(0) = 1$ (Moisan, Shivarova and Trivelpiece, 1982a).

Fig. A12 shows the measured intensity of the radial electric field component E_r of the travelling wave along this time a TWD. As calculations in Fig. A11 already showed, it decreases radially almost exponentially.

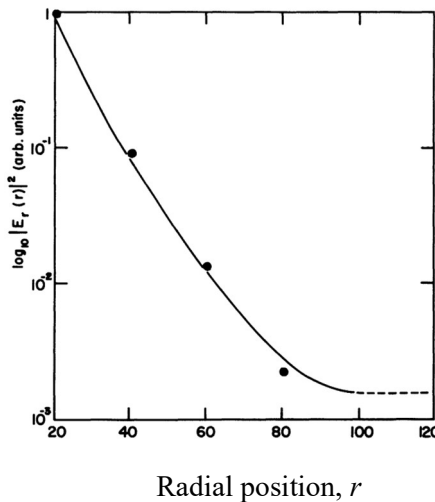


FIG. A12. The solid line is a recording of $\log_{10} [E_r(r)]^2$ as a function of radial position, as measured with a radially oriented electric-field type antenna (footnote 9), starting from the discharge tube outer wall. The position $r = 20$ mm corresponds to the tip of the antenna almost touching the tube external wall (Moisan *et al.* 1982b). The points are fitted with a modified Bessel function of the first kind, $K_1(r)$, as required for the *surface wave* field intensity distribution (Moisan and Nowakowska, 2018). As the fR product ($0.5 \text{ GHz} \times 1.15 \text{ cm} = 0.575 \text{ GHz cm}$) is much less than 2 GHz cm , it implies here the propagation of an azimuthally symmetric TM travelling wave with its three field components E_z , E_r and H_ϕ (Margot-Chaker *et al.*, 1989).

The wave Poynting vector which is given by $\mathbf{S} = \mathbf{E} \times \mathbf{H}$ (Lorrain and Corson, 1972) has thus two components due to the E_z and E_r field values, respectively:

$$\mathbf{S}_z = \mathbf{E}_r \times \mathbf{H}_\phi \quad (\text{A1})$$

and:

$$\mathbf{S}_r = -\mathbf{E}_z \times \mathbf{H}_\phi. \quad (\text{A2})$$

The measured values of the field intensity components E_z^2 and E_r^2 are easily obtained under standing wave conditions. As shown in Appendix C, the E_r^2 intensity of the radial electric field component is always larger than E_z^2 : consequently, \mathbf{S}_z is greater than \mathbf{S}_r meaning that the wave power primarily flows axially. The remainder of the total wave power flows radially into the plasma column to sustain it. This should put an end to the debate about how the wave propagates along the TWD and how it sustains it. Aliev, Boev and Shivarova first raised theoretically the possibility that most of the wave power circulates along the outer wall of the discharge tube in a vacuum (see Sec. 5.1.3 and 5.1.4).

Acknowledgments

We gratefully acknowledge the contribution of Dr. Helena Nowakowska (Institute of Flow Machinery, Polish Academy of Sciences, Gdansk, Poland) to the equations used in Section 4. Dr. Kinga Kutasi (Wigner Institute, Budapest, Hungary) is thanked for her relevant reading of Section 2. We would also like to thank Professors Émile Carbone (INRS-Énergie, Matériaux, Télécommunications, Varennes, Québec), Vasco Guerra (Instituto Superior Técnico, Lisbon, Portugal) and J. J. A. M. Van der Mullen (Eindhoven University of Technology, the Netherlands and Université Libre de Bruxelles, Belgium) for their comments on the manuscript during its preparation. We are also indebted to Dr Mariam Rachidi (Montréal, Québec) for her help with data processing. The Natural Sciences and Engineering Research Council of Canada (NSERC) covered the costs of editing and publishing this manuscript.

REFERENCES

- Aliev, Y.M., A. G. Boev, and A. Shivarova, 1982, “On the non-linear theory of a long gas discharge produced by an ionizing slow electromagnetic wave“, *Phys. Letters* **92**, 235-237.
- Aliev, Y.M., A. G. Boev, and A. Shivarova, 1984, “Slow ionizing high-frequency electromagnetic wave along a thin plasma column“, *Journal of Physics D: Applied Physics* **17**, 2233-2242.

- Aliev, Y.M., K. M. Ivanova, M. Moisan, and A. Shivarova, 1993, "Analytical expression for the axial structure of surface wave sustained plasmas under various regimes of charged particle loss". *Plasma Sources Science and Technology* **2**, 145-152.
- Aliev, Y.M., A. V. Maximov, H. Schluter, and A. Shivarova, 1995a, "On the axial structure of surface wave sustained discharges", *Physica Scripta* **51**, 257-262.
- Aliev, Y.M., A. V. Maximov, I. Ghanashev, A. Shivarova, and H. Schlüter, 1995b, "Axial structure of discharges sustained by ionizing fast electromagnetic surface waves". *IEEE Transactions on Plasma Science* **23**, 409-414.
- Babovic, V.M., B. A. Anicin, and D. M. Davidovic, 1997, "On the axial variation of the electron density in a plasma column of the surfatron type", *Physica Scripta* **55**, 86-87.
- Chaker, M., P. Nghiem, E. Bloyet, Ph. Leprince, and J. Marec, 1982, "Characteristics and energy balance of a plasma column sustained by a surface wave", *J. Physique-Lettres* **43**, L-71-L-75.
- Chaker, M., M. Moisan, and Z. Zakrzewski, 1986, "Microwave and RF surface-wave sustained discharges as plasma sources for plasma chemistry and plasma processing", *Plasma Chemistry and Plasma Processing* **6**, 79-96, doi:10.1007/BF00573823.
- Christova, M., E. Castañón-Martinez, M. D. Calzada, Y. Kabouzi, J. M. Luque, and M. Moisan, 2004, "Electron density and gas temperature from line broadening in an argon surface-wave-sustained discharge at atmospheric pressure", *Applied Spectroscopy* **58**, 1032-1037.
- Ferreira, C. M., 1981, "Theory of a plasma column sustained by a surface wave", *J. Phys. D: Appl. Phys.* **14**, 1811-30.
- Glaude, V.M.M., M. Moisan, R. Pantel, P. Leprince, and J. Marec, 1980, "Axial electron-density and wave power distributions along a plasma-column sustained by the propagation of a surface microwave", *Journal of Applied Physics* **51**, 5693-5698, doi:10.1063/1.327568.
- Gordiets, B., M. Pinheiro, E. Tatarova, F. M. Dias, C. M. Ferreira, and A. Ricard, 2000, "A travelling wave sustained hydrogen discharge: modelling and experiment", *Plasma Sources Science and Technology*, **9**, 295-303.
- Hamdan, A., F. Valade, J. Margot, F. Vidal, and J. P. Matte, 2017, "Space and time structure of helium pulsed surface-wave discharges at intermediate pressures (5–50 Torr)", *Plasma Sources Science and Technology* **26**, 015001 (10pp), doi:10.1088/0963-0252/26/1/015001.
- Hubert, J., M. Moisan, and Z. Zakrzewski, 1986, "On the supply and measurement of power in microwave induced plasmas", *Spectrochimica Acta* **41B**, 205-215.
- Kovačević, M.S., L. Kuzmanović, M. M. Milošević, A. Djordjevich, 2021, "An estimation of the axial structure of surface-wave produced plasma column", *Physics of Plasmas* **28**, 023502.
- Lorrain, P., and D. Corson, 1972, "Electromagnetic fields and waves", WH Freeman Company, San Francisco, USA.
- Margot-Chaker, J., M. Moisan, M. Chaker, V. M. M. Glaude, P. Lauque, J. Paraszczak, and G. Sauv e, 1989, "Tube diameter and wave frequency limitations when using the electromagnetic surface wave in the m=1 (dipolar) mode to sustain a plasma column", *Journal of Applied Physics* **66**, 4134-4148, doi:10.1063/1.343998.
- Mateev, E., I. Zhelyazkov, and V. Atanassov, 1983. "Propagation of a large amplitude surface wave in a plasma column sustained by the wave", *Journal of Applied Physics* **54**, 3049-3052.

- Moisan, M., A. Shivarova, and A. W. Trivelpiece, 1982a, "Experimental investigations of the propagation of surface-waves along a plasma-column", *Plasma Phys. Control. Fusion* **24**, 1331–1400. doi: 10.1088/0032-1028/24/11/001.
- Moisan M., C. M. Ferreira, Y. Hajlaoui D. Henry, J. Hubert, R. Pantel, A. Ricard, and Z. Zakrzewski, 1982b, "Properties and applications of surface wave produced plasmas", *Rev. Physique Appliquée* **17**, 707-727.
- Moisan, M., R. Pantel, J. Hubert, 1990, "Propagation of surface wave sustaining a plasma column at atmospheric pressure", *Contributions to Plasma Physics* **30**, 293-314. doi:10.1002/Ctpp.2150300213.
- Moisan, M., and Z. Zakrzewski, 1991, "Plasma sources based on the propagation of electromagnetic surface waves", *Journal of Physics D: Applied Physics* **25**, 1025-1048.
- Moisan, M., C. Barbeau, R. Claude, C. M. Ferreira, J. Margot, J. Paraszczak, A. B. Sá, G. Sauvé, and M. R. Wertheimer, 1991, "Radio-frequency or microwave plasma reactors - factors determining the optimum frequency of operation", *Journal of Vacuum Science and Technology B*, **9**, 8-25, doi:10.1116/1.585795.
- Moisan, M., D. Kéroack, and L. Stafford, 2016, "Physique atomique et spectroscopie optique". Collection Grenoble Sciences (EDP); Les Ulis: France.
- Moisan, M., and H. Nowakowska, 2018, "Contribution of surface-wave (SW) sustained plasma columns to the modeling of RF and microwave discharges with new insight into some of their features. A survey of other types of SW discharges (Topical review)", *Plasma Sources Science and Technology* **7** 073001 (43pp), doi: 10.1088/1361-6595/aac528.
- Moisan, M., P. Levif, and H. Nowakowska, 2019, "Space-wave (antenna) radiation from the wave launcher (surfatron) before the development of the plasma column sustained by the EM surface wave: a source of microwave power loss", *AMPERE Newsletter* **98**, 9-19.
- Moisan, M., Z. Zakrzewski, and J. C. Rostaing, 2001, "Waveguide-based single and multiple nozzle plasma torches: the TIAGO concept", **10**, 387-394, doi: 10.1088/0963-0252/10/3/301.
- Moisan, M., I. P. Ganachev, and H. Nowakowska, 2022, "Concept of power absorbed and lost per electron in surface-wave plasma columns and its contribution to the advanced understanding and modeling of microwave discharges", *Physical Review E* **106**, 04520.
- Morales-Calero, F. J., A. Cobos-Luque, J. M. Blazquez-Moreno, A. M. Raya, R. Rincon, J. Muñoz, A. Benítez, N. Y. Mendoza-Gonzalez, J. A. Alcuson, A. Caballero, and M. D. Calzada, 2024, "Increasing the production of high-quality graphene nanosheet powder: The impact of electromagnetic shielding of the reaction chamber on the TIAGO torch plasma approach", *Chemical Engineering Journal* **498**, 155088, <https://doi.org/10.1016/j.cej.2024.155088>.
- Pelletier, J., A. Lacoste, T. Lagarde, M. Moisan, Y. Arnal, and Z. Zakrzewski, 1999, "Diviseur de puissance pour dispositif à plasma", French patent application filed on 13 September 1999 as FR 99/11422, PCT publication under WO 01/20710. "Equal part microwave power divider into many ports along a waveguide, ensuring absence of influence of any port on others", US patent 6,727,656. Assignee: CNRS, Université de Montréal and Metal Process (French company).
- Rakem Z., P. Leprince, J. Marec, and S. Saada, 1986, Proc. 39th Gaseous Electronics Conf., Madison (University of Wisconsin) 1121.

- Rakem, Z., P. Leprince, and J. Marec, 1990, "Characteristics of a surface wave produced discharge operating under standing wave conditions", *Revue de Physique Appliquée* **25**, 125-130.
- Rakem, Z., P. Leprince, and J. Marec, 1992, "Modelling of a microwave discharge created by a standing surface wave", *J. Phys. D*: **25**, 953-959.
- Ricard, A., L. St-Onge, H. Malvos, A. Gicquel, J. Hubert, and M. Moisan, 1995, "Torche à plasma à excitation micro-onde : deux configurations complémentaires", *Journal de Physique III France* **5**, 1269-1285.
- Rincón, R., J. Muñoz, M. Sáez, and M. D. Calzada, 2013, "Spectroscopic characterization of atmospheric pressure argon plasmas sustained with the Torche à Injection Axiale sur Guide d'Ondes", *Spectrochimica Acta Part B* **81**, 26–35, doi.org/10.1016/j.sab.2012.12.006.
- Rincón, R., M. Jiménez, J. Muñoz, M. Sáez, and M. D. Calzada, 2014a, "Hydrogen production from ethanol decomposition by two microwave atmospheric pressure plasma sources: surfatron and TIAGO torch", *Plasma chemistry and plasma processing* **34**, 145-157, doi: 10.1007/s11090-013-9502-4.
- Rincón, R., J. Muñoz, M. Marinas, and M.D. Calzada, 2014b, "Hydrogen and by-products formation after the decomposition of ethanol by means of a microwave plasma torch at atmospheric pressure", *IEEE Transactions on plasma science*, **42**, 2770-2771, doi: 10.1109/TPS.2014.2325554.
- Rogers, J., and J. Asmussen, 1982, "Standing waves along a microwave generated surface wave plasma", *IEEE Transactions on Plasma Science* **10**, 11-16.
- Toman, J., M. Snírer, R. Rincón, O. Jašek, D. Všianský, A.M. Raya, F.J. Morales-Calero, J. Munoz, and M. D. Calzada, 2023, "On the gas-phase graphene nanosheet synthesis in atmospheric microwave plasma torch: Upscaling potential and graphene nanosheet-copper nanocomposite oxidation resistance", *Fuel Processing Technology* **239**, 107534 (13pp).
- Trivelpiece, W., and R.W. Gould, 1959, "Space charge wave in cylindrical plasma columns", *J. Appl. Phys.* **30**, 1784-1793. doi.org/10.1063/1.1735056.
- Wolinska-Szatowska, J., 1988, "The modelling of a discharge sustained by a standing surface wave", *Journal of Physics D: Applied Physics* **21**, 937-943.
- Zakrzewski, Z., M. Moisan, V. M. M. Glaude, C. Beaudry, and P. Leprince, 1977, "Attenuation of a surface wave in an unmagnetized R. F. plasma column", *Plasma Physics* **19**, 77-83.
- Zakrzewski, Z., 1983, "Conditions of existence and axial structure of long microwave discharges sustained by travelling waves", *Journal of Physics D: Applied Physics* **16**, 171-180, doi:10.1088/0022-3727/16/2/014.
- Zhelyazkov, I., E. Benova, and V. Atanassov, 1986, "Axial structure of a plasma column produced by a large-amplitude electromagnetic surface wave", *J. Appl. Phys.* **59**, 1466-1472.
- Zhelyazkov, I., and V. Atanassov, 1995, "Axial structure of low-pressure high-frequency discharges sustained by travelling electromagnetic surface waves", *Physics Reports* **255**, 79-201.
- Zhukov, V. I., and D. M. Karfidov, 2023, "Plasma distribution in a column of a low-pressure microwave discharge sustained by a standing surface wave", *Plasma Physics Reports* **49**, 975-983, doi:10.1134/S1063780X23600792.